

**INVESTIGATIONS OF CHARGE-CARRIER DYNAMICS AT
SEMICONDUCTOR/LIQUID INTERFACES**

Thesis by
William J. Royea

In Partial Fulfillment of the Requirements
For the Degree of Doctor of Philosophy

California Institute of Technology
Pasadena, California

2001
(Defended August 14, 2000)

© 2000

William J. Royea

All rights reserved

Acknowledgements

A wise old man once told me, “The more you learn, the more you realize how little you know.” I thank my advisor Prof. Nathan Lewis for helping me recognize how ignorant I truly am. Nate is an exceptional scientist and an outstanding mentor, and I am grateful to have had the fortunate opportunity to work for him.

With the exception of one individual, I am also indebted to all past and present members of the Lewis group with whom I have had the pleasure to work. Graduate school would have been a very unpleasant experience without my highly talented and supportive colleagues. Of all the wonderful people in the Lewis group, I am particularly thankful to a few individuals:

For everyone who joins the Lewis group, there is always one person who shows you how to make electrodes and how to use a potentiostat: if you’re fortunate, that person is not your advisor. For me, this individual was Dr. Mark Lonergan, and although he had plenty of laughs at my expense, I still thank him. In this regard, I also thank Dr. Stephen Doig, who was “instrumental” in getting me started in the lab and helping me to adjust to life in the Lewis group.

There are many members of the Lewis group with whom I have worked with closely on several of the projects described in this thesis. Dr. Arnel Fajardo provided key insights into the theoretical work described in Chapter 2, and for this I thank him. I also thank Arnel for his many years of guidance, for his friendship, and for not attempting to kick my ass when he should have. I am grateful to Dr. Olaf Krüger for providing the ToSCA simulations described in Chapter 4, as well as for many useful discussions on the topic of interfacial electron transfer. I thank both Agnes Juang and David Michalak who put several hours of lab work into the project described in Chapter 5. I would still be in the lab today if it were not for them. I am also grateful to Dr. Joel Haber who provided the modified silicon surfaces for the work described in Chapter 6.

Of everyone who has come and gone from the Lewis group, there has been only one proverbial fixture, Rob Rossi. I cannot count how many times Rob has bailed me out of predicaments and how many hours he has spent helping me. Even discounting for his mid-western upbringing, Rob is a good person, not to mention a model citizen, and I thank him for his friendship.

There are many others in the chemistry department to whom I am grateful. My committee members, Prof. Harry Gray, Prof. Jackie Barton, and Prof. Rudy Marcus are all extraordinary people who have always had their doors open to answer a question or help me with a problem. I am grateful to the electronically-inclined Tom Dunn and the mechanically-inclined Mike Roy and Guy Duremburg who made many impossible experiments possible. I thank an honorary member of the chemistry department, Mike Hill, who has been a great supporter and friend and whose astonishing stories of medical misfortunes never cease to entertain me. Although too numerous to mention all of them by name here, I thank all of Nate's administrative assistants for their many helping hands, and I also thank Maureen Renta for hers.

As much as I have learned in graduate school, I have learned nothing that compares to the lessons that my mother and my father, the wise old man, have taught me. I thank them for their unconditional love and support.

Last, but certainly not least, I thank my almost-wife Hallen, especially for her remarkable patience and understanding, but *especially* for making life fun.

Abstract

Theoretical and experimental investigations of charge-carrier dynamics at semiconductor/liquid interfaces, specifically with respect to interfacial electron transfer and surface recombination, are presented.

Fermi's golden rule has been used to formulate rate expressions for charge transfer of delocalized carriers in a nondegenerately doped semiconducting electrode to localized, outer-sphere redox acceptors in an electrolyte phase. The treatment allows comparison between charge-transfer kinetic data at metallic, semimetallic, and semiconducting electrodes in terms of parameters such as the electronic coupling to the electrode, the attenuation of coupling with distance into the electrolyte, and the reorganization energy of the charge-transfer event. Within this framework, rate constant values expected at representative semiconducting electrodes have been determined from experimental data for charge transfer at metallic electrodes. The maximum rate constant (i.e., at optimal exoergicity) for outer-sphere processes at semiconducting electrodes is computed to be in the range 10^{-17} – 10^{-16} $\text{cm}^4 \text{s}^{-1}$, which is in excellent agreement with prior theoretical models and experimental results for charge-transfer kinetics at semiconductor/liquid interfaces.

Double-layer corrections have been evaluated for semiconductor electrodes in both depletion and accumulation conditions. In conjunction with the Gouy-Chapman-Stern model, a finite difference approach has been used to calculate potential drops at a representative solid/liquid interface. Under all conditions that were simulated, the correction to the driving force used to evaluate the interfacial rate constant was determined to be less than 2% of the uncorrected interfacial rate constant.

Photoconductivity decay lifetimes have been obtained for Si(111) in contact with solutions of CH_3OH or tetrahydrofuran containing one-electron oxidants. Silicon surfaces in contact with electrolyte solutions having Nernstian redox potentials > 0 V vs.

SCE exhibited low effective surface recombination velocities regardless of the different surface chemistries. The formation of an inversion layer, and not a reduced density of electrical trap sites on the surface, is shown to be responsible for the long charge-carrier lifetimes observed for these systems. In addition, a method for preparing an air-stable, low surface recombination velocity Si surface through a two-step, chlorination/alkylation reaction is described.

Table of Contents

Acknowledgements	iii
Abstract	v
Table of Contents	vii
List of Figures	x
List of Tables	xiii
Chapter 1: Introduction to Charge-Carrier Dynamics at Semiconductor/Liquid Interfaces	1
I. Overview	2
II. Electron Transfer at Semiconductor/Liquid Interfaces	5
III. Surface Recombination at Semiconductor/Liquid Interfaces	8
IV. Summary	12
V. References	13
Chapter 2: Fermi Golden Rule Approach to Evaluating Outer-Sphere Electron-Transfer Rate Constants at Semiconductor/Liquid Interfaces	16
I. Introduction	17
II. Basic Kinetic Equations for Interfacial Charge-Transfer Reactions	19
III. Fundamental Expressions for Interfacial Electron-Transfer Rate Constants	21
A. Metallic Electrodes: Fixed-Distance Redox Species	21
B. Metallic Electrodes: Random Distribution of Dissolved Redox Species	23
C. Semiconducting Electrodes: Fixed-Distance Redox Species	25
D. Semiconducting Electrodes: Random Distribution of Dissolved Redox Species	26
IV. Relationships Between Rate Constants for Metal and Semiconductor Electrodes	30
A. Fixed-Distance Redox Acceptors	30
B. Random Distribution of Redox Acceptors	30
C. Relation Between Fixed-Distance Measurements at Metal Electrodes and Rate Constant Data for Randomly Dissolved Acceptors at Semiconductor Electrodes	31

D.	Relation Between Measurements Through Insulating Layers at Metal Electrodes and Rate Constant Data for Randomly Dissolved Acceptors at Semiconductor Electrodes	32
V.	Analysis of Experimental Data	33
VI.	Discussion	35
VII.	Summary	43
VIII.	References	44
Chapter 3: Theoretical Investigation of Interfacial Electron-Transfer Rate Constants at Semimetal Electrodes		48
I.	Introduction	49
II.	Rate Expressions for Charge Transfer at Semimetal/Liquid Interfaces	51
A.	Rate Law for Charge Transfer to a Random Distribution of Dissolved Redox Acceptors	51
B.	Fermi Golden Rule Expressions for Charge Transfer to a Random Distribution of Dissolved Redox Acceptors	51
C.	Comparison of Rate Expressions for Semimetal/Liquid and Metal/Liquid Junctions	53
III.	Evaluation of Interfacial Rate Constants at Graphite Electrodes from Analysis of Experimental Data	56
IV.	Discussion	62
V.	Summary	64
VI.	References	65
Chapter 4: Double-Layer Corrections for Interfacial Rate Constants at Semiconducting Electrodes		66
I.	Introduction	67
II.	Theory	69
III.	Results	76
A.	Depletion Conditions	76
B.	Accumulation Conditions	78
IV.	Discussion	91
V.	Summary	93
VI.	References	94
Chapter 5: Time-Resolved Photoconductivity Decay Measurements of Chemically Modified Silicon Surfaces		96
I.	Introduction	97

II.	Experimental	99
A.	Surface Treatments and Redox Solutions	99
B.	Photoconductivity Decay Measurements	100
C.	X-ray Photoelectron Spectroscopy Measurements	101
III.	Results	104
A.	Photoconductivity Decay Measurements of Hydrogen-Terminated Si(111) in Aqueous Acids and in Air	104
B.	Photoconductivity Decay Measurements of NH_4F -Etched Si(111) in CH_3OH or THF Solutions Containing Electrochemical Oxidants	105
C.	Photoconductivity Decay Measurements of Air-Oxidized Si(111) in CH_3OH or THF Solutions Containing Electrochemical Oxidants	107
D.	Photoconductivity Decay Measurements of Alkylated Si(111) in Air	108
IV.	Discussion	122
V.	Summary	127
VI.	References	128
Chapter 6: Electrochemical Measurements of Interfacial Electron Transfer at Chemically Modified Silicon Electrodes		131
I.	Introduction	132
II.	Experimental	134
A.	Electrodes and Solutions	134
B.	Electrochemical Cells and Instrumentation	135
III.	Results	136
IV.	Discussion	142
V.	Summary	143
VI.	References	144

List of Figures

Chapter 1

- Figure 1.1 Recombination pathways for an n-type semiconductor/liquid junction in depletion conditions. 4
- Figure 1.2 Schematic of capture and emission processes relevant to charge-carrier recombination at a semiconductor surface. 11

Chapter 2

- Figure 2.1 Energy diagram for a metal/liquid interface. 28
- Figure 2.2 Energy diagram for a semiconductor/liquid interface 29
- Figure 2.3 Plot of $k'_m(r, E)$ as a function of the relative distance of the redox species to the distance of closest approach to the electrode surface for various values of $H_{AB,m}^{o2}$. 40
- Figure 2.4 Plot of $k'_m(r, E)$ as a function of the relative distance of the redox species to the distance of closest approach to the electrode surface for various values of β_m . 42

Chapter 3

- Figure 3.1 Energy diagram for a semimetal/liquid junction at equilibrium. 55
- Figure 3.2 Plot of $D_{sm,eff}(E)$ for graphite near the Fermi level at the point of zero charge. 58
- Figure 3.3 Plot of the potential drop across the solution Helmholtz layer as a function of the potential applied to a graphite/liquid interface. 59

Chapter 4

- Figure 4.1a Potential drops at a semiconductor/liquid interface at the flat-band potential. 74
- Figure 4.1b Potential drops at a semiconductor/liquid interface in depletion conditions. 75
- Figure 4.2 Plots of E_{sc} as a function of $E - E_{fb}$ for an n-Si electrode in depletion. 81
- Figure 4.3 Plots of $1 - (E_h/E)$ as a function of $E - E_{fb}$ for an n-Si electrode in depletion. 82

Figure 4.4	Plots of $1 - (E_d/E)$ as a function of $E - E_{fb}$ for an n-Si electrode in depletion.	83
Figure 4.5	Plot of the ratio of the concentration of redox species at the OHP relative to the concentration of redox species in the bulk of the solution as a function of $E - E_{fb}$ for an n-type semiconductor electrode in depletion.	84
Figure 4.6	Plot of the Frumkin correction term for the heterogeneous rate constant for electron transfer from an n-type semiconductor electrode in depletion to a redox species in the solution phase.	85
Figure 4.7	Potential dropped across the semiconductor as a function of $E - E_{fb}$ for an n-Si electrode in accumulation.	86
Figure 4.8	Potential dropped across the Helmholtz layer as a function of $E - E_{fb}$ for an n-Si electrode in accumulation.	87
Figure 4.9	Potential dropped across the diffuse layer as a function of $E - E_{fb}$ for an n-Si electrode in accumulation.	88
Figure 4.10	Plot of the ratio of the concentration of redox species at the semiconductor surface to the concentration of redox species in the bulk of the solution vs. $E - E_{fb}$ for an n-Si electrode in accumulation.	89
Figure 4.11	A plot of the driving-force correction influencing the interfacial rate constant for electron transfer at an n-type semiconductor driven into accumulation.	90
 Chapter 5		
Figure 5.1	A schematic of the rf apparatus used to acquire photoconductivity decays.	103
Figure 5.2	Time-resolved photoconductivity decay of hydrogen-terminated Si(111) in contact with concentrated sulfuric acid and after air exposure.	110
Figure 5.3	Time-resolved photoconductivity decay of NH_4F -etched Si(111) in contact with $\text{CH}_3\text{OH}-\text{I}_2$ and in contact with N_2 .	111
Figure 5.4	Time-resolved photoconductivity decay of NH_4F -etched Si(111) in contact with $\text{CH}_3\text{OH}-\text{Fc}^{+/0}$ and in contact with $\text{N}_2(\text{g})$.	112
Figure 5.5	Time-resolved photoconductivity decay of NH_4F -etched Si(111) in contact with $\text{THF}-\text{I}_2$ and in contact with $\text{N}_2(\text{g})$.	113
Figure 5.6	Time-resolved photoconductivity decay of NH_4F -etched Si(111) in contact with $\text{THF}-\text{Fc}^{+/0}$ and in contact with $\text{THF}-\text{Me}_{10}\text{Fc}^{+/0}$.	114

Figure 5.7	Time-resolved photoconductivity decay of air-oxidized n-Si in contact with $\text{CH}_3\text{OH-Fc}^{+/0}$ and in contact with $\text{N}_2(\text{g})$.	115
Figure 5.8	Time-resolved photoconductivity decay of methylated Si(111) in air.	116
Figure 5.9	Time dependence of the mean carrier lifetimes for methylated Si in contact with air.	117
Figure 5.10	An energy diagram showing the Nernstian potentials of various redox couples relative to the band-edge positions of Si.	126
Chapter 6		
Figure 6.1	Plots of $\ln(J)$ vs E for a $\text{C}_{12}\text{H}_{25}$ -terminated Si(100) surface in contact with $\text{CH}_3\text{OH-MV}^{2+/+}$.	138
Figure 6.2	Mott-Schottky plot for a $\text{C}_{12}\text{H}_{25}$ -terminated Si(100) surface in contact with $\text{CH}_3\text{OH-MV}^{2+/+}$.	139
Figure 6.3	Plot of current density vs. potential for Si(100) surfaces terminated with three different-length alkyl chains.	140

List of Tables

Chapter 2

Table 2.1	Values of $k_{sc,max}$ as a function of the electronic coupling at contact.	39
Table 2.2	Values of $k_{sc,max}$ as a function of β_m .	41

Chapter 3

Table 3.1	Comparison of calculated and measured rate constants for interfacial electron transfer from a graphite electrode to various redox couples in aqueous solution.	61
-----------	--	----

Chapter 5

Table 5.1a	Measured lifetimes and surface recombination velocities for $\text{NH}_4\text{F}(\text{aq})$ -etched Si(111) following various surface treatments (assuming $\tau_b = \infty$).	118
Table 5.1b	Measured lifetimes and surface recombination velocities for $\text{NH}_4\text{F}(\text{aq})$ -etched Si(111) following various surface treatments.	119
Table 5.2a	Measured lifetimes and surface recombination velocities for air-oxidized Si(111) following various surface treatments (assuming $\tau_b = \infty$).	120
Table 5.2b	Measured lifetimes and surface recombination velocities for air-oxidized Si(111) following various surface treatments.	121

Chapter 6

Table 6.1	Measured kinetic parameters for chemically modified and unmodified Si(100) surfaces in $\text{CH}_3\text{OH}-\text{MV}^{2+/+}$ solutions.	141
-----------	---	-----

Chapter 1

Introduction to Charge-Carrier Dynamics at Semiconductor/Liquid Interfaces

I. OVERVIEW

This thesis describes studies of charge-carrier transport and recombination processes at semiconductor/liquid interfaces. The primary motivation for research in this subject is the development of liquid-based solar energy conversion devices.¹⁻⁸ Since surface processes can often influence, if not govern, the energy conversion efficiencies and stabilities of photoelectrochemical devices, a detailed understanding of the mechanism and kinetics of charge-carrier transport at solid/solution interfaces will likely lead to more rational approaches for designing liquid-based solar cells. In addition, surface processes are an important consideration in microelectronics applications.^{9,10} As device dimensions shrink, and surface-to-volume ratios correspondingly grow, charge-carrier dynamics at semiconductor surfaces will play an increasingly significant role in these technologies.

Two charge-carrier processes are the focus of this thesis: interfacial electron transfer and surface recombination. This chapter presents a brief introduction to the kinetics of both mechanisms. Chapter 2 follows directly from the discussion of interfacial charge-transfer kinetics, describing the development of a theoretical framework for relating interfacial electron-transfer rate constants of semiconductor/liquid contacts to that of metal/liquid contacts. Chapter 3 digresses from the topic of semiconductor/liquid junctions to extend the theoretical description of heterogeneous electron transfer to semimetal/liquid junctions. In Chapter 4, the results of a series of computer simulations are presented which quantify the magnitude of double-layer corrections necessary for evaluating experimental measurements of interfacial electron-transfer kinetics at semiconductor/liquid interfaces. Chapter 5 summarizes experimental measurements of carrier lifetimes and surface recombination velocities for chemically modified silicon surfaces, and finally, Chapter 6 presents the results of steady-state kinetic measurements on functionalized silicon electrodes in contact with solutions containing redox-active molecules.

Interfacial electron transfer and surface recombination are two of several charge-transport mechanisms that occur in semiconductor/liquid systems.^{10,11} Some of these processes are depicted in Figure 1.1 for the case of an n-type semiconductor in contact with a liquid containing an electroactive species. These processes include electron-hole recombination in the bulk of the semiconductor, electron-hole recombination in the depletion region, transfer of a conduction band electron to a redox-active acceptor in solution, tunneling of a conduction band electron through the semiconductor barrier, and electron-hole recombination at a surface trap. For a given semiconductor/liquid system, these processes occur simultaneously. A single pathway, however, usually dominates the net transport current, and that rate-determining process is determined by several factors such as the dopant density of the semiconductor, the position of the semiconductor band edges relative to the formal potential of the solution, the density of surface traps located within the band gap, and the concentrations of electrons and holes in the semiconductor bands. In the ensuing sections and in the theoretical work and computer simulations presented in Chapters 1 – 4, the rates of interfacial electron transfer and/or surface recombination are considered without regard to other concurrent processes. In experimental systems, however, observables such as steady-state currents and carrier decay profiles cannot be compared with theoretical formulations for a specific process unless the observables are shown to uniquely reflect the individual process of interest. For the experiments described in Chapters 5 and 6, these issues have been addressed and are discussed further in their respective chapters.

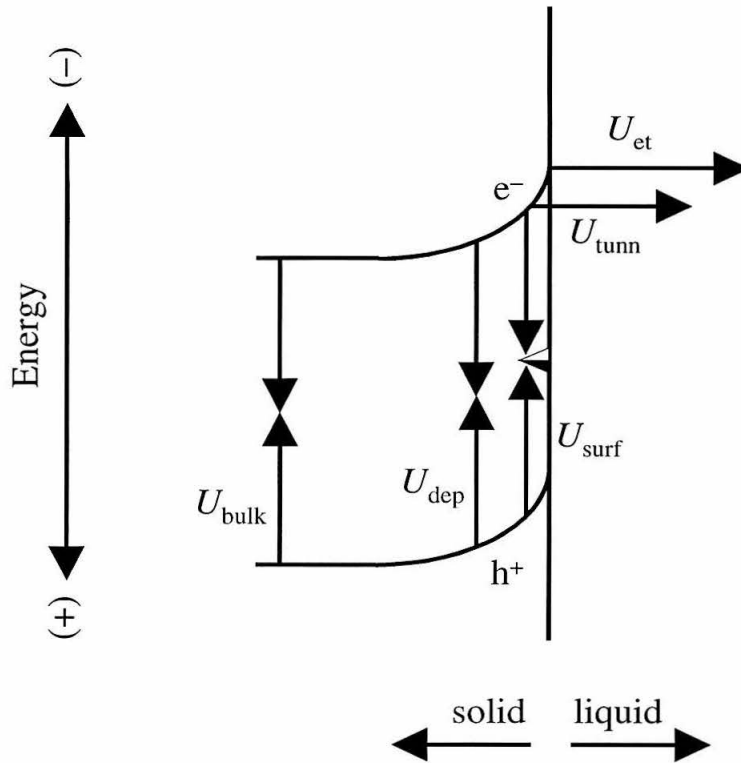


Figure 1.1: Recombination pathways for an n-type semiconductor/liquid junction in depletion conditions. The rates for processes such as bulk recombination (U_{bulk}), depletion region recombination (U_{dep}), and surface recombination (U_{surf}) are controlled by the concentration of minority carriers. The rates for other processes such as interfacial electron transfer (U_{et}) and electron tunneling (U_{tunn}) are controlled by majority carriers. Other recombination processes such as radiative recombination and Auger recombination (not shown) are also possible.

II. ELECTRON TRANSFER AT SEMICONDUCTOR/ LIQUID INTERFACES

Many theoretical and experimental aspects of electron transfer in molecular systems have been extensively developed.¹²⁻¹⁶ These processes are well understood in the context of Marcus theory, which relates the rate of an electron-transfer event to thermodynamic and electronic parameters of the reactants and products. The Marcus theory of electron transfer has also been extended to more complex systems such as DNA,¹⁷ porphyrins,¹⁸ and metal electrodes.¹⁹⁻²² For many years, additional efforts have been made to apply the Marcus formalism to interfacial charge-transfer reactions at semiconductor/liquid contacts.²³⁻³³

Unlike electron transfer at a metal/liquid interface which obeys a first-order rate law, the transfer of an electron in the conduction band of a semiconductor to an outer-sphere redox acceptor in solution is known to follow a second-order rate law given by:²⁷

$$\frac{-d[A]}{dt} = k_{sc}n_s[A] \quad (1.1)$$

where n_s is the concentration of surface electrons in the conduction band (in units of cm^{-3}), $[A]$ is the concentration of redox acceptors located near the surface of the solid (also in units of cm^{-3}), and k_{sc} is the electron-transfer rate constant. Since the right side of eq 1.1 must have units of a flux (i.e., $\text{cm}^{-2} \text{s}^{-1}$), the units of k_{sc} are, by definition, $\text{cm}^4 \text{s}^{-1}$. In the Marcus formalism, k_{sc} can be expressed as follows:

$$k_{sc} = \nu_n \kappa_{el} \exp\left(\frac{-(\Delta G^{o'} + \lambda)^2}{4\lambda k_b T}\right) \quad (1.2)$$

where ν_n is the nuclear vibration frequency, κ_{el} is the electronic factor that accounts for orbital interactions in the semiconductor/liquid system, $\Delta G^{o'}$ is the standard driving force for the interfacial electron-transfer process, λ is the total reorganization energy, k_b is the Boltzmann constant, and T is the temperature.

In the past decade, there has been significant controversy regarding the rate of

interfacial electron transfer at the semiconductor/liquid interface.^{24,25,27,29,30,34–38} At issue has been the magnitude of $k_{sc,max}$, which is the value of k_{sc} at optimal exoergicity (i.e., when $-\Delta G^{\circ} = \lambda$ in eq 1.2). While many robust experimental measurements have indicated that $k_{sc,max}$ is on the order of 10^{-17} – 10^{-16} $\text{cm}^4 \text{s}^{-1}$,^{24,25,27,29,30,39} other reports have suggested that, in certain cases, $k_{sc,max}$ can be as large as 10^{-12} – 10^{-10} $\text{cm}^4 \text{s}^{-1}$.^{34–36} If values of $k_{sc,max}$ this large could in fact be attained, the resulting rate of interfacial electron transfer would have dramatic implications for liquid-based solar energy conversion devices. At these rates, it would be possible for interfacial electron transfer to compete effectively with thermal relaxation in the conduction band of the semiconductor. Photoexcited electrons in a working photoelectrochemical cell could then, in principle, produce useful electrical work at higher thermodynamic energies thereby leading to significantly higher light-to-energy conversion efficiencies than previously expected. In many cases, however, recombination processes would also be much more rapid, dramatically limiting the efficiencies of such systems.

One seemingly plausible explanation that could account in part for the discrepancies observed in experimental measurements of $k_{sc,max}$ involves the influence of double-layer corrections. For measurements of interfacial rate constants at metal/liquid contacts, double-layer corrections are necessary to account for the partitioning of potential between the solid and liquid phases.⁴⁰ In the work described in Chapter 4, computer simulations have been performed to determine the magnitude of such corrections for semiconductor/liquid systems. The results from this study unequivocally demonstrate that such effects are extremely small for electron transfer at the semiconductor/liquid interface. Double-layer effects can therefore not account for the observed differences in measurements of $k_{sc,max}$.

Among all published experimental measurements of $k_{sc,max}$, one report is particularly compelling.²⁴ In this study, steady-state current-voltage and differential-capacitance measurements were used to characterize the interfacial charge-transfer

kinetics and energetics for n-Si in contact with a series of substituted viologens dissolved in methanol. Unlike earlier experiments, which only quantified $k_{\text{sc,max}}$ for individual semiconductor-redox couple systems, this investigation showed that the expected rate constant vs. driving force behavior, as described by Marcus theory (eq 1.2), was obeyed for an entire set of redox couples with different formal potentials. The reported value of $k_{\text{sc,max}}$ in this system was $6 \times 10^{-17} \text{ cm}^4 \text{ s}^{-1}$,²⁴ consistent with many earlier measurements of $k_{\text{sc,max}}$ in other semiconductor/liquid systems.

Although persuasive, the experimental result described above does not preclude the possibility of higher values of $k_{\text{sc,max}}$ in other systems. The work described in Chapter 2 was therefore undertaken to determine if values of $k_{\text{sc,max}} \approx 10^{-12}$ – $10^{-10} \text{ cm}^4 \text{ s}^{-1}$ are theoretically feasible. The approach taken in these studies was to develop a framework based on quantum-mechanical principles that relates interfacial electron-transfer rate constants for metal and semiconductor electrodes. The resulting model was then used to predict rate constants for semiconductor electrodes based on well-established experimental quantities of metal electrodes. The results from this theoretical approach are, in fact, remarkably consistent with the experimental measurements of $k_{\text{sc,max}} \approx 10^{-17}$ – $10^{-16} \text{ cm}^4 \text{ s}^{-1}$ and further suggest that significantly larger values of $k_{\text{sc,max}}$ are physically unrealistic. To date, it appears that the theoretical work described in Chapter 2, as well as its corresponding predictions, are gaining widespread acceptance in the photoelectrochemistry community.

III. SURFACE RECOMBINATION AT SEMICONDUCTOR/LIQUID INTERFACES

A statistical formalism describing charge-carrier recombination in semiconductors was developed over 50 years ago by Shockley and Read,⁴¹ and independently by Hall.⁴² The Shockley-Read-Hall treatment applies generally to all semiconductor recombination processes, and the theory has been verified in a large body of experimental work.¹⁰ In this section, the Shockley-Read-Hall formalism is used to derive an analytical expression for the rate of surface recombination in an n-type semiconductor.

For a given number density of recombination traps at the surface of a semiconductor, $N_{t,s}$, the net rate of surface recombination is given by the rate of carrier capture minus the rate of thermal emission out of the recombination centers (Figure 1.2). For electrons, this rate, $U_{n,s}$, is given by:

$$U_{n,s} = n_s N_{t,s} (1 - f_{t,s}) k_{n,s} - n_{1,s} N_{t,s} f_{t,s} k_{n,s} \quad (1.3)$$

where $f_{t,s}$ is the occupancy of surface traps and $k_{n,s}$ is the electron capture coefficient at the semiconductor surface. The term $n_{1,s}$, which describes the surface electron concentration when the Fermi level is located at the energy of the recombination center, is given by the following expression:

$$n_{1,s} = N_c \exp\left(\frac{\mathbf{E}_{c,s} - \mathbf{E}_{t,s}}{k_b T}\right) \quad (1.4)$$

Here, N_c is the density of electronic states in the conduction band, $\mathbf{E}_{c,s}$ is the energy of the conduction band edge at the semiconductor surface, and $\mathbf{E}_{t,s}$ is the energy of the recombination center. An expression analogous to eq 1.3 describes the net rate of hole recombination at the surface, $U_{p,s}$, as follows:

$$U_{p,s} = p_s N_{t,s} f_{t,s} k_{p,s} - p_{1,s} N_{t,s} (1 - f_{t,s}) k_{p,s} \quad (1.5)$$

where p_s is the surface concentration of holes in the valence band, $k_{p,s}$ is the hole capture

coefficient at the semiconductor surface, and $p_{1,s}$ is the surface hole concentration when the Fermi level is located at the energy of the recombination center, which is given by:

$$p_{1,s} = N_v \exp\left(\frac{\mathbf{E}_{t,s} - \mathbf{E}_{v,s}}{kT}\right) \quad (1.6)$$

In this expression, N_v is the density of electronic states in the valence band, and $\mathbf{E}_{v,s}$ is the energy of the valence band edge at the semiconductor surface.

Under steady state conditions, the net rates of electron and hole recombination are equal. Thus, setting eq 1.3 equal to eq 1.5 and eliminating $f_{t,s}$ yields the following:

$$U_s \equiv U_{n,s} = U_{p,s} = N_{t,s} \frac{k_{n,s}k_{p,s}(n_s p_s - n_{1,s} p_{1,s})}{k_{n,s}(n_s + n_{1,s}) + k_{p,s}(p_s + p_{1,s})} \quad (1.7)$$

In order to relate this expression to experimental data, it is convenient to rewrite the carrier concentrations in eq 1.7 explicitly as the sum of equilibrium ($n_{s,o}$ and $p_{s,o}$) and excess (Δn_s and Δp_s) carrier concentrations (for electrons and holes, respectively).

Substituting these terms into eq 1.7 and recognizing that $n_{1,s} p_{1,s}$ and $n_{s,o} p_{s,o}$ are equivalent (i.e., both yielding the square of the intrinsic carrier concentration at the surface) results in the following expression:

$$U_s = N_{t,s} \frac{k_{n,s}k_{p,s}(n_{s,o}\Delta p_s + p_{s,o}\Delta n_s + \Delta n_s\Delta p_s)}{k_{n,s}(n_{s,o} + \Delta n_s + n_{1,s}) + k_{p,s}(p_{s,o} + \Delta p_s + p_{1,s})} \quad (1.8)$$

Eq 1.8 thus represents the net rate of surface recombination for traps located at a single energy, $\mathbf{E}_{t,s}$. For a distribution of traps located at various energies, the right side of eq 1.8 must be integrated over all energies.

A key parameter commonly used to characterize surface recombination is the surface recombination velocity, S , which is defined as the rate of recombination divided by the excess minority carrier concentration (i.e., $S \equiv U_s/\Delta p_s$). From eq 1.8, S can be expressed as:

$$S = N_{t,s} \frac{k_{n,s}k_{p,s} [n_{s,o} + (p_{s,o} \Delta n_s / \Delta p_s) + \Delta n_s]}{k_{n,s}(n_{s,o} + \Delta n_s + n_{l,s}) + k_{p,s}(p_{s,o} + \Delta p_s + p_{l,s})} \quad (1.9)$$

The parameter S , which has units of cm s^{-1} , represents a pseudo-first-order rate constant for surface recombination, analogous to k_{sc} for interfacial electron transfer. Because S varies linearly with the concentration of both surface electrons and surface holes, the parameter depends on many variables such as illumination level, applied potential, and temperature. In practice, however, these variables can be controlled, allowing for quantitative extraction of the density of electrical surface traps.

Measured values for S typically range from 10^1 cm s^{-1} to 10^5 cm s^{-1} . For silicon surfaces with high-quality thermally grown oxide layers, S values as low as 3 cm s^{-1} have been reported.^{43,44} Such low values of S are typically desirable for device applications, and experimental efforts have therefore been largely directed at minimizing surface recombination using other surface treatments. The work described in Chapter 5 presents one such method for electrically passivating Si using a novel surface modification route that has been developed recently. In the context of the Shockley-Read-Hall treatment, the work in Chapter 5 also address shortcomings of other seemingly successful methods for electrically passivating silicon surfaces.

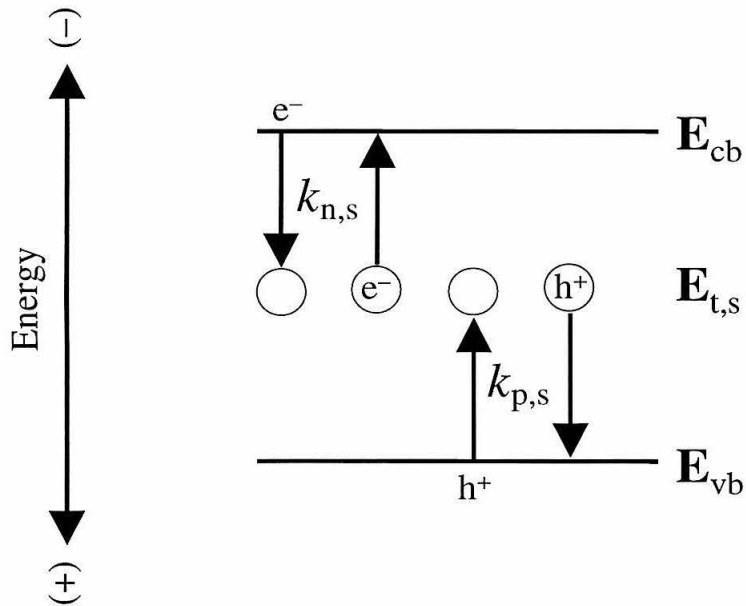


Figure 1.2: A schematic of capture and emission processes relevant to charge-carrier recombination at a semiconductor surface. By the principle of microscopic reversibility, the carrier capture coefficient and emission coefficient are equivalent for a given carrier type. The terms E_{cb} and E_{vb} are the conduction and valence band-edge energies, respectively. All other parameters are given in the text.

IV. SUMMARY

Charge-carrier processes at semiconductor/liquid interfaces play an important role in a number of applications. This thesis describes theoretical and experimental efforts aimed at elucidating the kinetics of interfacial electron transfer and surface recombination. The behavior of interfacial electron-transfer reactions are shown to be consistent with previous experimental measurements for both semiconductor/liquid and metal/liquid interfaces, as well as with classical Marcus formulations of electron transfer. In addition, the Shockley-Reed-Hall formalism has been used successfully to characterize surface-recombination behavior observed at a variety of silicon surfaces.

V. REFERENCES

1. Wrighton, M. S. *Acc. Chem. Res.* **1979**, *12*, 303.
2. Heller, A. *Acc. Chem. Res.* **1981**, *14*, 154.
3. Fonash, S. J. *Solar Cell Device Physics*; Academic: New York, 1981.
4. Lewis, N. S. *Acc. Chem. Res.* **1990**, *23*, 176.
5. Koval, C. A.; Howard, J. N. *Chem. Rev.* **1992**, *92*, 411.
6. Tan, M. X.; Laibinis, P. E.; Nguyen, S. T.; Kesselman, J. M.; Stanton, C. E.; Lewis, N. S. *Prog. Inorg. Chem.* **1994**, *41*, 21.
7. Nozik, A. J.; Memming, R. *J. Phys. Chem.* **1996**, *100*, 13061.
8. Lewis, N. S. *J. Phys. Chem. B* **1998**, *102*, 4843.
9. Wolf, S.; Tauber, R. N. *Silicon Processing for the VLSI Era*; Lattice Press: Sunset Beach, CA, 1986.
10. Sze, S. M. *The Physics of Semiconductor Devices*, 2nd ed.; Wiley: New York, 1981.
11. Lewis, N. S.; Rosenbluth, M. L. Theory of Semiconductor Materials. In *Photocatalysis: Fundamentals and Applications*; Serpone, N., Pelizzetti, E., Eds.; John Wiley & Sons: New York, 1989.
12. Marcus, R. A.; Sutin, N. *Biochim. Biophys. Acta.* **1985**, *811*, 265.
13. Barbara, P. F.; Meyer, T. J.; Ratner, M. A. *J. Phys. Chem.* **1996**, *100*, 13148.
14. Bowler, B. E.; Raphael, A. L.; Gray, H. B. *Prog. Inorg. Chem.* **1990**, *38*, 259.
15. Closs, G. L.; Miller, J. R. *Science* **1988**, *240*, 440.
16. Miller, J. R.; Calcaterra, L. T.; Closs, G. L. *J. Am. Chem. Soc.* **1984**, *106*, 3047.
17. Murphy, C. J.; Arkin, M. R.; Jenkins, Y.; Ghatila, N. D.; Bossmann, S. H.; Turro, N. J.; Barton, J. K. *Science* **1993**, *262*, 1025.
18. Gust, D.; Moore, T. A.; Moore, A. L.; Macpherson, A. N.; Lopez, A.; DeGraziano, J. M.; Gouni, I.; Bittersmann, E.; Seely, G. R.; Gao, F.; Nieman, R. A.; Ma, X. C.; Demanche, L. J.; Hung, S.; Luttrull, D. K.; Lee, S.; Kerrigan, P. K. *J. Am. Chem. Soc.* **1993**, *115*, 11141.
19. Smalley, J. F.; Feldberg, S. W.; Chidsey, C. E. D.; Linford, M. R.; Newton, M. D.; Liu, Y. P. *J. Phys. Chem.* **1995**, *99*, 13141.

20. Chidsey, C. E. D. *Science* **1991**, *251*, 919.
21. Finklea, H. O.; Hanshew, D. D. *J. Am. Chem. Soc.* **1992**, *114*, 3173.
22. Terrettaz, S.; Becka, A. M.; Traub, M. J.; Fettingner, J. C.; Miller, C. J. *J. Phys. Chem.* **1995**, 11216.
23. Gerischer, H.; Eyring, H. In *Physical Chemistry: An Advanced Treatise*; Yost, W., Ed.; Academic: New York, 1970; Vol. 9A.
24. Fajardo, A. M.; Lewis, N. S. *Science* **1996**, *274*, 969.
25. Fajardo, A. M.; Lewis, N. S. *J. Phys. Chem.* **1997**, *101*, 11136.
26. Gerischer, H. *J. Phys. Chem.* **1991**, *95*, 1356.
27. Lewis, N. S. *Annu. Rev. Phys. Chem.* **1991**, *42*, 543.
28. Marcus, R. A. *J. Phys. Chem.* **1991**, *95*, 2010.
29. Pomykal, K. E.; Fajardo, A. M.; Lewis, N. S. *J. Phys. Chem.* **1996**, *100*, 3652.
30. Pomykal, K. E.; Lewis, N. S. *J. Phys. Chem. B* **1997**, *101*, 2476.
31. Royea, W. J.; Fajardo, A. M.; Lewis, N. S. *J. Phys. Chem. B* **1997**, *101*, 11152.
32. Farzad, F.; Thompson, D. W.; Kelly, C. A.; Meyer, G. J. *J. Am. Chem. Soc.* **1999**, *121*, 5577.
33. Dang, X. J.; Hupp, J. T. *J. Am. Chem. Soc.* **1999**, *121*, 8399.
34. Rosenwaks, Y.; Thacker, B. R.; Ahrenkiel, R. K.; Nozik, A. J. *J. Phys. Chem.* **1992**, *96*, 10096.
35. Rosenwaks, Y.; Thacker, B. R.; Nozik, A. J.; Ellingson, R. J.; Burr, K. C.; Tang, C. L. *J. Phys. Chem.* **1994**, *98*, 2739.
36. Smith, B. B.; Halley, J. W.; Nozik, A. J. *Chem. Phys.* **1996**, *205*, 245.
37. Casagrande, L. G.; Juang, A.; Lewis, N. S. *J. Phys. Chem. B* **2000**, *104*, 5436.
38. Ellingson, R.; Meier, A.; Kocha, S.; Smith, B. B.; Rosenwaks, Y.; Halley, J. W.; Schelling, P.; Hanna, M.; Nozik, A. J. Third International Meeting on New Trends in Photoelectrochemistry, 1997, Estes Park, CO.
39. Horrocks, B. R.; Mirkin, M. V.; Bard, A. J. *J. Phys. Chem.* **1994**, *98*, 9106.
40. Bard, A. J.; Faulkner, L. R. *Electrochemical Methods: Fundamentals and Applications*; Wiley: New York, 1980.
41. Shockley, W.; Read, W. T. *Phys. Rev.* **1952**, *87*, 835.

42. Hall, R. N. *Phys. Rev.* **1952**, 87, 387.
43. Yablonovitch, E.; Gmitter, T. J. *Sol. St. Electron.* **1992**, 35, 261.
44. Eades, W. D.; Swanson, R. M. *J. Appl. Phys.* **1985**, 58, 4267.

Chapter 2

Fermi Golden Rule Approach to Evaluating Outer-Sphere Electron-Transfer Rate Constants at Semiconductor/Liquid Interfaces

I. INTRODUCTION

Rate constants for interfacial charge transfer at metallic and semiconducting electrodes have been the focus of several studies in recent years.¹⁻⁸ Measurements of rate constants at metallic electrodes have been possible due to the development of pinhole-free, insulating organic layers³ and the use of redox reagents incorporated into self-assembled monolayers,^{1,2,4,9} both of which allow for precise measurements of rate constant vs. distance relationships. In addition, the preparation of nearly defect-free semiconductor electrodes that obey the expected second-order rate law for interfacial charge transfer has permitted measurements of rate constants by straightforward experimental techniques.^{6-8,10,11} For both semiconducting and metallic electrodes, measurements of the dependence of the interfacial rate constant on the driving force for charge transfer are consistent with the predictions of electron-transfer theory with respect to the contribution of nuclear terms.^{1,2,4,7,8,12-14}

To date, a comparison between the absolute magnitude of the rate constants at metallic and semiconducting electrodes has been unavailable. Such a comparison is not straightforward, since the charge-transfer processes in these systems, as measured using common laboratory techniques, obey different rate laws.¹⁴ The purpose of this chapter is to present a framework that readily facilitates such a comparison on a common basis, specifically, the electronic coupling of the redox species to an electronic state of the electrode.

A brief review of the rate laws that describe charge-transfer processes at four types of interfaces is first presented. The rate-constant relationships for these four systems are then derived using a common theoretical framework. Finally, this framework is used to establish analytical formulas that allow comparison between these rate constants based on reference to readily measured observables. The four systems are (a) a metallic electrode with redox acceptor species located at a known, fixed distance from the electrode surface, (b) a metallic electrode with a random distribution of redox acceptors dissolved in the

solution phase, (c) a semiconducting electrode with redox acceptor species located at a known, fixed distance from the electrode surface, and (d) a semiconducting electrode with a random distribution of redox acceptors dissolved in the solution phase. Although the equations given herein have been derived for electron transfer from the electrode to the solution (cathodic current flow), analogous expressions are readily obtained for electron transfer from the solution to the electrode (anodic current flow).

II. BASIC KINETIC EQUATIONS FOR INTERFACIAL CHARGE-TRANSFER REACTIONS

For a metal electrode with redox acceptors located at a distance r from the electrode surface, the electron flux that defines the charge-transfer rate, $rate_m(r,E)$, at a specific electrode potential, E , is given by

$$rate_m(r,E) = k_m(r,E)C(r) \quad (2.1)$$

where $C(r)$ is the acceptor coverage, in cm^{-2} , that is present at a distance r from the electrode surface. The rate constant $k_m(r,E)$ has units of s^{-1} so that a flux is obtained from this rate expression. For a set of redox acceptors affixed to the electrode, eq 2.1 is a potential-dependent function that must be evaluated at the particular distance of interest.

In the case of a metal electrode with redox acceptors randomly distributed in solution, the rate expression is

$$rate_m(E) = k_m(E)[A] \quad (2.2)$$

where $[A]$ is the concentration, in cm^{-3} , of the redox species in the interfacial region, and $k_m(E)$ is the conventional charge-transfer rate constant at a metal electrode.¹⁵ The units of $k_m(E)$ are therefore $cm\ s^{-1}$.

For a semiconducting electrode with redox acceptors located at a distance r from the electrode surface, the appropriate expression is

$$rate_{sc}(r,E) = k_{sc}(r)n_s(E)C(r) \quad (2.3)$$

where $rate_{sc}(r,E)$ and $k_{sc}(r)$ are the rate (flux) and the distance-dependent interfacial rate constant, respectively. In this expression, the electron concentration at the surface of the semiconductor, $n_s(E)$, is explicitly written in the rate law. This occurs because, unlike at a metal electrode, the value of $n_s(E)$ for a semiconductor electrode is a quantity that can be varied experimentally.¹⁴⁻¹⁶ Since the observed flux is linearly proportional to the value of $n_s(E)$, the flux must be divided by $n_s(E)$ in order to obtain the rate constant for

this electrochemical process. As a result, the value of $k_{sc}(r)$ has units of $\text{cm}^3 \text{s}^{-1}$.

In the case of a semiconducting electrode with redox acceptors randomly distributed in solution, the rate expression is

$$rate_{sc}(E) = k_{sc}n_s(E)[A] \quad (2.4)$$

where $rate_{sc}(E)$ is the rate (flux) and k_{sc} is the interfacial rate constant. Following the same reasoning as above, k_{sc} has units of $\text{cm}^4 \text{s}^{-1}$ for charge transfer from a semiconductor electrode to a random distribution of redox acceptor species dissolved in solution.¹⁴

III. FUNDAMENTAL EXPRESSIONS FOR INTERFACIAL ELECTRON-TRANSFER RATE CONSTANTS

To unify the rate expressions for these four different systems, reference is made to a theoretical treatment, based on Fermi's golden rule, which describes the rate of a kinetic process in terms of fundamental, quantum-mechanical parameters.¹⁷⁻¹⁹ Specifically, Fermi's golden rule relates the rate of a state crossing to the electronic coupling matrix element for the process and to the Franck-Condon density of states for an isoenergetic electron-transfer event at each energy of concern. This approach is valid only for nonadiabatic electron-transfer events, and modifications will be introduced where appropriate to account for situations in which adiabatic effects arise.^{12,13,18,20}

A. Metallic Electrodes: Fixed-Distance Redox Species

For this scenario, basic equations, outlined by Levich²¹ and restated more recently by Chidsey and co-workers,^{1,4} that describe the situation in the classical Marcus limit of interfacial electron transfer are employed.¹⁷ In this formalism, the electron-transfer rate at a metal electrode as a function of r is given by

$$\text{rate}_m(r, E) = \frac{2\pi^{3/2}C(r)}{h(k_b T \lambda_m)^{1/2}} \int_{-\infty}^{\infty} \overline{H_{AB,m}^2(r, \mathbf{E})} \mathcal{F}(\mathbf{E}, E) \rho_{m,\text{eff}}(\mathbf{E}) \times \exp\left[-(\mathbf{E} - qE^{o'} + \lambda_m)^2 / 4\lambda_m k_b T\right] d\mathbf{E} \quad (2.5)$$

In this equation, h is Planck's constant, $\rho_{m,\text{eff}}(\mathbf{E})$ is the effective density of states in the metal (in units of states eV^{-1}) at the energy \mathbf{E} that couples in the charge-transfer event, k_b is Boltzmann's constant, T is the temperature, λ_m is the reorganization energy of the acceptor at the electrode surface, $\mathcal{F}(\mathbf{E}, E)$ is the Fermi occupancy function as a function of energy at the electrode potential E ,²² q is the charge of an electron, and $E^{o'}$ is the formal potential of the redox species.²³ The quantity $\overline{H_{AB,m}^2(r, \mathbf{E})}$ represents the square of the matrix element that couples reactant and product states at \mathbf{E} , averaged over all degenerate

states in the metal having an energy \mathbf{E} in a plane parallel to the solid/liquid interface. The value of $\overline{H_{AB,m}^2}(r, \mathbf{E})$ has units of $\text{eV}^2 \text{state}^{-1}$.

Assuming the effective density of states²⁴ and the matrix coupling elements¹ are independent of energy, eq 2.5 can be recast as follows:

$$\text{rate}_m(r, E) = \frac{2\pi^{3/2}C(r)}{h(k_bT\lambda_m)^{1/2}} \overline{H_{AB,m}^2}(r)\rho_{m,\text{eff}} \int_{-\infty}^{\infty} \mathcal{F}(\mathbf{E}, E) \times \exp\left[-(\mathbf{E} - qE^{o'} + \lambda_m)^2 / 4\lambda_m k_bT\right] d\mathbf{E} \quad (2.6)$$

The definite integral in eq 2.6 defines the energy range over which the charge-transfer process occurs and properly weights the rate constant at each energy according to the appropriate Franck-Condon density of states for the reaction (Figure 2.1). This density of states arises from the nuclear reorganization required by the reactants and products to achieve an isoenergetic electron-transfer event. If λ_m and E are known, then the value of the definite integral can be computed by numerical integration.

The only remaining quantity required to compute the rate constant is therefore the number of states eV^{-1} that participate in the charge-transfer process, $\rho_{m,\text{eff}}$. The density of states, D_m , is known for most metals from application of the Drude free-electron gas model.²⁴ Taking the electron concentration, N_m (in electrons cm^{-3}), at the Fermi level of the metal and dividing by the Fermi energy, \mathbf{E}_f , yields

$$D_m = \frac{3}{2} \left(\frac{N_m(\mathbf{E}_f)}{\mathbf{E}_f} \right) \quad (2.7)$$

Here D_m is assumed to be approximately independent of energy.²⁴ The number of states per atom per eV in the metal, ρ_m , can then be obtained by dividing D_m by the atomic density of the solid, d_m . For gold, $\rho_m = 0.27 \text{ states atom}^{-1} \text{ eV}^{-1}$.

Of these states, however, only a certain fraction will be effective in facilitating the interfacial charge-transfer event. This fraction is l_m/δ_m , where l_m (in cm) is the effective coupling length of the redox acceptor wave function into the metal and δ_m is the average

diameter of an atom in the metal lattice (in units of cm atom^{-1}). Thus, the effective density of states for the charge-transfer process is

$$\rho_{\text{m,eff}} = \rho_{\text{m}} \left(\frac{l_{\text{m}}}{\delta_{\text{m}}} \right) \approx \frac{D_{\text{m}} l_{\text{m}}}{d_{\text{m}}^{2/3} (6/\pi)^{1/3}} \quad (2.8)$$

Assuming an effective coupling length, l_{m} , taken by Chidsey to be 1×10^{-8} cm into the electrode,¹ therefore allows calculation of the total number of effective states eV^{-1} that participate in the charge-transfer process. With $l_{\text{m}} \approx 3 \times 10^{-8}$ cm, approximately one atom is effective in the coupling process, yielding a total effective density of states of approximately 0.27 states eV^{-1} .

Since the rate is measured as a flux of charge through the electrode surface, comparison of the rate law of eq 2.1 and the rate expression of eq 2.6 shows that

$$k_{\text{m}}(r, E) = \frac{2\pi^{3/2}}{h(k_{\text{b}}T\lambda_{\text{m}})^{1/2}} \overline{H_{\text{AB,m}}^2(r)} \rho_{\text{m,eff}} I(\lambda_{\text{m}}, E) \quad (2.9)$$

where $I(\lambda_{\text{m}}, E)$ is the definite integral in eq 2.6. For a redox species located at a specific, fixed distance r_{A} from the electrode, the rate constant, $k_{\text{m},r_{\text{A}}}(E)$, is given by

$$k_{\text{m},r_{\text{A}}}(E) = \frac{2\pi^{3/2}}{h(k_{\text{b}}T\lambda_{\text{m}})^{1/2}} \overline{H_{\text{AB,m},r_{\text{A}}}^2} \rho_{\text{m,eff}} I(\lambda_{\text{m}}, E) \quad (2.10)$$

where $\overline{H_{\text{AB,m},r_{\text{A}}}^2}$ is the value of $\overline{H_{\text{AB,m}}^2(r)}$ at $r = r_{\text{A}}$. Measurement of the rate constant $k_{\text{m},r_{\text{A}}}(E)$ thus allows calculation of the coupling per state from eq 2.10, assuming that the reorganization energy is known or has been determined experimentally for the process of concern.

B. Metallic Electrodes: Random Distribution of Dissolved Redox Species

Equation 2.2 serves as the basis for an expression to obtain the rate constant, $k_{\text{m}}(E)$, that describes charge transfer from a metal electrode to a random distribution of dissolved

redox species. In its simplest form, the nuclear coupling terms are taken to be independent of distance (see refs 4, 25, and 26 for restrictions on this approximation), and the electronic coupling in the nonadiabatic regime decays approximately exponentially with distance from the electrode.^{4,18,27} Thus, the expected rate expression is

$$rate_m(E) = \frac{2\pi^{3/2}[A]}{h(k_b T \lambda_m)^{1/2}} \int_{r_0}^{\infty} \int_{-\infty}^{\infty} \overline{H_{AB,m}^{\circ 2}(\mathbf{E})} \exp[-\beta_m(r - r_0)] \mathcal{F}(\mathbf{E}, E) \times \rho_{m,eff}(\mathbf{E}) \exp\left[-(\mathbf{E} - qE^{o'} + \lambda_m)^2 / 4\lambda_m k_b T\right] d\mathbf{E} dr \quad (2.11)$$

where $\overline{H_{AB,m}^{\circ 2}(\mathbf{E})}$ is the square of the electronic coupling matrix element observed at r_0 , the distance of closest approach of the redox species to the electrode surface, averaged over all degenerate states at each \mathbf{E} and averaged over the plane that lies parallel to the electrode surface, and β_m is the coupling attenuation factor. If $\rho_{m,eff}(\mathbf{E})$ and $\overline{H_{AB,m}^{\circ 2}(\mathbf{E})}$ are taken to be independent of energy, eq 2.11 reduces to

$$rate_m(E) = \frac{2\pi^{3/2}[A]}{h(k_b T \lambda_m)^{1/2}} \overline{H_{AB,m}^{\circ 2}} \beta_m^{-1} \rho_{m,eff} I(\lambda_m, E) \quad (2.12)$$

where $\overline{H_{AB,m}^{\circ 2}}$ is the square of the electronic coupling matrix at r_0 , averaged over all degenerate states in a plane parallel to the solid/liquid contact for each \mathbf{E} . Comparison of this expression with eq 2.2 indicates that the rate constant for this process is

$$k_m(E) = \frac{2\pi^{3/2}}{h(k_b T \lambda_m)^{1/2}} \overline{H_{AB,m}^{\circ 2}} \beta_m^{-1} \rho_{m,eff} I(\lambda_m, E) \quad (2.13)$$

Another approach to determining the electronic coupling to a random distribution of redox acceptors is to perform a series of kinetic measurements on electrodes having blocking layers of different thicknesses.³ Extrapolation to zero thickness of the blocking layer then allows determination of the electronic coupling matrix element that would be present with no barrier layer present.

C. Semiconducting Electrodes: Fixed-Distance Redox Species

The same formalisms can be used to obtain an expression for the rate constant at a semiconducting electrode. For acceptor ions located at any distance r from the electrode surface, the fundamental integral that relates the electronic coupling to the observed rate is exactly the same as that given in eq 2.5:

$$rate_{sc}(r, E) = \frac{2\pi^{3/2}C(r)l_{sc}}{h(k_b T \lambda_{sc})^{1/2} d_{sc}^{2/3} (6/\pi)^{1/3}} \int_{-\infty}^{\infty} \overline{H_{AB,sc}^2}(r, \mathbf{E}) \mathcal{F}(\mathbf{E}, E) \times D_{sc}(\mathbf{E}) \exp\left[-(\mathbf{E} - qE^{o'} + \lambda_{sc})^2 / 4\lambda_{sc}k_b T\right] d\mathbf{E} \quad (2.14)$$

where the subscripts sc denote the appropriate values of quantities for the semiconductor electrode and a relationship analogous to that of eq 2.8 has been used to express the effective density of states that couples in the charge-transfer event.

A significant difference between a semiconducting and a metallic electrode is in the form of the density of states, $D_{sc}(\mathbf{E})$, and in the occupancy of these states at room temperature. For a semiconductor, electron transfer occurs only through a narrow distribution of energies near the bottom of the conduction band edge at the semiconductor/liquid interface (Figure 2.2). Thus, the nuclear terms are essentially constant over the region where the integrand in eq 2.14 is non-negligible, and one obtains

$$rate_{sc}(r, E) = \frac{2\pi^{3/2}C(r)l_{sc}}{h(k_b T \lambda_{sc})^{1/2} d_{sc}^{2/3} (6/\pi)^{1/3}} \exp\left[-(\mathbf{E}_{cb} - qE^{o'} + \lambda_{sc})^2 / 4\lambda_{sc}k_b T\right] \times \overline{H_{AB,sc}^2}(r) \int_{-\infty}^{\mathbf{E}_{cb}} \mathcal{F}(\mathbf{E}, E) D_{sc}(\mathbf{E}) d\mathbf{E} \quad (2.15)$$

where \mathbf{E}_{cb} represents the energy of the conduction band edge at the surface of the semiconductor. In eq 2.15, the electronic coupling represented by $\overline{H_{AB,sc}^2}(r)$ has been averaged over all degenerate states at \mathbf{E} in a plane parallel to the electrode surface and has been assumed to be independent of energy over the range of interest, as was done for the situation at a metallic electrode in eqs 2.6 and 2.12.

The integral in eq 2.15 equals the effective density of states in the conduction band of the semiconductor, N_c (in units of states cm^{-3}), multiplied by the value of the Fermi function evaluated at the potential of interest.^{28–30} For a non-degenerately doped semiconductor, Boltzmann statistics can be used to describe accurately the value of the Fermi function for a semiconductor electrode under depletion conditions, and the integral in eq 2.15 reduces to^{28–30}

$$\int_{-\infty}^{\mathbf{E}_{\text{cb}}} \mathcal{F}(\mathbf{E}, E) D_{\text{sc}}(\mathbf{E}) d\mathbf{E} = N_c \exp\left[\left(\mathbf{E}_{\text{cb}} - qE(A/A^-) - qE\right)/k_b T\right] \equiv n_s(E) \quad (2.16)$$

This definition is thermodynamically rigorous at equilibrium, i.e., for $E = E(A/A^-) = \mathbf{E}_f/q$. As long as a Boltzmann-type relationship holds between the electron concentration at the surface of the solid and its value in the bulk, the definition in eq 2.16 is valid for any electrode potential E . Substituting eq 2.16 into eq 2.15 therefore yields

$$\text{rate}_{\text{sc}}(r, E) = \frac{2\pi^{3/2} C(r) l_{\text{sc}}}{h (k_b T \lambda_{\text{sc}})^{1/2} d_{\text{sc}}^{2/3} (6/\pi)^{1/3}} \exp\left[-\left(\mathbf{E}_{\text{cb}} - qE^{o'} + \lambda_{\text{sc}}\right)^2 / 4\lambda_{\text{sc}} k_b T\right] \times \frac{1}{\overline{H_{\text{AB,sc}}^2}(r) n_s(\mathbf{E})} \quad (2.17)$$

The rate at optimal exoergicity occurs when $qE^{o'} - \mathbf{E}_{\text{cb}} = \lambda_{\text{sc}}$. Comparing the rate expression of eq 2.17 when $qE^{o'} - E_{\text{cb}} = \lambda_{\text{sc}}$ with the rate law of eq 2.3, the rate constant at optimal exoergicity, $k_{\text{sc,max}}(r)$, is

$$k_{\text{sc,max}}(r) = \frac{2\pi^{3/2} l_{\text{sc}}}{h (k_b T \lambda_{\text{sc}})^{1/2} d_{\text{sc}}^{2/3} (6/\pi)^{1/3}} \overline{H_{\text{AB,sc}}^2}(r) \quad (2.18)$$

D. Semiconducting Electrodes: Random Distribution of Dissolved Redox Acceptors

In the case of a semiconductor electrode in contact with a random distribution of redox species dissolved in solution, the rate expression is identical to that given in eq 2.11:

$$rate_{sc}(E) = \frac{2\pi^{3/2}l_{sc}[A]}{h(k_bT\lambda_{sc})^{1/2}d_{sc}^{2/3}(6/\pi)^{1/3}} \int_{r_0}^{\infty} \int_{-\infty}^{\infty} \overline{H_{AB,sc}^2(\mathbf{E})} \exp[-\beta_{sc}(r-r_0)] \times \mathcal{F}(\mathbf{E}, E) D_{sc,eff}(\mathbf{E}) \exp\left[-(\mathbf{E} - qE^{o'} + \lambda_{sc})^2 / 4\lambda_{sc}k_bT\right] d\mathbf{E}dr \quad (2.19)$$

where the subscript sc again denotes the parameters for a semiconductor electrode.

Applying the same treatment as above to remove the nuclear terms from the integral, analytically evaluating the remaining terms of the integral with respect to distance, and substituting eq 2.16 into eq 2.19 results in the following expression:

$$rate_{sc}(E) = \frac{2\pi^{3/2}l_{sc}[A]}{h(k_bT\lambda_{sc})^{1/2}d_{sc}^{2/3}(6/\pi)^{1/3}} \exp\left[-(\mathbf{E}_{cb} - qE^{o'} + \lambda_{sc})^2 / 4\lambda_{sc}k_bT\right] \frac{\overline{H_{AB,sc}^2} \beta_{sc}^{-1} n_s(\mathbf{E})}{\overline{H_{AB,sc}^2} \beta_{sc}^{-1} n_s(\mathbf{E})} \quad (2.20)$$

where $\overline{H_{AB,sc}^2}$ has again been assumed to be independent of energy.

The rate constant at optimal exoergicity is thus readily obtained by relating the rate expressions of eqs 2.4 and 2.20 when $qE^{o'} - \mathbf{E}_{cb} = \lambda_{sc}$:

$$k_{sc,max} = \frac{2\pi^{3/2}l_{sc}}{h(k_bT\lambda_{sc})^{1/2}d_{sc}^{2/3}(6/\pi)^{1/3}} \overline{H_{AB,sc}^2} \beta_{sc}^{-1} \quad (2.21)$$

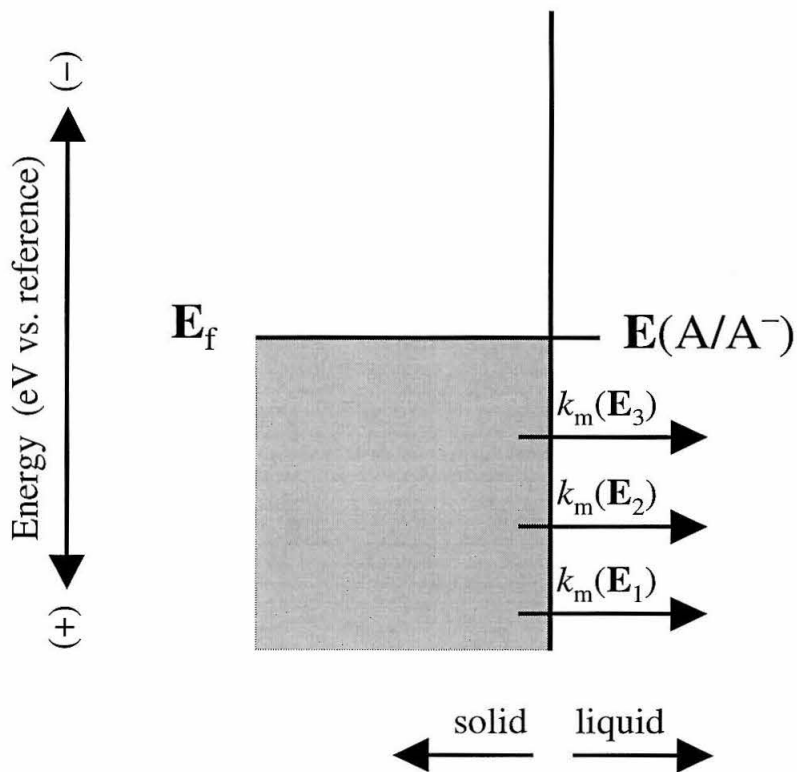


Figure 2.1: An energy diagram for a metal/liquid interface. The quantity $E(A/A^-)$ is the electrochemical potential of the solution, $k_m(E_n)$ is the charge-transfer rate constant at energy E_n , and E_f is the Fermi level of the electrode. The shaded region represents the occupied states in the metal.

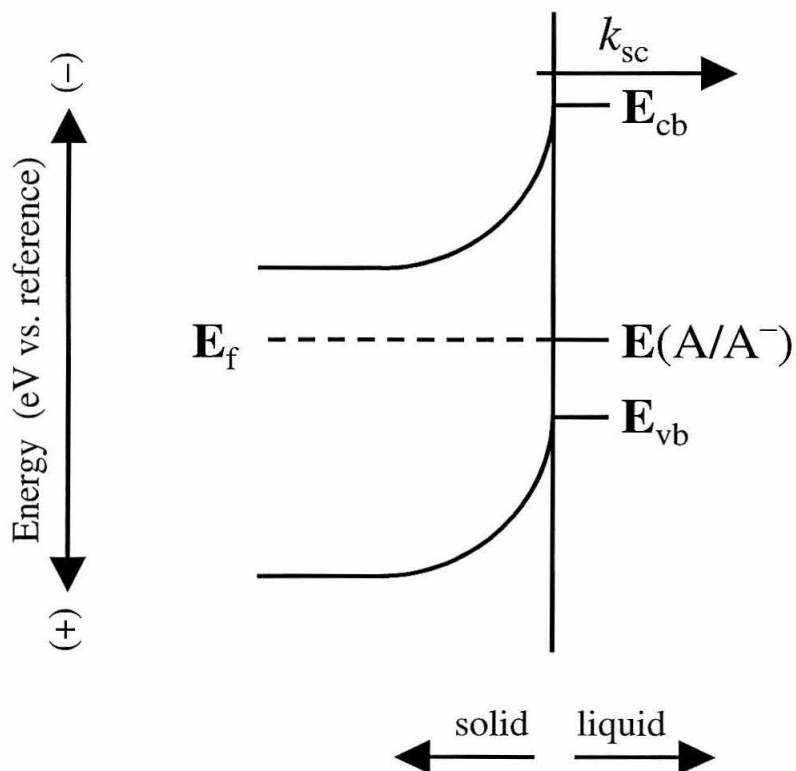


Figure 2.2: An energy diagram for a semiconductor/liquid interface. The energy of the conduction band at the surface of the semiconductor is given by E_{cb} , the energy of the valence band at the surface of the semiconductor is given by E_{vb} , and the rate constant at energies $E \approx E_{cb}$ is k_{sc} .

IV. RELATIONSHIPS BETWEEN RATE CONSTANTS FOR METAL AND SEMICONDUCTOR ELECTRODES

A. Fixed-Distance Redox Acceptors

From eqs 2.8, 2.9, and 2.18, the following expression for the rate constant ratio between $k_{\text{sc,max}}(r)$ and $k_{\text{m}}(r,E)$ is obtained:

$$\frac{k_{\text{sc,max}}(r)}{k_{\text{m}}(r,E)} = D_{\text{m}}^{-1} \frac{\overline{H_{\text{AB,sc}}^2}(r)}{\overline{H_{\text{AB,m}}^2}(r)} \left(\frac{l_{\text{sc}}}{l_{\text{m}}} \right) \left(\frac{d_{\text{m}}}{d_{\text{sc}}} \right)^{2/3} \left(\frac{\lambda_{\text{m}}}{\lambda_{\text{sc}}} \right)^{1/2} I^{-1}(\lambda_{\text{m}}, E) \quad (2.22)$$

The two kinetic quantities $k_{\text{m}}(r,E)$ and $k_{\text{sc,max}}(r)$ can be related experimentally if D_{m} is known and if the numerical value of the definite integral, I , in eq 2.6 can be determined for the specific situation of concern. Under these conditions, assuming that the average coupling per state is the same for a metal and a semiconductor electrode (i.e., $\overline{H_{\text{AB,m}}^2}(r) = \overline{H_{\text{AB,sc}}^2}(r)$), that the penetration length of the acceptor wave function into the solid is the same for a metal and a semiconductor electrode (i.e., $l_{\text{m}} = l_{\text{sc}}$), and that the ratio of the reorganization energies at each interface is unity, one obtains³¹

$$k_{\text{sc,max}}(r) = k_{\text{m}}(r,E) D_{\text{m}}^{-1} \left(\frac{d_{\text{m}}}{d_{\text{sc}}} \right)^{2/3} I^{-1}(\lambda_{\text{m}}, E) \quad (2.23)$$

Evaluation of eq 2.23 at a particular distance therefore results in the desired relationship for the case of fixed-distance redox acceptors.

B. Random Distribution of Redox Acceptors

A similar analysis, but including the integration of the electronic coupling over distance, and assuming the ratio of β_{m} to β_{sc} is unity, allows one to relate the rate constants at metal (eq 2.13) and semiconductor (eq 2.21) electrodes for a random distribution of acceptor species. In the nonadiabatic limit

$$\frac{k_{\text{sc,max}}}{k_{\text{m}}(E)} = D_{\text{m}}^{-1} \frac{\overline{H_{\text{AB,sc}}^2}}{H_{\text{AB,m}}^2} \left(\frac{\beta_{\text{m}}}{\beta_{\text{sc}}} \right) \left(\frac{l_{\text{sc}}}{l_{\text{m}}} \right) \left(\frac{d_{\text{m}}}{d_{\text{sc}}} \right)^{2/3} \left(\frac{\lambda_{\text{m}}}{\lambda_{\text{sc}}} \right)^{1/2} I^{-1}(\lambda_{\text{m}}, E) \quad (2.24)$$

In this case, assumptions analogous to those that led to eq 2.23 yield

$$k_{\text{sc,max}} = k_{\text{m}}(E) D_{\text{m}}^{-1} \left(\frac{d_{\text{m}}}{d_{\text{sc}}} \right)^{2/3} I^{-1}(\lambda_{\text{m}}, E) \quad (2.25)$$

A simple, first-order approach to account for adiabaticity is to use eq 2.23 at each distance to relate $k_{\text{sc,max}}(r)$ to $k_{\text{m}}(r, E)$, with the constraint that $k_{\text{m}}(r, E) < k_{\text{m,ad}}$, where $k_{\text{m,ad}}$ is the maximum rate constant for charge transfer in the adiabatic limit.^{20,32} Typically $k_{\text{m,ad}} = 10^{13} \text{ s}^{-1}$ in polar solvents,¹⁷ which is the value that will be used herein. The integration over distance must then be performed numerically in order to obtain a value for $k_{\text{sc,max}}$:

$$k_{\text{sc,max}} = \left[\int_{r_0}^{\infty} k'_{\text{m}}(r, E) dr \right] D_{\text{m}}^{-1} \left(\frac{d_{\text{m}}}{d_{\text{sc}}} \right)^{2/3} I^{-1}(\lambda_{\text{m}}, E) \quad (2.26)$$

where

$$k'_{\text{m}}(r, E) \equiv \begin{cases} k_{\text{m,ad}} & \text{for } k_{\text{m}}(r, E) > k_{\text{m,ad}} \\ k_{\text{m}}(r, E) & \text{for } k_{\text{m}}(r, E) \leq k_{\text{m,ad}} \end{cases} \quad (2.27)$$

C. Relation Between Fixed-Distance Measurements at Metal Electrodes and Rate Constant Data for Randomly Dissolved Acceptors at Semiconductor Electrodes

The relationship between the rate constant $k_{\text{sc,max}}$ obtained for a random distribution of acceptor species at a semiconductor electrode and the distance-dependent measurements of $k_{\text{m}}(r, E)$ for species immobilized on a metal electrode can also be derived from the fundamental rate equations given above. If the value of $k_{\text{m}}(r, E)$ is known at a distance $r = r_{\text{A}}$, and β_{m} is known from experiment, then in the nonadiabatic limit, $k_{\text{m}}(E)$ can be determined from the following:

$$k_m(E) = k_{m,r_A}(E) \beta_m^{-1} \exp(\beta_m r_A) \quad (2.28)$$

Then, substituting eq 2.28 into eq 2.25, one obtains

$$k_{sc,max} = k_{m,r_A}(E) \beta_m^{-1} \exp(\beta_m r_A) D_m^{-1} \left(\frac{d_m}{d_{sc}} \right)^{2/3} I^{-1}(\lambda_m, E) \quad (2.29)$$

To incorporate adiabatic effects, the integral must be computed numerically using eqs 2.26 and 2.27.

D. Relation Between Measurements Through Insulating Layers at Metal Electrodes and Rate Constant Data for Randomly Dissolved Acceptors at Semiconductor Electrodes

The formalism presented above can also be used to relate $k_{sc,max}$ to a rate constant for charge transfer through a blocking layer on a metal electrode to a random distribution of acceptor species. If the thickness of the blocking layer is r_b , the attenuation coefficient through the blocking layer is $\beta_{m,b}$, and the potential-dependent rate constant observed for the metal electrode at this thickness is $k_{m,r_b}(E)$, then in the nonadiabatic limit, extrapolation to zero thickness of the blocking layer yields $k_m(E)$:

$$k_m(E) = k_{m,r_b}(E) \exp(\beta_{m,b} r_b) \quad (2.30)$$

Again using eq 2.24, and assuming $\beta_{m,b}$ has been determined experimentally, one can determine $k_{sc,max}$:

$$k_{sc,max} = k_{m,r_b}(E) \exp(\beta_{m,b} r_b) D_m^{-1} \left(\frac{d_m}{d_{sc}} \right)^{2/3} I^{-1}(\lambda_m, E) \quad (2.31)$$

V. ANALYSIS OF EXPERIMENTAL DATA

The equations presented above can be used to compare the experimental results of various electrode systems in terms of the values of their electronic coupling. In addition, the equations can be used to relate the rate constant measured at a metallic electrode to the rate constant that would be measured for the same redox species at a semiconducting electrode, within the constraints of the assumptions described above. In this section, such comparisons are performed for various electrochemical systems of current interest.

Potential-step experiments using Au electrodes modified with ferrocene-terminated alkanethiols $[(\eta^5\text{-C}_5\text{H}_5)\text{Fe}(\eta^5\text{-C}_5\text{H}_4)\text{CO}_2(\text{CH}_2)_{16}\text{SH}]$ have provided data that are especially suitable for such an analysis.¹ In this system, an interfacial charge-transfer rate constant, $k_{m,rA}(E)$, of 6000 s^{-1} was observed at an overpotential of -0.68 V . A fit to the kinetic data at several values of the overpotential yielded a reorganization energy of 0.85 eV . Numerical integration at $\lambda_m = 0.85\text{ eV}$ and $E - E^{o'} = -0.68\text{ V}$ results in a value of $I(\lambda_m, E) = 0.112\text{ eV}$. Assuming a value of $\beta_m = 1.11$ per CH_2 unit,⁴ and 19 effective methylene units linking the redox species to the metal surface, the value of $k_m(E)/I(\lambda_m, E)$ can be established from eq 2.28 as $7.3 \times 10^5\text{ cm eV}^{-1}\text{ s}^{-1}$. Use of eq 2.29 yields a predicted value of $k_{sc,max} = 5.1 \times 10^{-17}\text{ cm}^4\text{ s}^{-1}$ for this system.

A similar system, employing thiols terminated with pentaamine(pyridine)ruthenium $[(\text{HS}(\text{CH}_2)_{15}\text{CONHCH}_2(\text{py}))\text{Ru}(\text{NH}_3)_5]^{2+}$,² has yielded values of $k_{m,rA}(E) = 202\text{ s}^{-1}$ at an overpotential of -0.37 V . Under these conditions, $I(\lambda_m, E) = 0.0439\text{ eV}$ for the experimentally determined values of $\lambda = 0.6\text{ eV}$ and $E - E^{o'} = -0.37\text{ V}$. Applying the measured value of $\beta_m = 0.98\text{ \AA}^{-1}$ for this system, and assuming that the electroactive group is separated from the electrode by 19 effective methylene units² (24 \AA), $k_m(E)/I(\lambda_m, E)$ and $k_{sc,max}$ are computed to be $7.7 \times 10^5\text{ cm eV}^{-1}\text{ s}^{-1}$ and $5.4 \times 10^{-17}\text{ cm}^4\text{ s}^{-1}$, respectively. Adiabatic effects were not considered in either of the two systems described above, since the computed values of $k_{m,rA}(E)$ never exceeded $k_{m,ad}$, even at $r = r_o$.

Experimental rate constants for randomly dissolved species at metal electrodes coated with a blocking layer, $k_{m,rb}(E)$, can also be related to $k_{sc,max}$ for semiconductor electrodes. In this situation, use of eq 2.31 is required. Terrettaz et al. have published voltammetric data for the reaction of freely diffusing $[\text{Fe}(2,2'\text{-bipyridine})_2(\text{CN})_2]^+$ on insulated Au electrodes. These data have yielded excellent agreement with the predicted dependence of $k_{m,rb}(E)$ on E (eq 2.12). Specifically, a value of $k_{m,rb}(E) = 7.8 \times 10^{-3} \text{ cm s}^{-1}$ has been reported at an applied bias of $-0.73 E$ vs. $E^{o'}$, and a fit of the entire data set yielded a value of $\lambda = 0.79 \text{ eV}$ for this redox couple at Au electrodes.³ With these values of $E - E^{o'}$ and λ , the definite integral $I(\lambda_m, E)$ can be evaluated numerically to be 0.195 eV. Extrapolation of $k_{m,rb}(E)$ to zero thickness of the blocking layer can be performed with the experimentally observed $\beta_{m,b}$ of 1.08 per methylene unit and assuming a 16-methylene-unit barrier length. This yields an expected value of $k_m(E)/I(\lambda_m, E) = 1.3 \times 10^6 \text{ cm eV}^{-1} \text{ s}^{-1}$ for the reaction of $[\text{Fe}(2,2'\text{-bipyridine})_2(\text{CN})_2]^+$ at an unmodified Au electrode. Use of eq 2.31 thus predicts $k_{sc,max} = 8.9 \times 10^{-17} \text{ cm}^4 \text{ s}^{-1}$ for this system.

VI. DISCUSSION

The calculations presented above indicate that experimental data support previous estimates, based on various semiclassical and statistical mechanical models, that $k_{sc,max}$ for charge transfer from a semiconductor electrode to a randomly distributed, non-adsorbing, outer-sphere redox species should be approximately 10^{-17} – 10^{-16} $\text{cm}^4 \text{s}^{-1}$.^{14,33} This value is in accord with recent experimental data for InP/liquid and Si/liquid contacts.^{6–8} Moreover, this value for $k_{sc,max}$ is consistent with the upper bounds set on the charge-transfer rate constant from earlier kinetic studies of n-GaAs/CH₃CN-ferrocene⁺⁰ interfaces.⁵

It is interesting to note that theory and experimental data comparing the behavior of semiconductor and metal electrodes appear to agree very closely even though a number of approximations have been made in the theoretical analysis of this work. The electronic coupling between redox acceptors and atoms in either the semiconductor or the metal electrode has been assumed to be constant in eq 2.23, even though this is most certainly only a rough approximation of the true physical situation. Similarly, the classical limit of the Marcus expression has been used in this work, as opposed to the full quantum-mechanical treatment of electron-transfer events.^{19,34} This limit seems to be an appropriate description of the experimental data available to date for charge transfer at metal/liquid interfaces,^{1,4} but more refined models would explicitly incorporate quantum modes of the electron-transfer events into treatments that describe charge transfer at both semiconductor and metal electrode systems.^{19,34} Additionally, the Drude model has been used in the present work to provide an estimate of the density of states in the metal electrode, but more refined models would use band structure calculations and photoemission data to obtain more accurate values of ρ_m (and the energy dependence of ρ_m) for the specific metals used in the comparison with semiconductor electrodes. Similarly, the present level of analysis ignores the constraint of momentum conservation on the electron-transfer process. To date, such a level of detail has not been used to

analyze the experimental data obtained on metal electrodes^{1,4} and thus has not been used in the present comparison, although it would be included in a more complete theoretical treatment of both systems. Finally, the comparisons between rate constants for charge transfer to random distributions of acceptors at metal and semiconductor electrodes implicitly assume similar dependencies of the solvent reorganization energy on the distance between the electrode and the acceptor in both types of solid/liquid contacts. Despite these approximations, the order-of-magnitude estimates of $k_{sc,max}$ obtained from the current level of theoretical treatment seem to be in excellent accord with the experimental data available at present on these electrode systems.

Nozik and co-workers have proposed that rate constants at semiconductor electrodes can possibly have values of 10^{-12} – 10^{-10} $\text{cm}^4 \text{ s}^{-1}$,^{35–39} although no robust experimental data to support such large rate-constant values are currently available in the literature.⁴⁰ The expressions presented above allow an evaluation of the electronic coupling that would be required in order to produce such a value of $k_{sc,max}$.

Figure 2.3 plots the value of $k'_m(r, E)$ calculated from eqs 2.9 and 2.27 as a function of $r - r_o$ for various values of the electronic coupling at contact, $\overline{H_{AB,m}^2}$, and $l_{sc} = 3 \times 10^{-8}$ cm. The corresponding values of $k_{sc,max}$, calculated using eq 2.26, are given in Table 2.1. Figure 2.4 plots the value of $k'_m(r, E)$ as a function of $r - r_o$ for various values of β_m , and Table 2.2 lists the corresponding values of $k_{sc,max}$.

In the nonadiabatic limit, the rate constant at each distance, and therefore the value of $k_{sc,max}$, increases linearly with the square of the electronic coupling per unit energy to the electrode. According to eq 2.26 with $l_{sc} = 3 \times 10^{-8}$ cm, this behavior occurs up to $k_{sc,max} = 10^{-16}$ $\text{cm}^4 \text{ s}^{-1}$. At this point, the electronic coupling matrix element at contact, i.e., at $r = r_o$, is at, or is very close to, the adiabatic limit at room temperature. This is also the situation observed experimentally for coupling between Au surfaces and a variety of redox species,^{1,4} indicating that, to first order, the behavior of semiconducting electrodes can be understood quantitatively using the same framework that has been

developed to describe charge transfer in metallic electrode systems. The value for $k_{sc,max} = 10^{-17}$ – 10^{-16} cm⁴ s⁻¹ thus not only agrees with the theoretical expectations for a semiconducting electrode system that has a nearly adiabatic coupling at contact and a coupling attenuation factor similar in magnitude to that measured at metallic electrodes (eqs 2.26 and 2.27) but also agrees with the experimental behavior of such systems ($k_{sc,max}$ for Si/CH₃OH = 6×10^{-17} cm⁴ s⁻¹; $k_{sc,max}$ for n-InP/CH₃OH = 3×10^{-16} cm⁴ s⁻¹)⁶⁻⁸ in satisfying detail.

Inspection of Tables 2.1 and 2.2 also reveals that the value of $k_{sc,max}$ is close to 10^{-16} – 10^{-17} cm⁴ s⁻¹ for a wide range of parameters that are chemically reasonable for an outer-sphere charge-transfer process. For $\overline{H_{AB,m}^{o2}} = 5 \times 10^{-2}$ eV² state⁻¹ and $l_{sc} = 3 \times 10^{-8}$ cm, a variation over all chemically reasonable values of the coupling attenuation factor for electron tunneling through solvent,⁴¹⁻⁴³ from $0.1 < \beta_m < 1.5$ Å⁻¹, yields $k_{sc,max} = 10^{-17}$ – 10^{-16} cm⁴ s⁻¹. Above this limit, $k_{sc,max}$ is rather insensitive to changes in $\overline{H_{AB,m}^{o2}}$, l_{sc} , and β_m . Even a very large electronic coupling of 5 eV² state⁻¹, which would certainly produce adsorption and other profound, readily observable chemical interactions between the redox species and the electrode (and thus probably would not produce a system that obeyed the rate law of eq 2.4), only produces $k_{sc,max} = 4.1 \times 10^{-16}$ cm⁴ s⁻¹ if $\beta_m = 1.0$ Å⁻¹.⁴⁴ The Fermi golden rule-based treatment, at the level of analysis adopted in this work, thus appears to agree well with experimental data and with prior theoretical models predicting $k_{sc,max} = 10^{-17}$ – 10^{-16} cm⁴ s⁻¹ for outer-sphere charge-transfer processes at experimentally accessible semiconductor/liquid contacts.

Values of $k_{sc,max} \gg 10^{-16}$ cm⁴ s⁻¹ thus appear to require adiabatic charge transfer to occur over a significant distance into the electrolyte. In lieu of explicitly evaluating a full Landau-Zener expression for the transition between adiabatic and nonadiabatic limits,^{18,20} a value of $k_{sc,max}$ incorporating adiabaticity can be computed by assuming, for simplicity, a limiting value of $k_{m,ad} = 10^{13}$ s⁻¹.¹⁷ Using this approximation and eq 2.26, a value of $k_{sc,max} = 10^{-15}$ cm⁴ s⁻¹ requires adiabatic charge transfer over ≈ 16 Å into the electrolyte.

Similarly, a value of $k_{sc} = 10^{-12} \text{ cm}^4 \text{ s}^{-1}$ would require adiabatic charge transfer over $\approx 1.6 \times 10^4 \text{ \AA}$ into the electrolyte, while $k_{sc} = 10^{-10} \text{ cm}^4 \text{ s}^{-1}$ would require adiabatic charge transfer over $\approx 0.2 \text{ mm}$ into the solution phase. Note that these values are not limited by any diffusional processes of redox species in the electrolyte solution, because if the charge-transfer rate constant to a redox species at a fixed distance falls below the value of $k_{m,ad}$ at a shorter distance from the electrode surface, then the result of an integration of the rate constant over distance into the electrolyte (eq 2.26) must produce a lower value of $k_{sc,max}$. The extremely rapid charge-transfer processes at extraordinarily long distances implied by $k_{sc} \geq 10^{-14} \text{ cm}^4 \text{ s}^{-1}$ appear to have no precedent in electrochemical¹⁻⁴ or donor/acceptor systems.^{41-43,45-48} In view of the analysis presented above, it seems far more likely that such anomalously large interfacial rate constant values result from adsorption of redox species, charge transfer through surface states, or other types of interfacial kinetic processes that can produce large majority carrier currents at semiconductor/liquid contacts without reflecting the outer-sphere interfacial kinetic processes that are the focus of this theoretical analysis.

Symbol in Figure 2.1	$\overline{H_{AB,m}^0}$ (eV ² state ⁻¹)	$k_{sc,max}$ (cm ⁴ s ⁻¹)
●	5×10^{-4}	1.6×10^{-18}
○	5×10^{-2}	1.2×10^{-16}
■	5×10^0	4.1×10^{-16}
□	5×10^2	6.9×10^{-16}
▲	5×10^4	9.8×10^{-16}
△	5×10^6	1.3×10^{-15}

Table 2.1: Values of $k_{sc,max}$ as a function of the electronic coupling at contact for the data plotted in Figure 2.3. A value of $\beta_m = 1.0 \text{ \AA}^{-1}$ was used to determine $k_{sc,max}$.

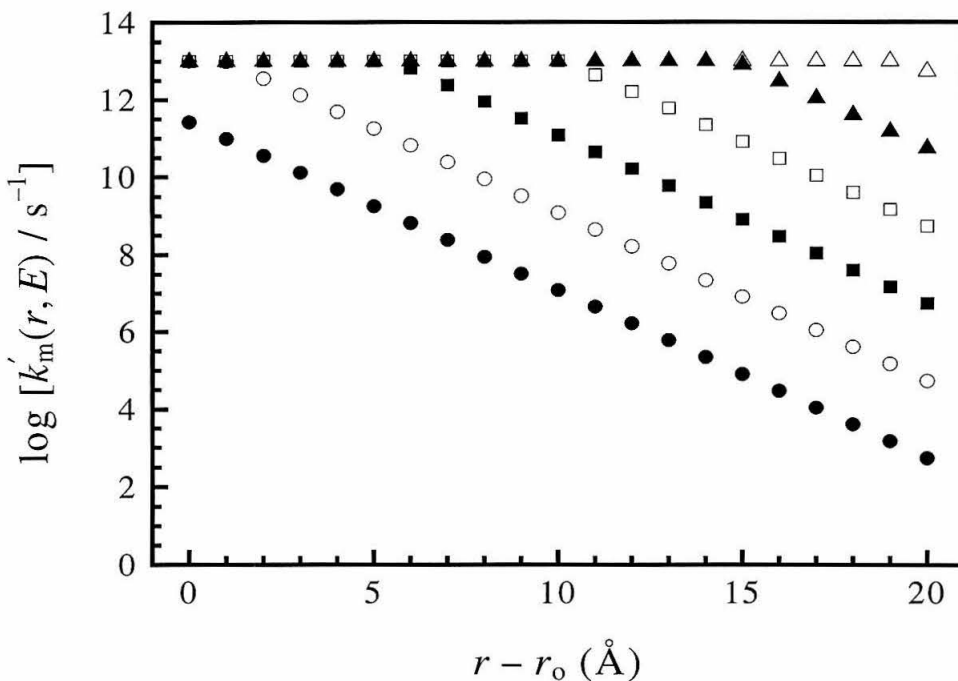


Figure 2.3: Plot of $k'_m(r, E)$ as a function of the relative distance of the redox species to the distance of closest approach to the electrode surface for various values of $\overline{H_{AB,m}^2}$ as indicated in Table 2.1. The value of β_m was taken to be 1.0 \AA^{-1} .

Symbol in Figure 2.2	β_m (\AA^{-1})	$k_{\text{sc,max}}$ ($\text{cm}^4 \text{s}^{-1}$)
●	0.1	1.2×10^{-15}
○	0.5	2.4×10^{-16}
■	0.75	1.6×10^{-16}
□	1.0	1.2×10^{-16}
▲	1.25	9.7×10^{-17}
△	1.5	8.1×10^{-17}

Table 2.2: Values of $k_{\text{sc,max}}$ as a function of β_m for the data plotted in Figure 2.4. A value of $\overline{H_{\text{AB,m}}^2} = 5 \times 10^{-2} \text{ eV}^2 \text{ state}^{-1}$ was used for these calculations.

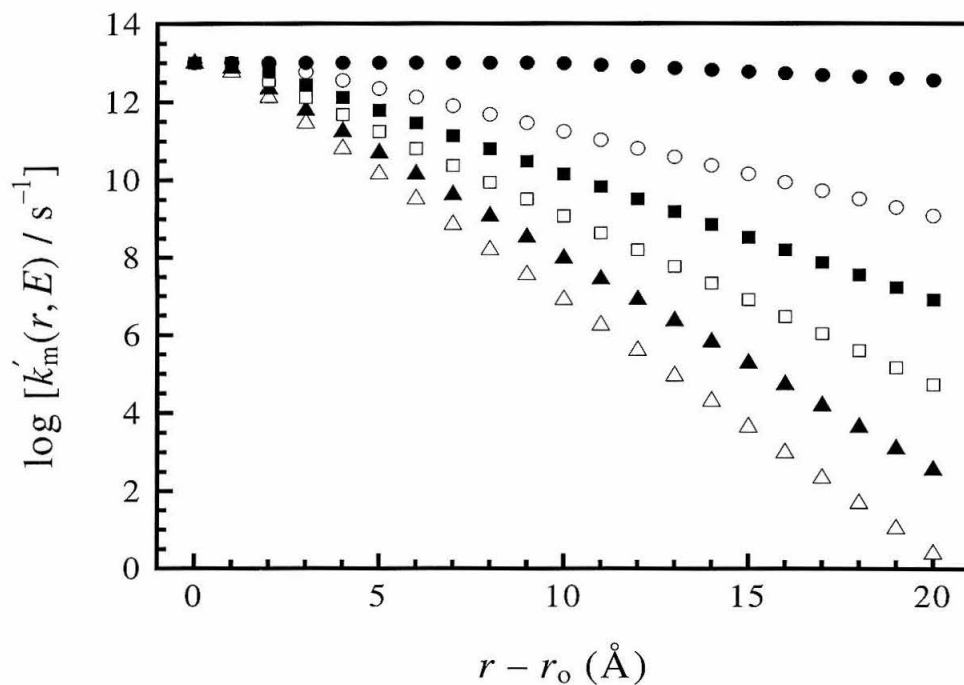


Figure 2.4: Plot of $k'_m(r, E)$ as a function of the relative distance of the redox species to the distance of closest approach to the electrode surface for various values of β_m as indicated in Table 2.2. The value of $\overline{H_{AB,m}^2}$ was taken to be 1.0 \AA^{-1} .

VII. SUMMARY

As demonstrated, it is possible to understand, in a unified framework, charge-transfer processes at metal/liquid and semiconductor/liquid contacts. Rate constants for these systems can be described in terms of the electronic coupling matrix elements that relate the two processes, and the two types of electrochemical rate constants can also be related to quantities commonly used in the literature to evaluate, both experimentally and theoretically, intermolecular and intramolecular donor/acceptor electron-transfer events. The quantum-mechanical, Fermi golden rule-based description of charge-transfer kinetics at semiconductor/liquid contacts agrees with prior statistical mechanical treatments and with prior electronic coupling estimates for such charge-transfer processes. It is also in excellent accord with robust experimental data available for the rate constants of such processes. The treatment also makes certain predictions regarding the experimental behavior of charge-transfer processes involving redox species immobilized on semiconducting electrode surfaces and forms the basis for further experimental investigations of such systems.

VIII. REFERENCES

1. Chidsey, C. E. D. *Science* **1991**, *251*, 919.
2. Finklea, H. O.; Hanshew, D. D. *J. Am. Chem. Soc.* **1992**, *114*, 3173.
3. Terrettaz, S.; Becka, A. M.; Traub, M. J.; Fettinger, J. C.; Miller, C. J. *J. Phys. Chem.* **1995**, 11216.
4. Smalley, J. F.; Feldberg, S. W.; Chidsey, C. E. D.; Linford, M. R.; Newton, M. D.; Liu, Y. P. *J. Phys. Chem.* **1995**, *99*, 13141.
5. Pomykal, K. E.; Fajardo, A. M.; Lewis, N. S. *J. Phys. Chem.* **1996**, *100*, 3652.
6. Pomykal, K. E.; Lewis, N. S. *J. Phys. Chem. B* **1997**, *101*, 2476.
7. Fajardo, A. M.; Lewis, N. S. *Science* **1996**, *274*, 969.
8. Fajardo, A. M.; Lewis, N. S. *J. Phys. Chem.* **1997**, *101*, 11136.
9. Chidsey, C. E. D.; Bertozzi, C. R.; Putvinski, T. M.; Mujisce, A. M. *J. Am. Chem. Soc.* **1990**, *112*, 4301.
10. Bard, A. J.; Mirkin, M. V.; Horrocks, B. R. *J. Phys. Chem.* **1994**, *98*, 2739.
11. Uhlendorf, I.; Reineke-Koch, R.; Memming, R. *J. Phys. Chem.* **1996**, *100*, 4930.
12. Marcus, R. A. *Annu. Rev. Phys. Chem.* **1964**, *15*, 155.
13. Marcus, R. A. *J. Chem. Phys.* **1965**, *43*, 679.
14. Lewis, N. S. *Annu. Rev. Phys. Chem.* **1991**, *42*, 543.
15. Bard, A. J.; Faulkner, L. R. *Electrochemical Methods: Fundamentals and Applications*; Wiley: New York, 1980.
16. Tan, M. X.; Laibinis, P. E.; Nguyen, S. T.; Kesselman, J. M.; Stanton, C. E.; Lewis, N. S. *Prog. Inorg. Chem.* **1994**, *41*, 21.
17. Marcus, R. A.; Sutin, N. *Biochim. Biophys. Acta.* **1985**, *811*, 265.
18. Newton, M. D. *Chem. Rev.* **1991**, *91*, 767.
19. Ulstrup, J.; Jortner, J. *J. Chem. Phys.* **1975**, *63*, 4358.
20. Brunschwig, B. S.; Logan, J.; Newton, M. D.; Sutin, N. *J. Am. Chem. Soc.* **1980**, *102*, 5798.
21. Levich, V. G. In *Advances in Electrochemistry and Electrochemical Engineering*; Delahay, P., Tobias, C. W., Eds.; Interscience: New York, 1966; Vol. 4.

22. The conventional electrochemical sign convention where positive energies are further from the vacuum level is used throughout this thesis; hence
- $$\mathcal{F}(\mathbf{E}, E) = \left[1 + \exp \left[\left(qE + \mathbf{E}(A/A^-) - \mathbf{E} \right) / kT \right] \right]^{-1},$$
- where $\mathbf{E}(A/A^-)$ is the electrochemical potential of the solution. Also, q is unsigned, and electrochemical potentials $\mathbf{E}(A/A^-)$ are related to their Nernst potentials, $E(A/A^-)$, by $\mathbf{E}(A/A^-) = qE(A/A^-)$, so that positive redox energies and potentials are both further from the vacuum level. All redox potentials in this work are written as reduction potentials, so that more negative conduction band energies indicate larger driving forces for charge transfer to an acceptor of formal potential $E^{\circ}(A/A^-)$. Thus, under such conditions the effective driving force for interfacial charge transfer, ΔG° , equals $-nF \left[E^{\circ}(A/A^-) - \mathbf{E}_{\text{cb}}/q \right]$, and ΔG° is negative for a thermodynamically favorable reduction of the acceptor A by an electron in the conduction band of the semiconductor.
23. The Fermi level is strictly defined for equilibrium conditions; thus the equations presented herein are only rigorously applicable for calculation of the rate of the equilibrium exchange process between the solid and the liquid. However, as long as the rates of electron equilibration and thermalization in the solid are sufficiently rapid, the equations presented herein are readily modified to describe the situation away from equilibrium through use of a quasi-Fermi level formalism which describes the occupancy statistics of carriers in the solid when a potential, E , is applied to the solid/liquid contact. The occupancy of states in the solid under such conditions can be computed according to the definition of $\mathcal{F}(\mathbf{E}, E)$ given in footnote 21 for any potential E , including the equilibrium case in which $E = E(A/A^-)$. This treatment allows recovery of the conventional Marcus-type or Butler-Volmer type current-potential relationships at a metal electrode and recovery of the standard exponential diode-like behavior of a semiconductor at various applied potentials from the equations presented herein; systems for which this Fermi level occupancy treatment do not apply are beyond the scope of this work and must be treated by a more sophisticated analysis than is available, to our knowledge, for any electrochemical system to date.
24. Kittel, C. *Introduction to Solid State Physics*, 6th ed.; Wiley: New York, 1986.
25. Marcus, R. A. *J. Phys. Chem.* **1991**, *95*, 2010.
26. Smith, B. B.; Koval, C. A. *J. Electroanal. Chem.* **1991**, *319*, 19.
27. Barbara, P. F.; Meyer, T. J.; Ratner, M. A. *J. Phys. Chem.* **1996**, *100*, 13148.
28. Sze, S. M. *The Physics of Semiconductor Devices*, 2nd ed.; Wiley: New York, 1981.

29. Fonash, S. J. *Solar Cell Device Physics*; Academic: New York, 1981.
30. Blakemore, J. S. *Semiconductor Statistics*; Dover Publications: New York, 1987.
31. It is not necessary that the conditions $\overline{H_{AB,m}^2}(r) = \overline{H_{AB,sc}^2}(r)$ and $l_m = l_{sc}$ are satisfied separately to obtain eq 2.23. Only the product of the coupling per state and the coupling depth into the electrode affects the measured rate constant so it is therefore sufficient that $\overline{H_{AB,m}^2}(r)l_m = \overline{H_{AB,sc}^2}(r)l_{sc}$ in order to obtain eq 2.23 and the relationships derived therefrom.
32. A more rigorous approach to account for adiabaticity would be to incorporate a Landau-Zener-type treatment for the probability of crossing from the reactant to the product diabatic surface,²⁰ but the treatment used herein is reasonably accurate in most cases.
33. Gerischer, H. *J. Phys. Chem.* **1991**, *95*, 1356.
34. Gehlen, J. N.; Chandler, D. *J. Phys. Chem.* **1992**, *97*, 4958.
35. Nozik, A. J.; Memming, R. *J. Phys. Chem.* **1996**, *100*, 13061.
36. Ellingson, R.; Meier, A.; Kocha, S.; Smith, B. B.; Rosenwaks, Y.; Halley, J. W.; Schelling, P.; Hanna, M.; Nozik, A. J. Third International Meeting on New Trends in Photoelectrochemistry, 1997, Estes Park, CO.
37. Smith, B. B.; Halley, J. W.; Nozik, A. J. *Chem. Phys.* **1996**, *205*, 245.
38. Rosenwaks, Y.; Thacker, B. R.; Ahrenkiel, R. K.; Nozik, A. J. *J. Phys. Chem.* **1992**, *96*, 10096.
39. Rosenwaks, Y.; Thacker, B. R.; Nozik, A. J.; Ellingson, R. J.; Burr, K. C.; Tang, C. L. *J. Phys. Chem.* **1994**, *98*, 2739.
40. Although values of $k_{sc} \approx 10^{-12} \text{ cm}^4 \text{ s}^{-1}$ have been reported for certain InP and GaAs electrodes,^{38,39} careful examination of these rate constants reveals that experimental artifacts resulting from electrode corrosion and/or passivation are likely responsible for these systems. Also see: Bansal, A.; Tan, M. X.; Tufts, B. J.; Lewis, N. S. *J. Phys. Chem.* 1993, *97*, 7309 and Nozik, A. J. Presented at the 211th National Meeting of the American Chemical Society; New Orleans, LA, March 1996, paper PHYS 11.
41. Bowler, B. E.; Raphael, A. L.; Gray, H. B. *Prog. Inorg. Chem.* **1990**, *38*, 259.
42. Closs, G. L.; Miller, J. R. *Science* **1988**, *240*, 440.
43. Murphy, C. J.; Arkin, M. R.; Jenkins, Y.; Ghatila, N. D.; Bossmann, S. H.; Turro, N.

- J.; Barton, J. K. *Science* **1993**, *262*, 1025.
44. Note that this treatment has assumed that the coupling per state that is reached at the adiabatic limit is similar for a metal and for a semiconductor electrode, allowing eqs 2.26 and 2.27 to be derived. A treatment in which the adiabatic limit for the semiconductor electrode is defined as the coupling obtained when the prefactor in eq 2.18 has a value of 10^{13} s^{-1} produces limiting rate constants that are smaller by a factor of 10–20 than those calculated using eqs 2.26 and 2.27 as described in the text. A more detailed theoretical analysis would be required in order to obtain more improved estimates of $k_{\text{sc,max}}$ relative to those provided by these procedures and also to treat the transition region between the adiabatic and nonadiabatic situations in depth.
 45. Miller, J. R.; Calcaterra, L. T.; Closs, G. L. *J. Am. Chem. Soc.* **1984**, *106*, 3047.
 46. Gust, D.; Moore, T. A.; Moore, A. L.; Macpherson, A. N.; Lopez, A.; DeGraziano, J. M.; Gouni, I.; Bittersmann, E.; Seely, G. R.; Gao, F.; Nieman, R. A.; Ma, X. C.; Demanche, L. J.; Hung, S.; Luttrull, D. K.; Lee, S.; Kerrigan, P. K. *J. Am. Chem. Soc.* **1993**, *115*, 11141.
 47. Franzen, S.; Goldstein, R. F.; Boxer, S. G. *J. Phys. Chem.* **1993**, *97*, 3040.
 48. For example, assuming an attenuation coefficient of $\beta = 1.0 \text{ \AA}^{-1}$ for the electronic coupling matrix element through the solvent, the electronic coupling at contact that would be required to achieve a value of $k_{\text{sc,max}} = 10^{-12} \text{ cm}^4 \text{ s}^{-1}$ is $\approx 10^{70,000} \text{ GeV}^2/\text{state}$, which is clearly nonphysical.

Chapter 3

Theoretical Investigation of Interfacial Electron-Transfer Rate Constants at Semimetal Electrodes

I. INTRODUCTION

Charge transfer at the semimetal/liquid interface is increasingly a subject of both academic and practical interest. For several years, semimetal electrodes such as glassy carbon and graphite have been employed in electrosynthetic and electroanalytical investigations of redox processes.¹⁻⁷ More recently, these materials have also been used in electrochemical scanning probe studies of localized surface reactions.⁸ In addition, carbon-based semimetals have been used extensively as electrode materials in energy-storage devices such as dry-cell batteries^{9,10} and methanol fuel cells.^{11,12} A better understanding of the kinetic behavior of charge-transfer reactions at the semimetal/liquid interface could lead to improvements in these technologies.

Although numerous electrochemical reactions have been characterized experimentally using semimetal electrodes, few efforts have been made to interpret the kinetic behavior observed for these systems in the context of a fundamental, non-phenomenological charge-transfer model. One notable exception is an investigation by McCreery and co-workers in which rate constants were measured for interfacial charge transfer between highly ordered pyrolytic graphite (HOPG) electrodes and a variety of dissolved outer-sphere redox species having various reorganization energies and formal potentials.³ In this study, a correlation between the measured charge-transfer rate constant and the driving force as predicted by Marcus theory was not observed. Based on the work presented in the previous chapter, however, it appears that a more rigorous treatment than that employed in the work of McCreery is necessary to appropriately account for parameters such as the reorganization energies and densities of states.

In Chapter 2, a formalism based on Fermi's golden rule was introduced for evaluating rate constants at semiconductor/liquid interfaces. In this chapter, a parallel approach is used to extend this formalism to interfacial charge transfer at semimetal/liquid interfaces. A similar framework is developed to relate rate constants for charge transfer at semimetal/liquid interfaces to those of metal/liquid interfaces.

Estimates of rate-constant values are made for graphite electrodes in contact with a variety of redox couples that have been examined previously by McCreery and co-workers. Although there is still considerable discrepancy between the theoretically derived and experimentally measured rate constants, possible reasons for these differences are discussed.

II. RATE EXPRESSIONS FOR CHARGE TRANSFER AT SEMIMETAL/LIQUID INTERFACES

A. Rate Law for Charge Transfer to a Random Distribution of Dissolved Redox Acceptors

The rate laws describing interfacial charge-transfer kinetics at semimetal electrodes are identical to those of metal electrodes. In the case of a semimetal electrode in contact with redox acceptors randomly distributed in an electrolyte solution, the appropriate rate expression is given by

$$rate_{sm}(E) = k_{sm}(E)[A] \quad (3.1)$$

where $rate_{sm}(E)$ is the charge-transfer flux in units of $cm^{-2} s^{-1}$, k_{sm} is the rate constant for charge transfer in units of $cm s^{-1}$, and $[A]$ is the concentration of redox acceptors in solution in units of cm^{-3} . As in the case for a metal electrode, the electron concentration at the surface of a semimetal electrode is not a parameter that can be controlled independently of the rate constant, and it is therefore not explicitly written in the rate law.

B. Fermi Golden Rule Expressions for Charge Transfer to a Random Distribution of Dissolved Redox Acceptors

For a semimetal electrode in contact with a solution containing a random distribution of outer-sphere redox acceptors, the Fermi golden rule expression for the charge-transfer rate in the nonadiabatic limit is given by:

$$rate_{sm}(E) = \frac{2\pi^{3/2}[A]}{h(k_b T \lambda_{sm})^{1/2}} \int_{r_0}^{\infty} \int_{-\infty}^{\infty} \overline{H_{AB,sm}^2(\mathbf{E})} \exp[-\beta_{sm}(r - r_0)] \mathcal{F}(\mathbf{E}, E) \times \rho_{sm,eff}(\mathbf{E}) \exp\left[-(\Delta G^{o'} + \lambda_{sm})^2 / 4\lambda_{sm} k_b T\right] d\mathbf{E} dr \quad (3.2)$$

where h is Planck's constant, k_b is Boltzmann's constant, T is the temperature, and λ_{sm} is the reorganization energy of the acceptor at the surface of the semimetal electrode. In this expression, $\overline{H_{AB,sm}^2(\mathbf{E})}$ represents the square of the electronic coupling matrix

element (in units of $\text{eV}^2 \text{state}^{-1}$) that couples reactant and product states at the energy \mathbf{E} . This term has been averaged over all degenerate states having an energy \mathbf{E} and also spatially over a plane parallel to the surface located at the distance of closest approach, r_o , of the redox acceptor to the semimetal surface. Also, β_{sm} is the electronic coupling attenuation coefficient, r is the distance between the electrode surface and the redox acceptor, $\mathcal{F}(\mathbf{E}, E)$ is the value of the Fermi occupancy function as function of energy, \mathbf{E} , and electrode potential, E , $\rho_{\text{sm,eff}}(\mathbf{E})$ is the density of states (in units of states eV^{-1}), and $\Delta G^{o'}$ is the driving force under standard conditions.

Making the assumption that the electronic coupling matrix element is independent of energy,¹³ solving the integral over distance, and rewriting the density of states as an effective volume density of states, $D_{\text{sm,eff}}(\mathbf{E})$ (see Chapter 2), allows reformulation of eq 3.2 as:

$$\text{rate}_{\text{sm}}(E) = \frac{2\pi^{3/2}l_{\text{sm}}[\text{A}]}{h(k_{\text{b}}T\lambda_{\text{sm}})^{1/2}d_{\text{sm}}^{2/3}(6/\pi)^{1/3}} \overline{H_{\text{AB,sm}}^2} \beta_{\text{sm}}^{-1} \int_{-\infty}^{\infty} \mathcal{F}(\mathbf{E}, E) D_{\text{sm,eff}}(\mathbf{E}) \times \exp\left[-(\Delta G^{o'} + \lambda_{\text{sm}})^2 / 4\lambda_{\text{sm}}k_{\text{b}}T\right] d\mathbf{E} \quad (3.3)$$

where l_{sm} is the effective coupling length of the acceptor wavefunction into the solid and d_{sm} is the atomic density of the solid.

In its current form, eq 3.3 is identical to the analogous rate expression for a semiconductor/liquid or a metal/liquid junction, but two key features distinguish charge transfer at a semimetal/liquid junction. As in the case for a metal electrode, charge flow at a semimetal electrode proceeds from a continuum of states below the Fermi level (Figure 3.1). Unlike the situation for a metal electrode, however, in a semimetal the density of states is not a weak function of energy near the Fermi level, and consequently $D_{\text{sm,eff}}(\mathbf{E})$ cannot be removed from the integral in eq 3.3. Evaluation of the rate expression therefore requires specific knowledge of the energy dependence of $D_{\text{sm,eff}}(\mathbf{E})$. Another property that must be considered involves the partitioning of the potential at the

solid/liquid interface. In most instances, the potential applied to a semiconductor/liquid contact drops almost entirely across the solid, while the potential applied to a metal/liquid contact drops almost exclusively across a small layer of solution near the interface (see Chapter 4). A semimetal electrode, however, represents an intermediate case in which a portion of the applied potential drops across the solid, and the remainder drops across the solution.¹⁴ As a result, the driving-force term in eq 3.3 must be adjusted to reflect the actual energy difference of surface electrons and redox acceptors near the interface.

Writing the driving-force term explicitly and including the potential correction yields:

$$rate_{sm}(E) = \frac{2\pi^{3/2}l_{sm}[A]}{h(k_bT\lambda_{sm})^{1/2}d_{sm}^{2/3}(6/\pi)^{1/3}} \overline{H_{AB,sm}^{\circ 2}\beta_{sm}^{-1}} \int_{-\infty}^{\infty} \mathcal{F}(\mathbf{E}, E) D_{sm,eff}(\mathbf{E}) \times \exp\left[-(\mathbf{E} - qE_h - qE^{o'} + \lambda_{sm})^2 / 4\lambda_{sm}k_bT\right] d\mathbf{E} \quad (3.4)$$

where E_h is the potential drop across the Helmholtz layer, $E^{o'}$ is the formal potential of the solution, and q is the charge on an electron. Combining eq 3.1 with eq 3.4 results in the following expression for the charge-transfer rate constant:

$$k_{sm}(E) = \frac{2\pi^{3/2}l_{sm}}{h(k_bT\lambda_{sm})^{1/2}d_{sm}^{2/3}(6/\pi)^{1/3}} \overline{H_{AB,sm}^{\circ 2}\beta_{sm}^{-1}} I_{sm}(\lambda_{sm}, E) \quad (3.5)$$

where $I_{sm}(\lambda_{sm}, E)$ represents the integral in eq 3.4.

C. Comparison of Rate Expressions for Semimetal/Liquid and Metal/Liquid Junctions

In Chapter 2, an expression similar to eq 3.5 for electron transfer from a metal electrode to a random distribution of dissolved redox acceptors was determined to be:

$$k_m(E) = \frac{2\pi^{3/2}l_m}{h(k_bT\lambda_m)^{1/2}d_m^{2/3}(6/\pi)^{1/3}} \overline{H_{AB,m}^{\circ 2}\beta_m^{-1}} D_{m,eff} I_m(\lambda_m, E) \quad (3.6)$$

All parameters in eq 3.6 are analogous to the quantities described above for a semimetal,

and for these terms, the subscript m has been used to denote that the terms refer to a metal electrode. Taking the ratio of eq 3.5 to eq 3.6 yields the following expression:

$$\frac{k_{\text{sm}}(E)}{k_{\text{m}}(E)} = D_{\text{m,eff}}^{-1} \frac{H_{\text{AB,sm}}^{\circ 2}}{H_{\text{AB,m}}^{\circ 2}} \left(\frac{\beta_{\text{m}}}{\beta_{\text{sc}}} \right) \left(\frac{l_{\text{sm}}}{l_{\text{m}}} \right) \left(\frac{d_{\text{m}}}{d_{\text{sm}}} \right)^{2/3} \left(\frac{\lambda_{\text{m}}}{\lambda_{\text{sm}}} \right)^{1/2} \left(\frac{I_{\text{sm}}(\lambda_{\text{sm}}, E)}{I_{\text{m}}(\lambda_{\text{m}}, E)} \right) \quad (3.7)$$

To quantitatively evaluate $k_{\text{sm}}(E)$ from experimental kinetic measurements at metal electrodes, the variables in eq 3.7 must be determined for both electrode/electrolyte systems. Alternatively, several reasonable approximations can be made to facilitate evaluation of $k_{\text{sm}}(E)$. Assuming the average electronic couplings, the coupling attenuation factors, the orbital penetration depths, and the reorganization energies are approximately the same for both solid/liquid systems, eq 3.7 reduces to:

$$k_{\text{sm}}(E) = k_{\text{m}}(E) D_{\text{m,eff}}^{-1} \left(\frac{d_{\text{m}}}{d_{\text{sm}}} \right)^{2/3} \left(\frac{I_{\text{sm}}(\lambda_{\text{sm}}, E)}{I_{\text{m}}(\lambda_{\text{m}}, E)} \right) \quad (3.8)$$

Thus, $k_{\text{sm}}(E)$ can be computed provided the values of the integrals are known for the specific experimental conditions.

A similar treatment can also be used to compare charge-transfer kinetic measurements for a semimetal electrode in contact with a random distribution of redox acceptors to distance-dependent kinetic measurements of a metal electrode with redox acceptors fixed at a distance r_{A} from the electrode surface. In this approach, $k_{\text{m}}(E)$ is first determined from the following expression:

$$k_{\text{m}}(E) = k_{\text{m},r_{\text{A}}}(E) \beta_{\text{m}}^{-1} \exp(\beta_{\text{m}} r_{\text{A}}) \quad (3.9)$$

where $k_{\text{m},r_{\text{A}}}(E)$ is the measured rate constant for electron-transfer from the metal electrode to the redox acceptor at $r = r_{\text{A}}$. The value of $k_{\text{m}}(E)$ obtained using eq 3.9 is then substituted in eq 3.8 to give a value for $k_{\text{sm}}(E)$.

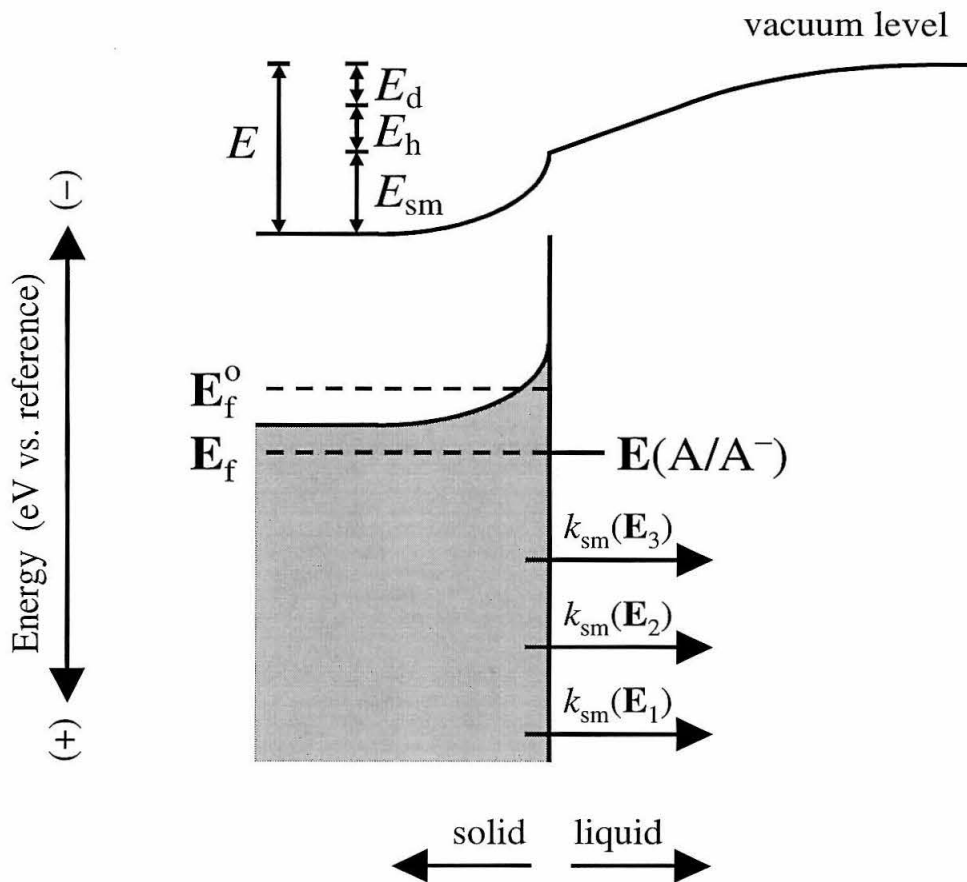


Figure 3.1: Energy diagram for a semimetal/liquid junction at equilibrium. The quantity E_f is the Fermi level, E_f^0 is the Fermi level at the potential of zero charge, $k_{sm}(E_n)$ is the interfacial charge-transfer rate constant at the energy E_n , $E(A/A^-)$ is the electrochemical potential of the solution (i.e., the Nernstian potential multiplied by q), E is the potential applied to the electrode versus the potential of zero charge, E_{sm} is the potential drop across the depletion layer of the semimetal, E_h is the potential drop across the Helmholtz layer, and E_d is the potential drop across the diffuse layer of the solution. The value $k_{sm}(E)$ is determined by integrating $k_{sm}(E_n)$ over all energies at a given applied potential, E .

III. EVALUATION OF INTERFACIAL RATE CONSTANTS AT GRAPHITE ELECTRODES FROM ANALYSIS OF EXPERIMENTAL DATA

In this section, the expressions derived above are used to determine values of $k_{\text{sm}}(E)$ for graphite in contact with various one-electron outer-sphere redox couples. The specific redox couples examined in this work are those for which kinetic measurements are available from a prior electrochemical investigation by McCreery and co-workers.

Two key variables must first be determined in order to evaluate $I_{\text{sm}}(\lambda_{\text{sm}}, E)$, and hence $k_{\text{sm}}(E)$: the volume density of states, $D_{\text{m,eff}}(\mathbf{E})$, for each energy near the Fermi level and the potential drop across the Helmholtz layer, E_{h} , at the applied potential of interest. Values of $D_{\text{m,eff}}(\mathbf{E})$ are readily available from capacitance measurements of graphite/electrolyte contacts reported previously by Gerischer and co-workers.¹⁴ The relevant results of this study are depicted in Figure 3.2, which shows $D_{\text{m,eff}}(\mathbf{E})$ for energies near the Fermi level at the point of zero net charge, $\mathbf{E}_{\text{f}}^{\circ}$. The data are well-fit with a 6th order polynomial function yielding a value of $D_{\text{m,eff}}(\mathbf{E}_{\text{f}}^{\circ}) = 2.4 \times 10^{-20}$ states $\text{eV}^{-1} \text{cm}^{-3}$. The capacitance measurements presented in the study of Gerischer also provide values for E_{h} as a function of the total applied potential vs. $\mathbf{E}_{\text{f}}^{\circ}$ (Figure 3.3). Thus, for a redox couple having a known formal potential and reorganization energy, the value of $I_{\text{sm}}(\lambda_{\text{sm}}, E)$ can be computed numerically for any value of the applied potential. The values of E° , λ , and $I_{\text{sm}}(\lambda_{\text{sm}}, E)$ for several one-electron redox couples are listed in Table 3.1.

With the value of $I_{\text{sm}}(\lambda_{\text{sm}}, E)$ known, eqs 3.8 and 3.9 can be used to determine $k_{\text{sm}}(E)$ through reference to experimentally determined kinetic data for charge transfer between a metal electrode and a redox species immobilized on the electrode surface. Such data are available from a chronocoulometric investigation of Au electrodes modified with ferrocene-terminated alkanethiols $[(\eta^5\text{-C}_5\text{H}_5)\text{Fe}(\eta^5\text{-C}_5\text{H}_4)\text{CO}_2(\text{CH}_2)_{16}\text{-SH}]$.¹³ In this system, an interfacial rate constant, $k_{\text{m,rA}}(E)$, of 6000 s^{-1} was observed at an overpotential of -0.68 V . A fit to the kinetic data at several values of the

overpotential yielded a reorganization energy of 0.85 eV. Numerical integration with $\lambda_m = 0.85$ eV and $E - E^{o'} = -0.68$ V results in a value of $I_m(\lambda_m, E) = 0.112$ eV. Assuming a value of $\beta_m = 1.11$ per CH_2 unit, and 19 effective methylene units linking the redox species to the metal surface, $k_m(E)/I(\lambda_m, E)$ can be established from eq 3.9 as 7.3×10^5 $\text{cm eV}^{-1} \text{ s}^{-1}$. The resulting values of $k_{sm}(E)$, computed from eq 3.8, are listed in Table 3.1 for various one-electron redox couples.

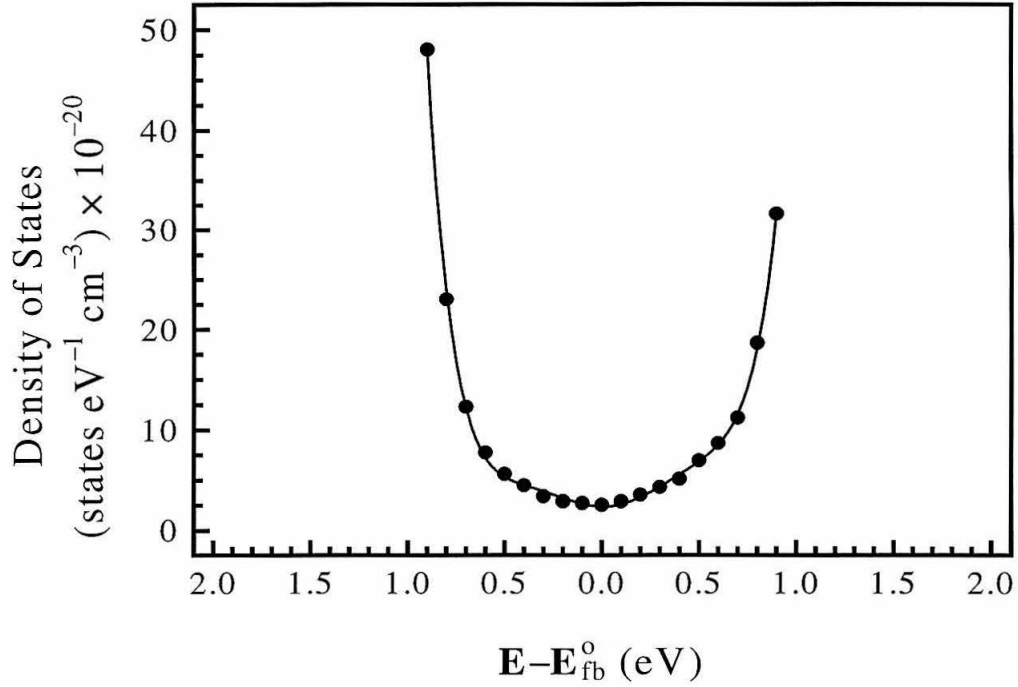


Figure 3.2: A plot of $D_{sm,eff}(\mathbf{E})$ for graphite near the Fermi level at the potential of zero charge.¹⁴ A sixth-order polynomial fit to the data is also shown.

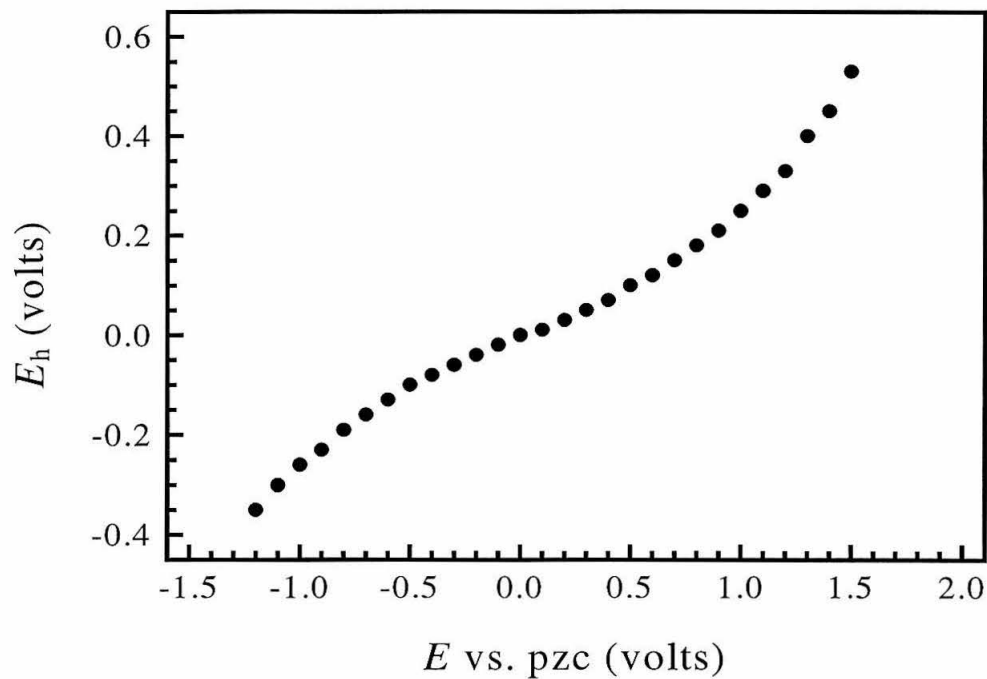


Figure 3.3: A plot of the potential drop across the solution Helmholtz layer as a function of the potential applied to a graphite/liquid interface relative to the potential of zero charge (pzc).¹⁴

Table 3.1: Comparison of calculated and measured rate constants for interfacial electron transfer from a graphite electrode to various redox couples in aqueous solution. Notes: ^a phen = 1,10-phenanthroline, MV = methylviologen, en = ethylenediamine, Fc = ferrocene, bpy = 2,2'-bipyridine, py = pyridine, sep = sepulchrate. ^b average of voltammetric peak potentials with respect to the potential of zero charge (≈ -0.24 V vs. SCE) as reported by McCreery and co-workers.³ ^c self-exchange rates obtained from ref 3 and references therein. ^d reorganization energies computed from self-exchange rate constants after ionic strength correction.¹⁵ ^e rate constant computed from eqs 3.8 and 3.9 at $E = E^{\circ}$. ^f rate constants measured in aqueous solutions using laser-activated HOPG at $E = E^{\circ}$.³

Redox System ^a	$E_{1/2}$ (V vs. pzc) ^b	k_{exchange} ($\text{M}^{-1} \text{s}^{-1}$) ^c	λ (eV) ^d	$I_{\text{sm}}(\mathcal{A}_{\text{sm}}, E^{o'})$	k_{sm}° (cm s^{-1}) ^e	k_{meas}° (cm s^{-1}) ^f
$\text{IrCl}_6^{2-/3-}$	0.98	2×10^5	0.88	6.00×10^{18}	1.87×10^2	3×10^{-3}
$\text{Ru}(\text{NH}_3)_6^{3+/2+}$	0.05	4×10^3	1.18	2.23×10^{14}	6.95×10^{-3}	9×10^{-4}
$\text{Co}(\text{phen})_3^{3+/2+}$	0.34	4×10^1	1.92	9.33×10^{11}	2.90×10^{-5}	2×10^{-5}
$\text{MV}^{2+/1+}$	-0.43	1×10^7	0.81	2.24×10^{15}	6.97×10^{-2}	1.7×10^{-2}
$\text{Fe}(\text{phen})_3^{3+/2+}$	1.10	3×10^8	0.30	2.84×10^{21}	8.83×10^4	$> 7 \times 10^{-2}$
$\text{Fe}(\text{CN})_6^{3-/4-}$	0.49	2×10^4	1.13	5.83×10^{15}	1.81×10^{-1}	1×10^{-6}
$\text{Co}(\text{en})_3^{3+/2+}$	-0.24	8×10^5	3.18	3.83×10^5	1.19×10^{-11}	2×10^{-5}
$\text{Ru}(\text{en})_3^{3+/2+}$	0.16	4×10^3	1.60	6.12×10^{12}	1.90×10^{-4}	1×10^{-4}
$\text{Fc}(\text{COOH})_2$	0.66	1×10^7	0.95	1.08×10^{17}	3.36×10^0	3×10^{-3}
$\text{Ru}(\text{bpy})_3^{3+/2+}$	1.28	2×10^9	0.09	2.07×10^{22}	6.44×10^5	$> 2 \times 10^{-2}$
$\text{Ru}(\text{NH}_3)_5\text{py}^{3+/2+}$	0.28	5×10^5	0.86	1.90×10^{16}	5.91×10^{-1}	2×10^{-3}
$\text{Co}(\text{sep})^{3+/2+}$	-0.38	5×10^0	2.05	1.57×10^{10}	4.88×10^{-7}	7×10^{-4}
$\text{Mo}(\text{CN})_8^{3-/4-}$	0.84	3×10^4	0.73	4.76×10^{18}	1.48×10^2	2×10^{-3}
$\text{W}(\text{CN})_8^{3-/4-}$	0.57	4×10^4	0.70	5.20×10^{17}	1.62×10^1	4×10^{-4}

IV. DISCUSSION

Although the computed values of $k_{sm}(E)$ for some redox couples listed in Table 3.1 are very similar to the values measured previously by McCreery and co-workers, there are substantial disparities for several redox systems examined in this work. For four redox couples, $\text{Ru}(\text{NH}_3)_6^{3+/2+}$, $\text{Co}(\text{phen})_3^{3+/2+}$, $\text{MV}^{2+/1+}$, and $\text{Ru}(\text{en})_3^{3+/2+}$, the computed rate constants agree to within one order of magnitude of their measured values. Moreover, the computed rate constants for two other redox couples, $\text{Fe}(\text{phen})_3^{3+/2+}$ and $\text{Ru}(\text{bpy})_3^{3+/2+}$, are consistent with the lower bounds determined experimentally. For the remaining redox couples, however, with the exception of $\text{Co}(\text{en})^{3+/2+}$ and $\text{Co}(\text{sep})^{3+/2+}$, the computed values of $k_{sm}(E)$ are significantly larger than the measured values.

In prior reports, deviations between electron-transfer rates measured using graphite electrodes and those measured using glassy carbon electrodes have often been attributed to the presence of reactive chemical sites or surface electronic defects. It is possible that the discrepancies described above may also result from such effects. In electrochemical kinetic measurements of $k_{sm}(E)$, however, McCreery and co-workers concluded from adsorption studies of anthraquinone-2,6-disulfonate that inner-sphere charge-transfer reactions with reactive chemical sites did not appreciably influence the kinetic data in the majority of the redox systems studied; only $\text{Fe}(\text{CN})_6^{3-/4-}$ appeared to react with sites on the electrode surface. Moreover, comparative studies of interfacial electron-transfer rates at various carbon electrodes (i.e., defective and non-defective HOPG and glassy carbon) by McCreery and others have demonstrated that the presence of electronic defect states result in larger apparent charge-transfer rates than on less defective surfaces. Since the computed rate constants were in several cases larger than the measured values of $k_{sm}(E)$, it is difficult to rationalize the observed differences on the basis of electronic defect states. Another explanation for the discrepancies could be that non-reacting surface overlayers were present on the graphite electrodes in the experimental measurements, attenuating the electronic coupling and thereby reducing the measured rate constants.

Because there were at least four cases in which theory and experiment agreed, however, it is improbable that such a blocking-layer effect was present since all redox couples should have been equally affected.

An alternative possibility for the observed differences might involve differences in electronic couplings among various redox couples. One of the key assumptions made in the calculations presented in this work is that the electronic coupling at contact *for all* semimetal/liquid junctions is equal to the electronic coupling at contact for a metal/liquid junction. While this assumption appears to be valid when comparing interfacial rate constants at semiconductor/liquid and metal/liquid junctions, such a postulation may not be suitable for a graphite electrode. Electronic couplings between the directed π orbitals exposed at the surface of basal plane graphite and redox molecules in solution may likely require more selective molecular configurations than those for systems in which the electrode surfaces have more diffuse orbital structures. If correct, the observed discrepancies between theory and experiment might be resolved if differences in the electronic coupling could be accurately assessed.

V. SUMMARY

Fermi's golden rule has been used to formulate fundamental rate expressions for semimetal/liquid contacts and to relate the rate expressions to those of metal/liquid junctions. The equations have been used to predict rate-constant values for a series of one-electron redox couples for which experimental kinetic data are available. Substantial disparities between the values of the computed and measured rate constants for several redox systems may be due to large variations in electronic coupling parameters that were not considered in the present work.

VI. REFERENCES

1. Bond, A. M. *Inorg. Chim. Acta* **226**, 226, 293.
2. Chen, P.; Fryling, M. A.; McCreery, R. L. *Anal. Chem.* **1995**, *67*, 3115.
3. Cline, K. K.; McDermott, M. T.; McCreery, R. L. *J. Phys. Chem.* **1994**, *98*, 5314.
4. Kinoshita, K. *Carbon: Electrochemical and Physicochemical Properties*; Wiley: New York, 1988.
5. Kneten, K.; McCreery, R. L. *Anal. Chem.* **1992**, *64*, 2518.
6. Liu, Y.; Freund, M. S. *Langmuir* **2000**, *16*, 283.
7. McCreery, R. L. Carbon Electrodes: Structural Effects on Electron Transfer Kinetics. In *Electroanalytical Chemistry*; Bard, A. J., Ed.; Marcel Dekker: New York, 1991; Vol. 17; pp 221.
8. Bard, A. J.; Mirkin, M. V.; Unwin, P. R.; Wipf, D. O. *J. Phys. Chem.* **1992**, *96*, 1861.
9. Novak, P.; Joho, F.; Imhof, R.; Panitz, J. C.; Haas, O. *J. Power Sources* **1999**, *82*, 212.
10. Trinidad, F.; Montemayor, M. C.; Fatas, E. *J. Electrochem. Soc.* **1991**, *138*, 3186.
11. Verma, L. K. *J. Power Sources* **2000**, *86*, 464.
12. Wasmus, S.; Kuver, A. *J. Electroanal. Chem.* **1999**, *461*, 14.
13. Chidsey, C. E. D. *Science* **1991**, *251*, 919.
14. Gerischer, H.; McIntyre, R.; Scherson, D.; Storck, W. *J. Phys. Chem.* **1987**, *91*, 1930.
15. Whereland, S.; Gray, H. B. *Proc. Natl. Acad. Sci. USA* **1976**, *73*, 2950.

Chapter 4

Double-Layer Corrections for Interfacial Rate Constants at Semiconducting Electrodes

I. INTRODUCTION

In contrast to the well-known equations that have been developed by Frumkin and others for correction of heterogeneous rate constants at metallic electrodes,^{1,2} few efforts have been made to determine the magnitude or form of such corrections for semiconducting electrodes. To date, experimental rate constant data for semiconductor electrodes have not been corrected for double-layer effects.³⁻⁹ Additionally, theoretical models that have been developed to estimate the maximum interfacial charge-transfer rate constant value under optimal exoergicity at a semiconductor/liquid contact have not considered such correction terms in their analysis of experimental data.¹⁰⁻¹² Such corrections might, however, be important when comparing the theoretically predicted charge-transfer rate constants to experimental kinetic data for charge-transfer processes across semiconductor/liquid interfaces. In fact, a recent analysis has asserted that experimental charge-transfer rate constants for reaction of non-adsorbed, outer-sphere redox species at semiconductor electrodes may require Frumkin-like double layer corrections of an order of magnitude to facilitate comparison to theoretical predictions.¹³ A quantitative evaluation of the Frumkin corrections for semiconducting electrodes is therefore the focus of this chapter.

Two cases are considered herein: a semiconductor electrode in depletion and one in accumulation.^{14,15} These two cases are treated separately, because there is a large difference in the magnitude of the differential capacitance of the semiconductor relative to the differential capacitance of the double layer under accumulation or depletion conditions.² For depletion conditions, an analytical treatment has been used to evaluate the Frumkin corrections. In accumulation, the Frumkin corrections were evaluated numerically, using digital simulation methods to solve for the potential dropped across the electrode as a function of the potential applied to the solid/liquid contact.

In both cases, the Gouy-Chapman-Stern (GCS) model has been used to describe the double layer in the electrolyte.² Although the GCS treatment is only approximately in

accord with experimental data,² the GCS model was adopted because it performs satisfactorily at the high electrolyte concentrations and low interfacial potential drops that are characteristic of most experimental situations encountered in interfacial kinetic measurements at semiconductor/liquid interfaces.^{3-5,8,9} In addition, the GCS model allows formulation of a numerical comparison between the results presented in this chapter and the Frumkin corrections for metallic electrodes.

II. THEORY

For a semiconductor electrode in depletion, the equations governing the Frumkin corrections can be expressed as follows:²

$$[A]_{\text{ohp}} = [A]_{\text{bulk}} \exp\left(-\frac{zq\phi_d}{k_bT}\right) \quad (4.1)$$

$$k_{\text{et},E_{\text{fb}}} = k_{\text{et},E} \frac{[A]_{\text{bulk}}}{[A]_{\text{ohp}}} \exp\left(\frac{\alpha q E_h}{k_bT}\right) \quad (4.2)$$

In these equations, $[A]_{\text{ohp}}$ is the concentration of oxidized species A at the outer Helmholtz plane, OHP (in units of molecules cm^{-3}), $[A]_{\text{bulk}}$ is the concentration of A in the bulk of the solution (in units of molecules cm^{-3}), z is the charge on A, ϕ_d is the potential drop across the diffuse layer, q is the electronic charge, k_b is the Boltzmann constant, T is the temperature, $k_{\text{et},E_{\text{fb}}}$ is the rate constant¹⁰ (in units of $\text{cm}^4 \text{s}^{-1}$) for interfacial charge transfer at the flat-band potential of the semiconductor, E_{fb} , $k_{\text{et},E}$ is the experimentally observed interfacial rate constant at a specific potential E of the semiconductor electrode, α is the transfer coefficient, and E_h is the potential dropped across the Helmholtz later at the applied potential of interest. Although an n-type semiconductor is used as an example throughout this paper, analogous equations are readily derived for p-type semiconductor electrodes.

Eq 4.1 accounts for the effect of the charge density in the electrode on the equilibrium concentration profile of a charged ion that undergoes faradaic charge transfer at the electrode surface. This equation is identical to the conventional Frumkin concentration-correction term for a metallic electrode.² Eq 4.2 is similar in form to the Frumkin correction of the rate constant for a metallic electrode, but significant modifications are required in order to apply this correction to semiconducting electrodes. Since each semiconductor has a unique position of its energy bands relative to the Nernstian potential of the solution, various semiconductor electrodes will produce

various driving forces for interfacial charge transfer even when the electrodes are maintained at identical potentials relative to the Nernst potential of the electrolyte. In addition, the Butler-Volmer expression with $\alpha = 0.5$ cannot be used to describe the dependence of the observed current density on the potential of a semiconductor electrode.¹⁰⁻¹² The conventional Frumkin correction, which uses the value of the overpotential and the Butler-Volmer relationship to relate the values of the experimentally observed rate constant to the value of the standard rate constant,² is therefore not a particularly informative quantity for a semiconductor/liquid contact.

Instead, a more convenient approach is to set the reference potential of the semiconductor/liquid contact to be equal to the flat-band potential of the semiconductor electrode E_{fb} . At this potential, zero net charge exists on the semiconductor electrode, so the Frumkin correction term of eq 4.1 vanishes (Figure 4.1a). Additionally, at the flat-band potential $\phi_d = 0$ and $E_h = 0$, so the redox acceptor experiences the full driving force for the interfacial charge-transfer process due to the potential difference between the conduction band edge of the semiconductor electrode and the formal potential of the redox species. At other applied potentials, some of the potential will drop across the Helmholtz layer (Figure 4.1b). This potential drop will change the value of the interfacial driving force (by an amount qE_h) experienced by a redox species located at the outer Helmholtz plane. It is assumed for simplicity that a Butler-Volmer relationship with $\alpha = 0.5$ can be used to describe the variation in this rate constant over small changes in interfacial driving force, although a more rigorous treatment would utilize the Marcus-Gerischer formalism to perform the relevant analysis.¹² Within these constraints, eq 4.2 incorporates both the concentration gradient correction term of eq 4.1 and the kinetic correction term due to apparent band-edge movement, in order to relate $k_{et,E}$ to the value of the rate constant that would be measured at the flat-band potential of the semiconductor, $k_{et,E_{fb}}$.²

In accumulation conditions, eq 4.1 also describes the Frumkin correction for the

concentration of the oxidized redox species at the OHP. However, in contrast to depletion conditions, the rate constant is not a simple function of the incremental change in interfacial driving force across the solid/liquid interface, because the distribution in energy of the occupied electronic states of the semiconductor changes significantly as the electrode is biased into accumulation. The interfacial rate constant is thus a complicated function of potential in this region. Consequently, for accumulation conditions, only the Frumkin-like correction that is required to describe the potential actually experienced by the redox species at the OHP at a given potential of the semiconductor electrode has been computed.

Within the GCS theory, the differential capacitance of the electrolyte is given by the reciprocal relationship²

$$\frac{1}{C_{\text{soln}}} = \frac{1}{C_d} + \frac{1}{C_h} \quad (4.3)$$

where C_h is the differential capacitance of the Helmholtz layer, C_d is the differential capacitance of the diffuse layer, and C_{soln} is the total differential capacitance of the solution.

At a semiconductor/liquid interface, the differential capacitance of the semiconductor space-charge region, C_{sc} , and the differential capacitance of the solution are represented by capacitors connected electrically in series. Thus, the total differential capacitance, C_{total} , of the semiconductor/liquid junction can be expressed as

$$\frac{1}{C_{\text{total}}} = \frac{1}{C_{\text{sc}}} + \frac{1}{C_h} + \frac{1}{C_d} \quad (4.4)$$

For an incremental applied potential ΔE , the potentials across the various capacitive elements are readily computed to be

$$\Delta E = \Delta E_{\text{sc}} + \Delta E_h + \Delta E_d \quad (4.5)$$

where

$$\Delta E_{sc} = \Delta E \times \left(1 - \frac{C_{total}}{C_d} - \frac{C_{total}}{C_h} \right) \quad (4.6)$$

$$\Delta E_h = \Delta E \times \left(1 - \frac{C_{total}}{C_{sc}} - \frac{C_{total}}{C_d} \right) \quad (4.7)$$

$$\Delta E_d = \Delta E \times \left(1 - \frac{C_{total}}{C_{sc}} - \frac{C_{total}}{C_h} \right) \quad (4.8)$$

The actual applied potential E is most conveniently defined for computational purposes relative to the flat-band potential, at which $E_h = E_d = 0$. From this reference potential, eqs 4.6, 4.7, and 4.8 can be integrated numerically, using a finite difference approach for steps of ΔE to produce the desired potential E . This process yields values of E_{sc} , E_d , and E_h , the integral potential drop across the semiconductor, the diffuse layer, and the Helmholtz layer respectively, as a function of the electrode potential. In this notation, $\phi_d = E_d = E - E_{sc} - E_h$. The distribution of electrons in the space charge region of the semiconductor was assumed to be insensitive to the presence of a faradaic current across the solid/liquid contact because the transport of charge carriers in the solid is much more rapid than the mass transport or diffusive motion of redox ions in the solution.

Figure 4.1: Potential drops at a semiconductor/liquid interface (a) at the flat-band potential and (b) in depletion conditions; E is the applied potential, E_{sc} is the potential dropped across the space charge region of the semiconductor, E_h is the potential dropped across the Helmholtz layer, and E_d is the potential across the diffuse layer of the solution (i.e., the potential drop at the OHP, x_{ohp}). The position of the local vacuum level reflects the change in electrostatic potential at various positions in space perpendicular to the plane of the semiconductor/liquid contact. The relative potential distribution is exaggerated in the figure due to the large differences in the magnitudes of the various potential drops at the semiconductor/liquid contact.

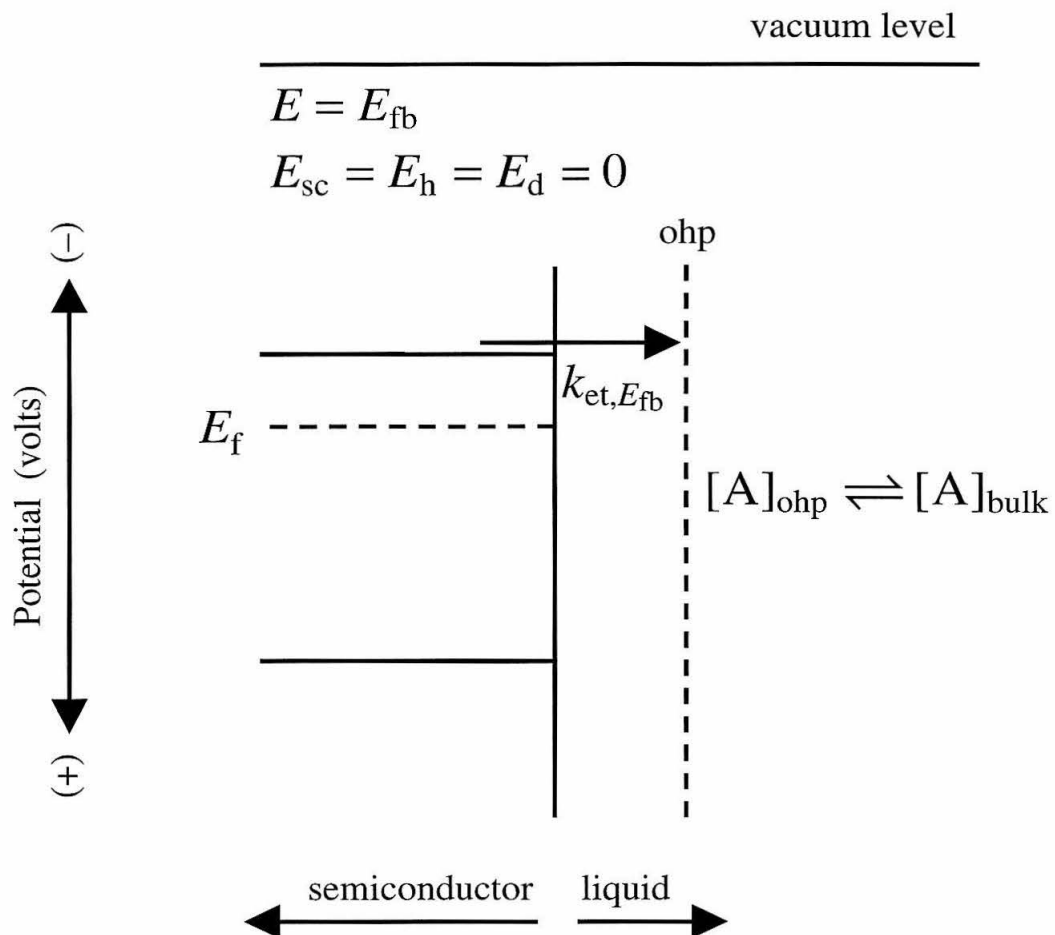


Figure 4.1a

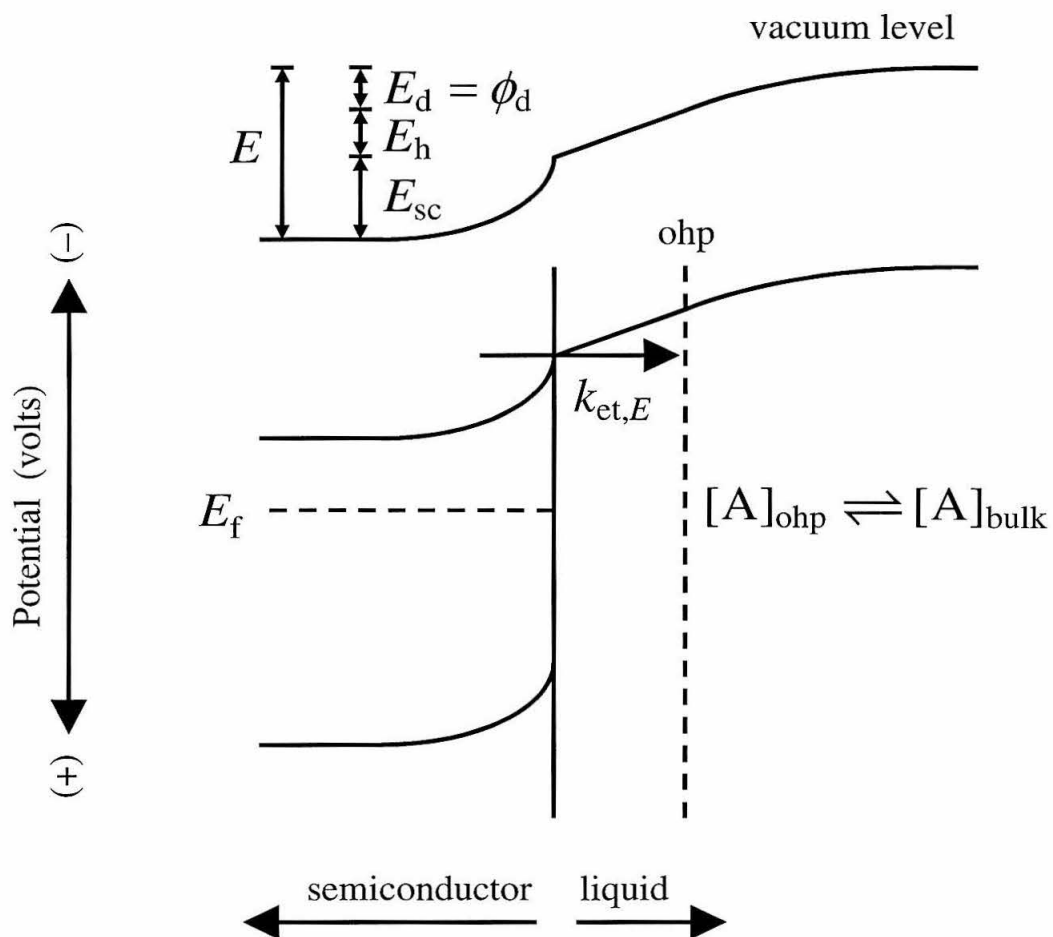


Figure 4.1b

III. RESULTS

A. Depletion Conditions

Under conditions that produce a depletion of majority carriers in the space-charge region of a non-degenerate semiconductor electrode, the differential capacitance of the semiconducting phase is given by the Mott-Schottky equation:¹⁶

$$C_{sc} = \left(\frac{q\epsilon_{sc}\epsilon_0 N_d}{2} \right)^{1/2} \left(E - E_{fb} - \frac{k_b T}{q} \right)^{-1/2} \quad (4.9)$$

where ϵ_{sc} and N_d are the dielectric constant and dopant density of the semiconductor respectively, and ϵ_0 is the permittivity of free space. Eq 4.9, which was obtained using the depletion approximation, has been shown to describe the value of C_{sc} to within a few percent for a semiconductor electrode under depletion conditions.¹⁷ A more exact treatment that includes the differential capacitance arising from mobile minority carriers under inversion conditions is available in the literature, but the simplified expression of eq 4.9 will be used in the discussion herein because this expression is a very accurate description of C_{sc} under moderate depletion conditions.

An expression for the differential capacitance of the solution containing a z:z electrolyte is given by²

$$\frac{1}{C_{soln}} = \frac{x_{ohp}}{\epsilon_s \epsilon_0} + \frac{1}{\left(\frac{2\epsilon_b \epsilon_0 zq[E]}{k_b T} \right)^{1/2} \cosh \left(\frac{zq\phi_d}{2k_b T} \right)} \quad (4.10)$$

where x_{ohp} is the width of the Helmholtz layer, ϵ_s is the dielectric constant of the solvent in the Helmholtz layer, ϵ_b is the dielectric constant of the bulk solvent, zq is the charge on the ions of the electrolyte, and $[E]$ is the concentration of electrolyte in the solution. The first term in eq 4.10 describes the differential capacitance of the Helmholtz layer, and the second term accounts for the differential capacitance of the diffuse layer.

It is useful (although not required) to introduce an approximation to aid in the

evaluation of ϕ_d as a function of E . Since the dopant density of non-degenerate semiconducting electrodes is typically only 10^{14} to 10^{17} cm^{-3} , a first-order calculation using eqs 4.9 and 4.10 at an electrolyte concentration $> 0.1\text{M}$ indicates that $C_{sc} \ll C_{soln}$ under depletion conditions. As a result, most of the potential drop will occur across the space charge region of the semiconductor. Thus ϕ_d will be sufficiently small that $zq\phi_d/2k_bT \ll 1$, so $\cosh(zq\phi_d/2k_bT) \approx 1.0$. This approximation can be checked for consistency after E_{sc} , E_d , and E_h are determined. Once the values of E_{sc} and E_h are known, ϕ_d can be computed, and the Frumkin terms of eqs 4.1 and 4.2 can then be calculated for the system of interest.

Figures 4.2 – 4.4 plot the values of E_{sc} , E_h , and E_d as a function of $E - E_{fb}$ for various dopant densities of an n-type semiconductor electrode in contact with a 1 M solution of a 1:1 electrolyte in CH_3OH . Since the values of E_h and E_d were very small under all conditions of interest, the quantities $1 - (E_h/E)$ and $1 - (E_d/E)$ have been plotted in Figure 4.3 and Figure 4.4 respectively. For these calculations, a Helmholtz layer thickness of $x_{ohp} = 5 \times 10^{-8}$ cm and a Helmholtz layer differential capacitance of $C_h = 5$ $\mu\text{f cm}^{-2}$, representative of methanolic solutions of 1.0 M LiCl,¹⁸ were used in eq 4.10. These values produce a dielectric constant of 3 for the solvent layer near the surface of the electrode, which is in agreement with experimental data on the differential capacitance of the Helmholtz layer for a 1 M electrolyte composition.¹⁸ Using these values, the computed value of E_h is generally on the order of 1 to 10 mV for semiconductors having a dopant density $< 1 \times 10^{16}$ cm^{-3} , while E_h is approximately 20 to 30 mV for a semiconductor with a dopant density of 1×10^{17} cm^{-2} (Figure 4.3). The value of ϕ_d is typically computed to be $< 1\text{mV}$ for all dopant densities investigated in this work (Figure 4.4).

Figure 4.5 depicts the values of the Frumkin correction term that describes the concentration profile of redox species in the electrolyte, for a semiconductor with dopant density 1×10^{15} cm^{-3} , resulting from the potential drop computations that are presented

in Figures 4.2 – 4.4. In these computations, the redox species was assumed to have a charge of $z = +2$, so that the Frumkin corrections of eqs 4.1 and 4.2 could be evaluated for some of the most highly charged outer-sphere redox species that have been used to date in kinetic measurements at semiconductor electrodes.^{3–9} As displayed in Figure 4.5, $[A]_{\text{ohp}}$ differed by no more than 2% from its value in the bulk of the solution, even at potentials greater than +1.0 V vs. E_{fb} . Even extreme cases which were not likely to be established experimentally, such as a semiconductor of dopant density $1 \times 10^{17} \text{ cm}^{-3}$ at an applied bias of +10 V vs. E_{fb} , only produced a 27% deviation of $[A]_{\text{ohp}}$ relative to $[A]_{\text{bulk}}$.

For a semiconductor of dopant density $1 \times 10^{15} \text{ cm}^{-3}$, Figure 4.6 depicts the value of $k_{\text{et},E_{\text{fb}}} / k_{\text{et},E}$ that results from eq 4.2. In no case was this correction significant in magnitude, with computed deviations of $k_{\text{et},E}$ relative to $k_{\text{et},E_{\text{fb}}}$ being $< 10\%$ for all conditions likely to be encountered experimentally. The corrections of eq 4.2 were $< 30\%$ of $k_{\text{et},E_{\text{fb}}}$ for semiconductors having dopant densities $\leq 1 \times 10^{16} \text{ cm}^{-3}$ (for $0.03 < E < 1.0 \text{ V}$), and were $< 100\%$ of $k_{\text{et},E_{\text{fb}}}$ for a semiconductor of dopant density $1 \times 10^{17} \text{ cm}^{-3}$ (for $0.03 < E < 0.6 \text{ V}$).

B. Accumulation Conditions

In accumulation, closed-form expressions have not been derived for C_{sc} as a function of E . A digital simulation was therefore utilized in order to evaluate the Frumkin corrections for the semiconductor/liquid interface in this applied potential regime. The GCS theory was again used to provide an approximate description of the potential distribution in the electrolyte. The simulation was performed with the ToSCA program, which self-consistently solves Poisson's equations in a semiconductor electrode as a function of potential, subject to various user-specified boundary conditions and initial conditions.^{19–21} The potential drops across the double layer of the solution were calculated from the conduction band-edge movements that were computed using the digital simulation program.

Figures 4.7 – 4.9 depict the dependence of E_{sc} , E_h , and E_d on $E - E_{fb}$ when an n-Si electrode of dopant density $1 \times 10^{15} \text{ cm}^{-3}$ is driven into accumulation. To perform these calculations, a 1:1 ratio of oxidized to reduced form of a cobaltocene redox couple was assumed. This redox solution produced a barrier height of 120 mV between the equilibrium conduction-band edge energy of the semiconductor at the solid/liquid junction and the equilibrium Fermi level of the semiconductor/liquid contact. A charge-transfer rate constant of $1 \times 10^{-18} \text{ cm}^4 \text{ s}^{-1}$ was used in order to produce current density-potential curves that displayed experimentally reasonable current densities. As displayed in Figure 4.7, the simulations with these input parameters reveal that an increasing fraction of the applied potential drops across the double layer of the solution as the potential of this n-type electrode becomes more negative. For example, a -1.0 V total applied bias vs. E_{fb} produces a total potential drop across the solution of approximately -0.63 V . The value of ϕ_d is also significant in accumulation, and determination of ϕ_d requires the incorporation of the hyperbolic cosine term in eq 4.10 to compute C_d . Values of C_d were obtained by computing E_d and successively re-evaluating C_d , E_d , and E_h until they converged to within 99.9% of their preceding values.

Figure 4.10 illustrates the Frumkin correction term of eq 1 that results from the potential distribution of Figures 4.7 – 4.9. For typical biases into accumulation, with $E_{fb} - E < 500 \text{ mV}$, $[A]_{ohp}$ differs from $[A]_{bulk}$ by up to a factor of 1.3. At an applied bias of -1.0 V vs. E_{fb} , the ratio of $[A]_{ohp}/[A]_{bulk}$ is 2.2.

Figure 4.11 displays the value of $(E - E_d)/E$, which represents the fractional deviation of the potential experienced by an acceptor species at the OHP from the value of the potential applied to the semiconductor/liquid interface, as a function of $E - E_{fb}$. In general, it is not possible to provide an analytical method to extrapolate the corrected rate constant to either the flat-band potential or to the standard Nernstian potential of the redox species, so the correction procedure for this situation was limited to computing the true potential experienced by the redox species at the OHP. In this fashion, the data of

Figure 4.11 allow correction of experimentally observed $k_{\text{et},E}-E$ data to the actual $k_{\text{et},E_{\text{fb}}}-E$ data to account for the actual potential experienced by the redox species undergoing the interfacial charge-transfer event. These rate constants can then be subjected to further analysis that might be appropriate to the system under study.

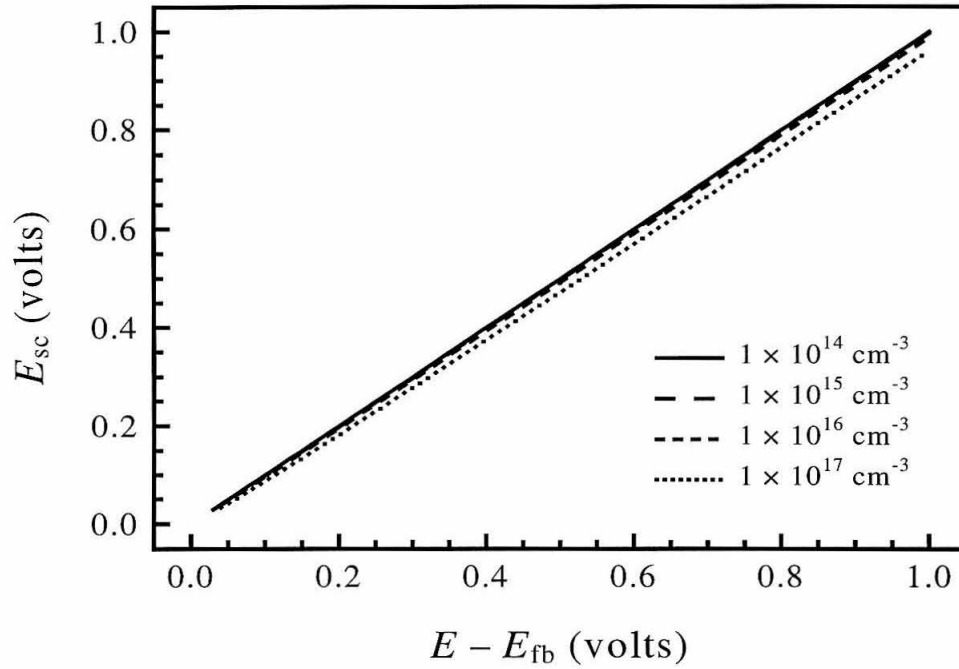


Figure 4.2: Plots of E_{sc} as a function of $E - E_{fb}$ for an n-Si electrode in depletion. Potentials were computed for the various dopant densities as indicated in the legend.

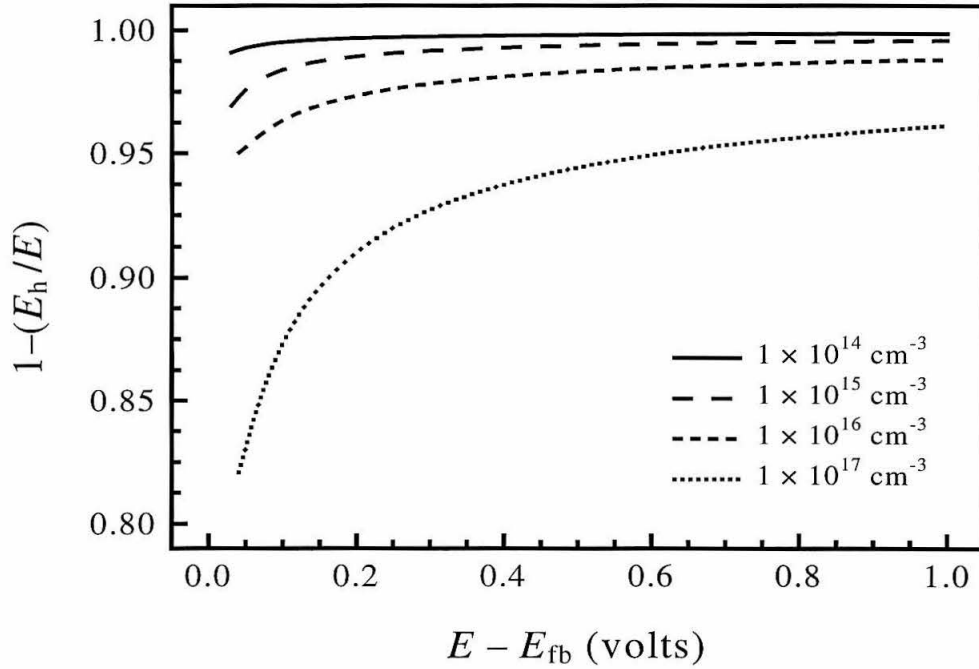


Figure 4.3: Plots of $1 - (E_h/E)$ as a function of $E - E_{fb}$ for an n-Si electrode in depletion.

Potentials were computed for the various dopant densities as indicated in the legend.

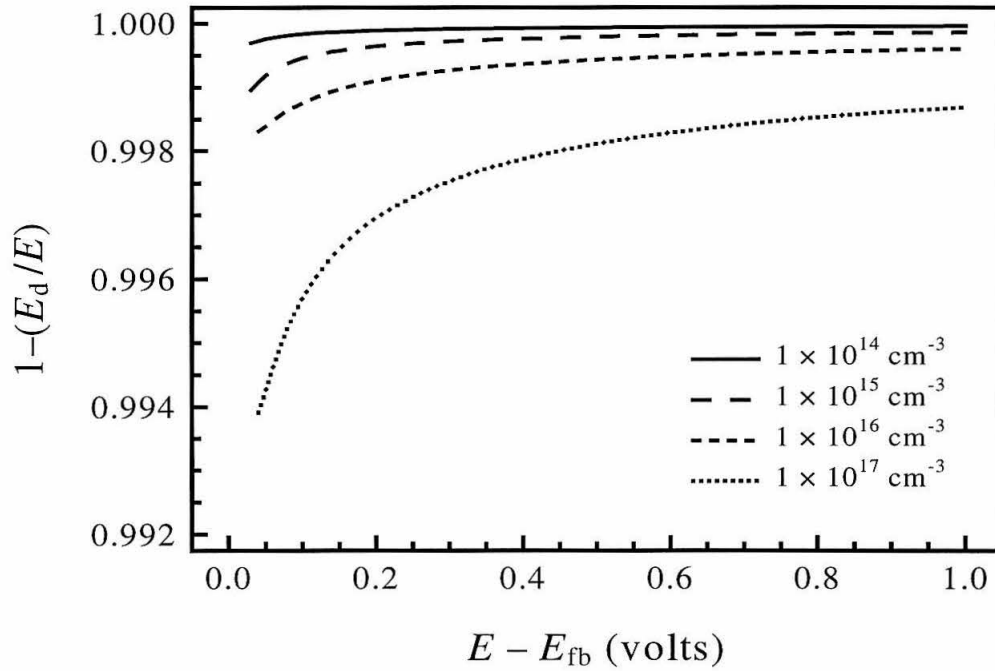


Figure 4.4: Plots of $1 - (E_d/E)$ as a function of $E - E_{fb}$ for an n-Si electrode in depletion. Potentials were computed for the various dopant densities as indicated in the legend.

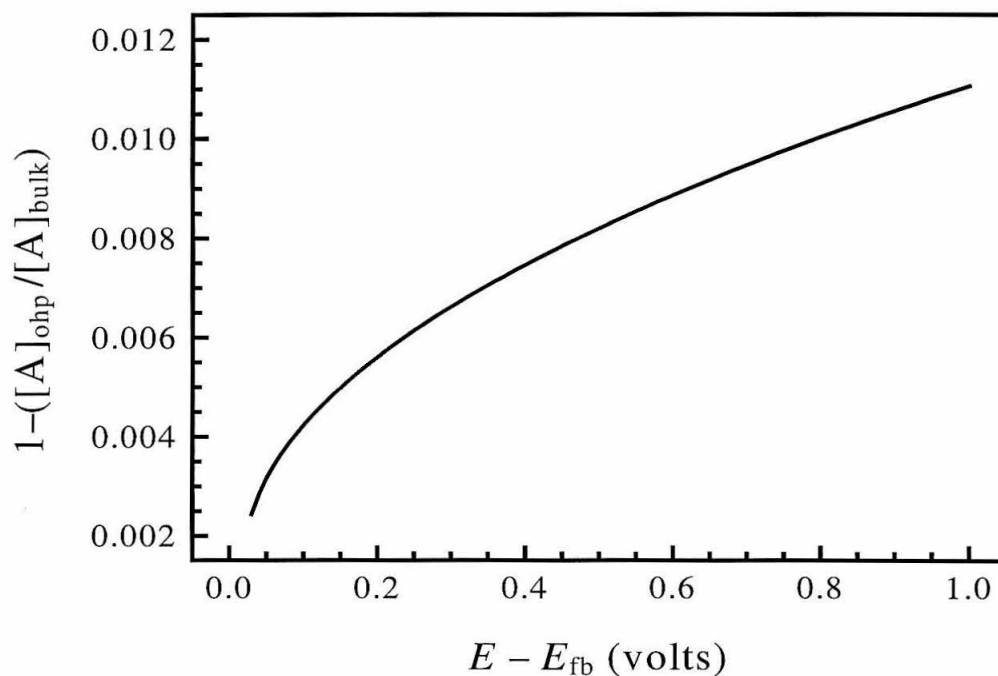


Figure 4.5: A plot of the ratio of the concentration of redox species at the OHP relative to the concentration of redox species in the bulk of the solution as a function of $E - E_{fb}$ for an n-type semiconductor electrode in depletion. A dopant density of $1 \times 10^{15} \text{ cm}^{-3}$ was used for these computations.

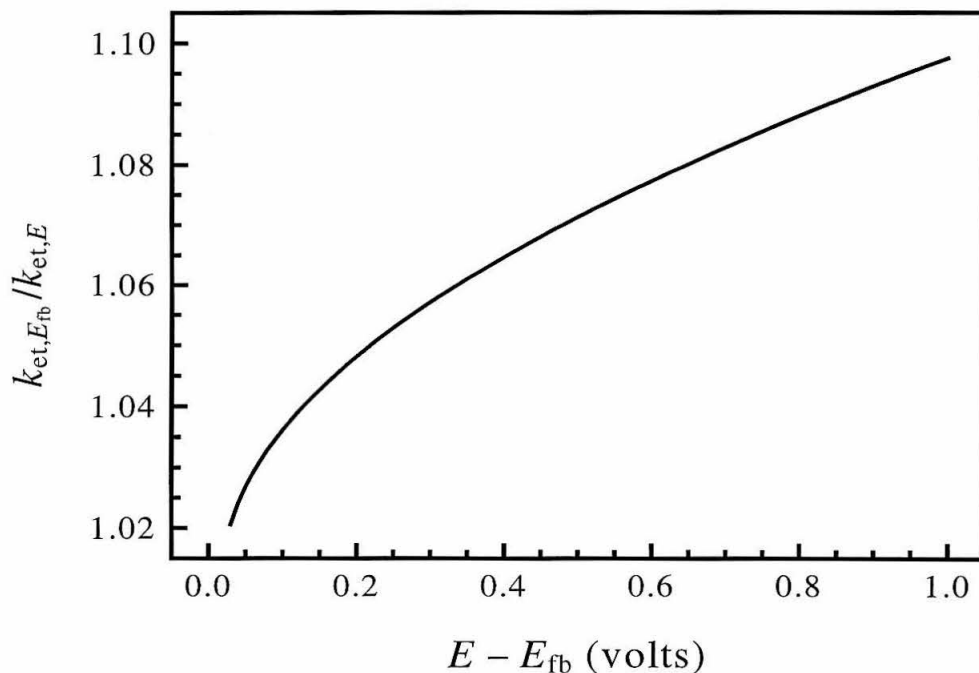


Figure 4.6: A plot of the Frumkin correction term for the heterogeneous rate constant for electron transfer from an n-type semiconductor electrode in depletion ($N_d = 1 \times 10^{15} \text{ cm}^{-3}$) to a redox species in the solution phase. The experimentally observed rate constant $k_{et,E}$ is corrected to its value at the point of zero net charge in the semiconductor, $k_{et,E_{fb}}$. The correction accounts for a potential drop across the Helmholtz layer affecting the rate constant as well as for effects of electrostatically-induced concentration gradients between the OHP and the bulk of the electrolyte solution.

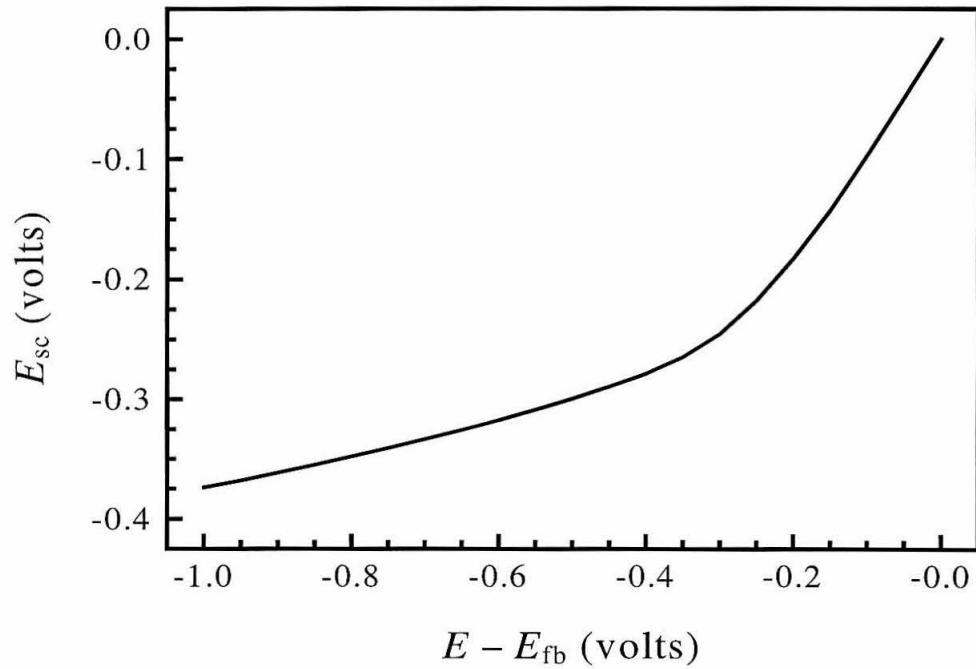


Figure 4.7: Potential dropped across the semiconductor as a function of $E - E_{fb}$ for an n-Si electrode in accumulation. All parameters are given in the text.

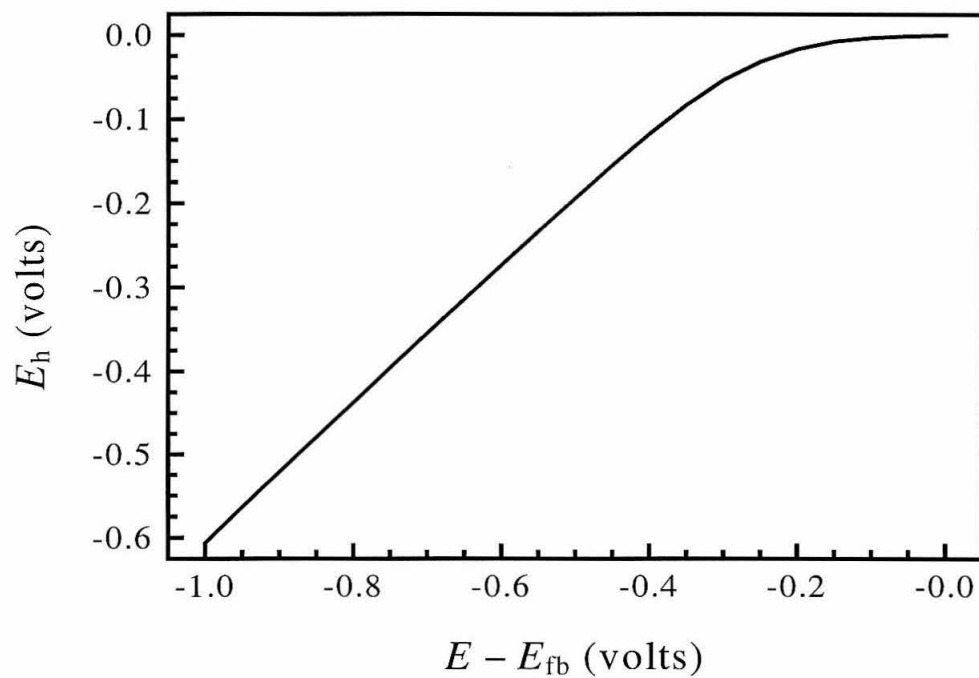


Figure 4.8: Potential dropped across the Helmholtz layer as a function of $E - E_{fb}$ for an n-Si electrode in accumulation. All parameters are given in the text.

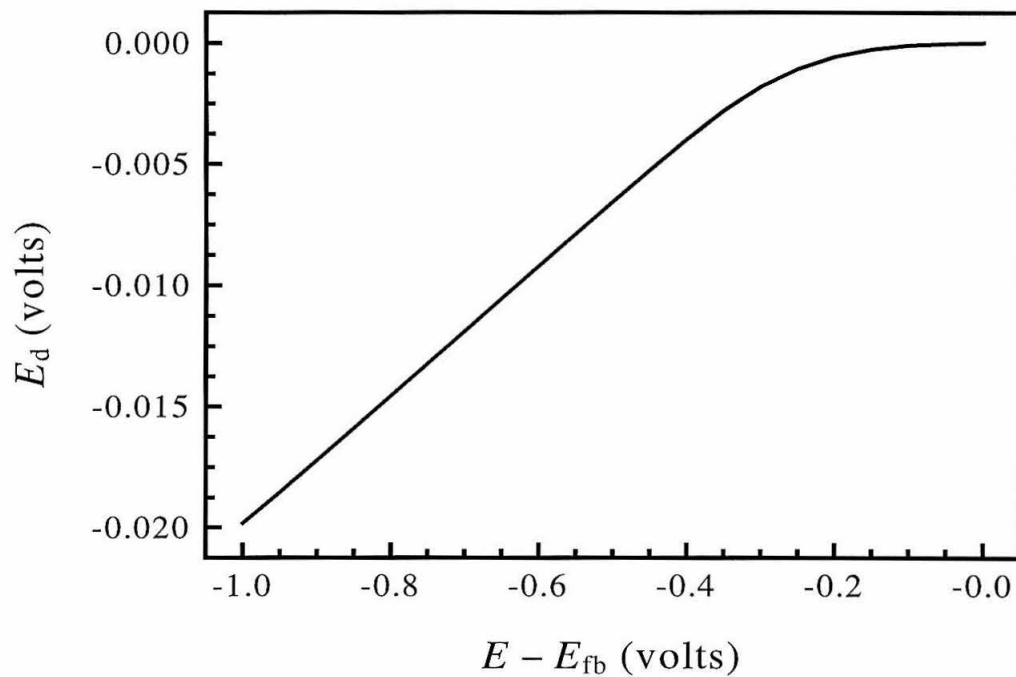


Figure 4.9: Potential dropped across the diffuse layer as a function of $E - E_{fb}$ for an n-Si electrode in accumulation. All parameters are given in the text.

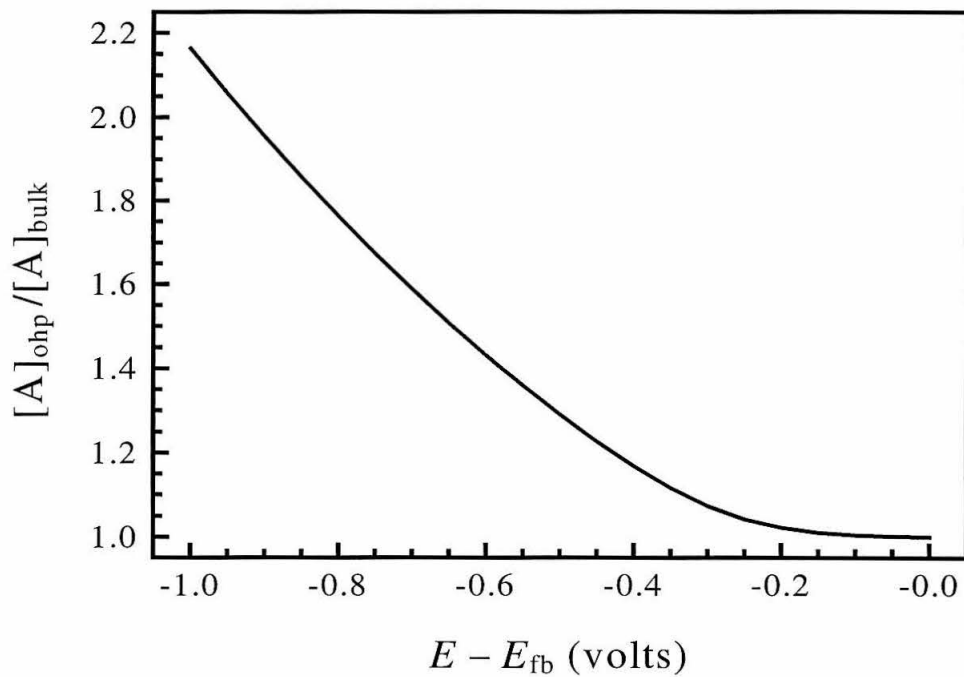


Figure 4.10: A plot of the ratio of the concentration of redox species at the semiconductor surface to the concentration of redox species in the bulk of the solution vs. $E - E_{\text{fb}}$ for an n-Si electrode in accumulation.

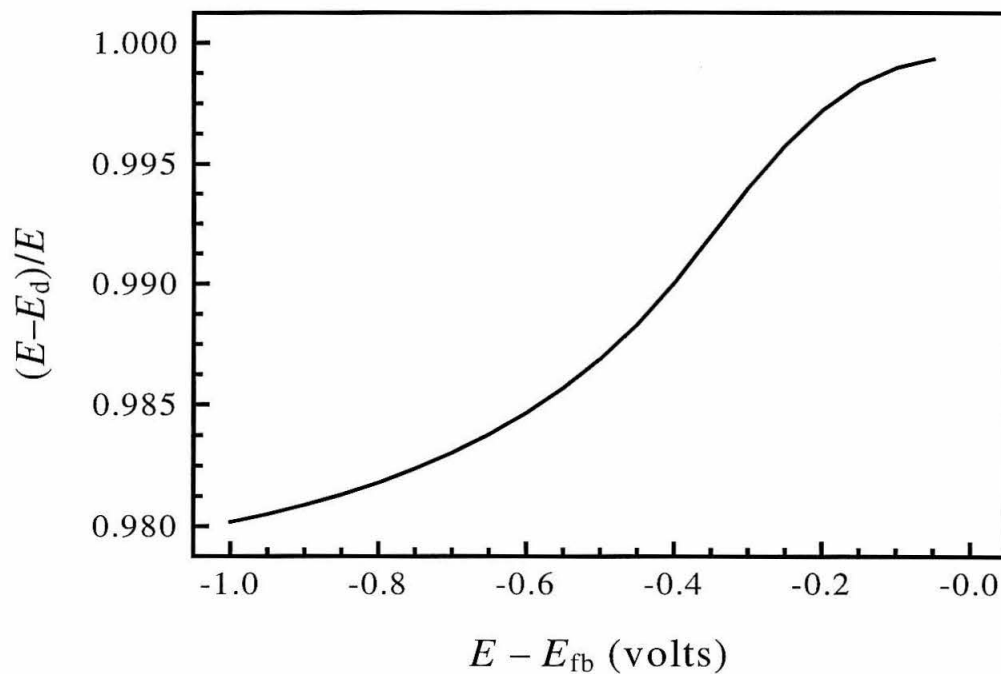


Figure 4.11: A plot of the driving-force correction influencing the interfacial rate constant for electron transfer at an n-type semiconductor driven into accumulation. The quantity $(E - E_d)/E$ represents the potential experienced by an acceptor species located at the OHP.

IV. DISCUSSION

The computations presented herein reveal that the Frumkin correction terms for a non-degenerately-doped semiconductor electrode in depletion are negligibly small compared to the typical error associated with the experimental determinations of charge-transfer rate constants of semiconductor electrodes. In depletion, the concentration of a non-adsorbing electroactive species at the OHP of a semiconductor/liquid contact is essentially identical to the concentration of the redox species in the bulk solution. Furthermore, the potential drop across the Helmholtz layer is a very small fraction of the potential applied to the electrode. Thus, within the framework of the GCS model, the observed rate constant is essentially the same as the Frumkin-corrected rate constant. Most experimental rate constant values that have been quoted previously in the literature for semiconductor/liquid contacts under depletion conditions therefore can be reliably viewed as excellent approximations to the Frumkin-corrected values for these charge-transfer rate constants.^{3-5,8,9}

This behavior can be readily understood from the basic properties of a semiconductor/liquid contact. In depletion, the small value of C_{sc} compared to C_h implies that even large positive excursions in the potential applied to an n-type semiconductor/liquid interface produce only small charge densities in the electrode. For instance, at $E = +1.0$ V vs. E_{fb} , the total charge density in a semiconducting electrode of dopant density $1 \times 10^{15} \text{ cm}^{-3}$ is only $9.3 \times 10^{-9} \text{ C cm}^{-2}$, whereas a +1.0 V potential applied to a metallic electrode (relative to its potential of zero charge) in contact with the same electrolyte produces a surface charge density of about $10^{-6} \text{ C cm}^{-2}$. Since the charge density in the semiconductor electrode is so small, the potential dropped across the liquid side of the double layer of a semiconductor/liquid junction is very small. Therefore, the Frumkin correction terms of eqs 4.1 and 4.2 are essentially negligible for these types of semiconductor/liquid contacts.

The computations underscore an advantage of semiconductor electrodes relative to

conventional solid metallic electrodes: since C_{sc} is so much smaller than C_{soln} , the flat-band potential, i.e., the point of zero charge, can be determined directly from differential capacitance vs. potential measurements. This arises because an analytical form of C_{sc} vs. E_{sc} is known for the space-charge region of the non-degenerately-doped semiconducting electrode (eq 4.9) and because $C_{sc} \approx C_{total}$ under depletion conditions for typical semiconductor/electrolyte contacts.

In accumulation, the situation is somewhat more complicated, because no closed-form expression has been obtained for the differential capacitance of the semiconductor electrode. In contrast to depletion conditions, a significant fraction of the applied potential will drop across the Helmholtz layer, and, under some circumstances, this potential drop may require a significant Frumkin correction to the surface concentration of redox species. The exact partitioning of the applied potential between the semiconductor and the Helmholtz layer will depend on the doping level of the semiconductor, the electrolyte concentration, and the faradaic interfacial charge-transfer kinetics, because rapid charge transfer will prevent accumulation of the carriers at the electrode surface, minimizing band-edge movement and minimizing the resulting potential drop across the Helmholtz layer. For the conditions simulated in this work, the correction to the driving force used to determine the true interfacial rate constant is less than 2% of the applied potential relative to the flat-band potential of the semiconductor electrode. Thus, the combined influence of the Frumkin correction terms will not significantly alter agreement between experiment and theory except at the most extreme applied biases in accumulation.

V. SUMMARY

Under moderate depletion conditions, a potential applied to a non-degenerately-doped semiconductor electrode drops almost entirely across the semiconductor space-charge layer and produces very little potential drop across the double layer of the electrolyte. For these conditions, the Frumkin corrections for charge-transfer rate constants within the GCS framework are small enough that they need not be considered except when an accuracy of better than 30% is required in determination of the heterogeneous charge-transfer rate constant. For semiconductor electrodes in accumulation, although a considerable portion of the applied bias can appear across the solution, significant Frumkin corrections are required only at potentials far removed from the flat-band potential of the semiconductor.

VI. REFERENCES

1. Frumkin, A. N. *Z. Phys. Chem. A* **1933**, *164*, 121.
2. Bard, A. J.; Faulkner, L. R. *Electrochemical Methods: Fundamentals and Applications*; Wiley: New York, 1980.
3. Horrocks, B. R.; Mirkin, M. V.; Bard, A. J. *J. Phys. Chem.* **1994**, *98*, 9106.
4. Howard, J. N.; Koval, C. A. *Anal. Chem.* **1994**, *66*, 4525.
5. Uhlendorf, I.; Reineke-Koch, R.; Memming, R. *J. Phys. Chem.* **1996**, *100*, 4930.
6. Rosenwaks, Y.; Thacker, B. R.; Ahrenkiel, R. K.; Nozik, A. J. *J. Phys. Chem.* **1992**, *96*, 10096.
7. Rosenwaks, Y.; Thacker, B. R.; Nozik, A. J.; Ellingson, R. J.; Burr, K. C.; Tang, C. L. *J. Phys. Chem.* **1994**, *98*, 2739.
8. Pomykal, K. E.; Fajardo, A. M.; Lewis, N. S. *J. Phys. Chem.* **1996**, *100*, 3652.
9. Fajardo, A. M.; Lewis, N. S. *Science* **1996**, *274*, 969.
10. Lewis, N. S. *Annu. Rev. Phys. Chem.* **1991**, *42*, 543.
11. Gerischer, H. *J. Phys. Chem.* **1991**, *95*, 1356.
12. Morrison, S. R. *Electrochemistry at Semiconductor and Oxidized Metal Electrodes*; Plenum: New York, 1980.
13. Smith, B. B.; Halley, J. W.; Nozik, A. J. *Chem. Phys.* **1996**, *205*, 245.
14. Finklea, H. O. *Semiconductor Electrodes*; Elsevier: New York, 1988.
15. Tan, M. X.; Laibinis, P. E.; Nguyen, S. T.; Kesselman, J. M.; Stanton, C. E.; Lewis, N. S. *Prog. Inorg. Chem.* **1994**, *41*, 21.
16. Gerischer, H.; Eyring, H. In *Physical Chemistry: An Advanced Treatise*; Yost, W., Ed.; Academic: New York, 1970; Vol. 9A; pp 463.
17. Many, A.; Goldstein, Y.; Grover, N. B. *Semiconductor Surfaces*; North-Holland: New York, 1965.
18. Schlichthörl, G.; Peter, L. M. *J. Electrochem. Soc.* **1995**, *142*, 2665.
19. Gajewski, H. *GAMM (Gesellschaft für Angewandte Mathematik und Mechanik) Mitteilungen* **1993**, *16*, 35.
20. Krüger, O.; Jung, C.; Gajewski, H. *J. Phys. Chem.* **1994**, *98*, 12653.

21. Krüger, O.; Kenyon, C. N.; Tan, M. X.; Lewis, N. S. *J. Phys. Chem.* **1997**, *101*, 2840.

Chapter 5

Time-Resolved Photoconductivity Decay Measurements of Chemically Modified Silicon Surfaces

I. INTRODUCTION

The passivation of Si to produce low surface recombination velocities is critical for a number of applications such as CMOS devices¹ and photovoltaics.^{2,3} In silicon/liquid systems, low surface recombination velocities are desirable for monitoring the presence of contaminants in electrolyte solutions during etching and wet-processing stages of device fabrication^{4,5} and for designing efficient Si-based photoelectrochemical energy conversion devices.⁶ Under certain nearly ideal conditions, the surface recombination velocity of a Si/SiO₂ interface can be as low as 3 cm s⁻¹.^{7,8} Although ultrathin Si oxides with such electrical characteristics are suitable for new generations of microelectronic devices, control of the interfacial properties and thicknesses of ultrathin Si oxides is often difficult. Hydrogen-terminated, (111)-oriented Si surfaces in contact with concentrated H₂SO₄(aq), concentrated HF(aq), and other acidic aqueous media also exhibit very low surface recombination velocities.⁹ However, the surface recombination velocities of these surfaces degrade rapidly upon exposure to ambient air.

Another method that has been used to produce low effective surface recombination velocities in silicon is immersion into methanol solutions containing one-electron oxidants such as 1,1'-dimethylferrocenium (Me₂Fc⁺⁰).¹⁰⁻¹² Silicon surfaces in contact with I₂ or Br₂ in methanol, ethanol, or tetrahydrofuran (THF) also exhibit low surface recombination velocities.^{4,13-16} The behavior of the Si surface in iodine-containing systems has been ascribed to passivation resulting from either formation of Si-I bonds¹⁵ or Si-alkoxide bonds.⁵ In this chapter, lifetime measurements have been performed to show that the previously observed carrier recombination dynamics are not due to an inherently low surface trap density, but rather, the formation of an inversion layer induced by electrochemical reactions between the Si and the oxidants in these redox-active electrolyte solutions. The studies presented herein also indicate that the trap density on the Si surface obtained from many of these surface reactions is in fact relatively high compared to that of the hydrogen-terminated Si surface in acid

electrolytes.

An alternative method for passivating silicon surfaces, based on recent developments in silicon surface chemistry, has also been explored in this work. Crystalline Si has been functionalized previously at atmospheric pressure with organic layers through the use of alkyl Grignard and alkyl lithium reagents,¹⁷ alkenes,¹⁸⁻²⁰ and phenyldiazonium salts,²¹ while the reaction chemistry of porous Si has been developed yet further to include the use of alkynes^{22,23} and organohalides.²⁴ The electrochemical properties of some of these surfaces have been detailed,^{25,26} but previously there have been no reports concerning the electrical properties of such systems. The work described in this chapter shows that crystalline Si functionalized through a two-step, wet-chemistry-based chlorination/alkylation procedure¹⁷ has an extremely low surface recombination velocity. Furthermore, the electrical passivation persists for extended time periods even for surfaces in contact with ambient air.

II. EXPERIMENTAL

A. Surface Treatments and Redox Solutions

Long bulk lifetime ($> 200 \mu\text{s}$), (111)-oriented float-zone silicon wafers were obtained from Virginia Semiconductor. The double-polished wafers were $190 - 200 \mu\text{m}$ thick and nominally n-type (phosphorous-doped) with resistivities of $3817 - 3826 \text{ ohm cm}$ as specified by the manufacturer. Photoconductivity decay measurements were made using samples $\approx 1 \text{ cm}^2$ in area cut from the wafers. Prior to alkylation reactions, samples were etched in 5:1 (v/v) 40% $\text{NH}_4\text{F}/49\% \text{ HF(aq)}$ (Transene Co.) for 30 seconds and subsequently in 40% NH_4F (aq) (Transene Co.) for 15 minutes, rinsed with distilled H_2O ($18.2 \text{ M}\Omega \text{ cm}$ resistivity), and dried in a stream of $\text{N}_2(\text{g})$. Prior to all other surface treatments, samples were etched in 40% NH_4F (aq) for 15 minutes, rinsed with distilled H_2O , and dried under a stream of $\text{N}_2(\text{g})$.

For alkylation reactions, anhydrous methanol (Aldrich) was used without further purification; for all other surface treatments, methanol was obtained from EM Science and distilled over magnesium turnings prior to use. Anhydrous tetrahydrofuran (THF), anhydrous acetonitrile, anhydrous chlorobenzene, phosphorous pentachloride, benzoyl peroxide, methylmagnesium chloride (in THF), octylmagnesium chloride (in THF), and iodine were purchased from Aldrich and used without further purification. Ferrocene (Fc^0) and bis(pentamethylcyclopentadienyl) iron ($\text{Me}_{10}\text{Fc}^0$) were acquired from Strem and were sublimed before use. Ferrocenium (Fc^+) was obtained from Aldrich and was recrystallized from a mixture of THF and acetonitrile. Bis(pentamethylcyclopentadienyl) iron tetrafluoroborate ($\text{Me}_{10}\text{Fc}^+$) was synthesized from sublimed $\text{Me}_{10}\text{Fc}^0$ according to published methods.²⁷ All solutions were prepared and stored in a $\text{N}_2(\text{g})$ -purged flushbox containing less than 10 ppm of $\text{O}_2(\text{g})$ as indicated by the absence of visible fumes from diethyl zinc. For solutions containing Fc^+ or $\text{Me}_{10}\text{Fc}^+$, the concentrations of oxidized redox species were determined by measuring the solution potentials vs. a CH_3OH -based calomel reference electrode.

Alkylation reactions of hydrogen-terminated silicon were performed under $N_2(g)$. Samples were first immersed in a solution of PCl_5 -saturated chlorobenzene containing $\approx 10^{-2}$ M benzoyl peroxide for 45 minutes at a temperature of 90 – 100 °C. After rinsing with anhydrous THF and CH_3OH , the samples were dried in a stream of $N_2(g)$. The samples were then immersed in a solution containing the appropriate Grignard reagent in THF. Alkylation reactions were performed at a temperature of 70 – 80 °C for either 8 hours (for CH_3MgBr) or 24 hours (for $C_8H_{17}MgBr$). The reacted samples were subsequently washed with THF followed by CH_3OH , sonicated in CH_3OH then CH_3CN (under an air ambient), and dried in a stream of $N_2(g)$.

B. Photoconductivity Decay Measurements

A schematic of the contactless rf conductivity apparatus used to measure photoconductivity decays is shown in Figure 5.1. In this system, the output from a high-frequency signal generator (Wavetek 2500A or Rohde & Schwarz SMY01) operating at 450 MHz was connected to a power splitter (Mini-Circuits ZSC2-1W). One output from the power splitter was connected through an amplifier (ANZAC AM-147, +17 dB gain) and a phase-shifter (General Radio 847-LTL) to the local oscillator input of a double-balanced frequency mixer (Mini Circuits ZAY-2), and the other output from the power splitter was connected through an amplifier (Mini-Circuits ZHL-1A, +20 dB gain) to the coupled port of a directional coupler (Merrimac CR-20-500, 20 dB isolation). An LC circuit consisting of a variable coupling capacitor (1-11 pF, air gap), a variable matching capacitor (1-11 pF, quartz), and a 3-turn coil (Cu wire, 1.1 mm diameter) placed in close proximity to the sample, was connected to the input port of the directional coupler. The output port of the directional coupler was then connected through an attenuator (Kay 0/400A, 0 to –13 dB) to the reference oscillator port of the double-balanced frequency mixer, and the output of the double-balanced frequency mixer was connected to a digital oscilloscope (Tektronix TDS-210) for measurement of the photoconductivity decay

signals. Prior to each measurement, the LC circuit was tuned to the resonant frequency of the sample by adjusting the variable capacitors and monitoring the amplitude of the reflected rf signal on a separate high frequency digital oscilloscope (Tektronix TDS-680c).

Samples were illuminated using 10 ns pulses from a Nd:YAG laser (Spectra-Physics INDI-30, 1064 nm) operating at a repetition rate of 10 Hz. The power density of the beam was attenuated using a beam splitter and neutral density filters, and the beam was expanded to approximately 3 cm² using a Gallilean beam expander. A holographic diffuser (Coherent, 1°) placed directly above the sample was used to produce a spatially uniform beam profile on the silicon substrate. Using the neutral density filters, the power density of the expanded, incident beam was adjusted to either 2×10^{-3} mJ pulse⁻¹ for high-level injection conditions or 3×10^{-6} mJ pulse⁻¹ for low-level injection conditions. A power meter (Coherent Fieldmaster GS) equipped with a pyroelectric sensor (Coherent LM-P10i) was used to determine the incident beam power. During measurements of the charge carrier lifetime, the sample was placed into a sealed glass vessel that allowed measurements of the sample in contact with N₂(g), air, or various liquid solutions. Time constants were obtained by fitting the average of 128 decays to a single exponential and averaging over a minimum of three samples for each type of surface at each measurement interval.

C. X-ray Photoelectron Spectroscopy Measurements

X-ray photoelectron (XP) spectra were acquired with an M-Probe surface spectrometer (Surface Science Instruments) operating at a base pressure of $< 6 \times 10^{-10}$ torr. Monochromatic, focused Al K $\alpha_{1,2}$ (1486.6 eV) irradiation was used to excite the sample, and the beam was directed at the surface of the substrate at an angle of 35° from the surface plane. Photoejected electrons were collected using a hemispherical analyzer also positioned at an angle of 35° from the surface plane. Spectra in the Si 2p region

were recorded in unscanned mode for 15 minute intervals (54.5 eV pass energy) using a circular X-ray spot with a diameter of 300 μm . Oxide coverages were determined by use of an overlayer model that has been described previously.^{28,29}

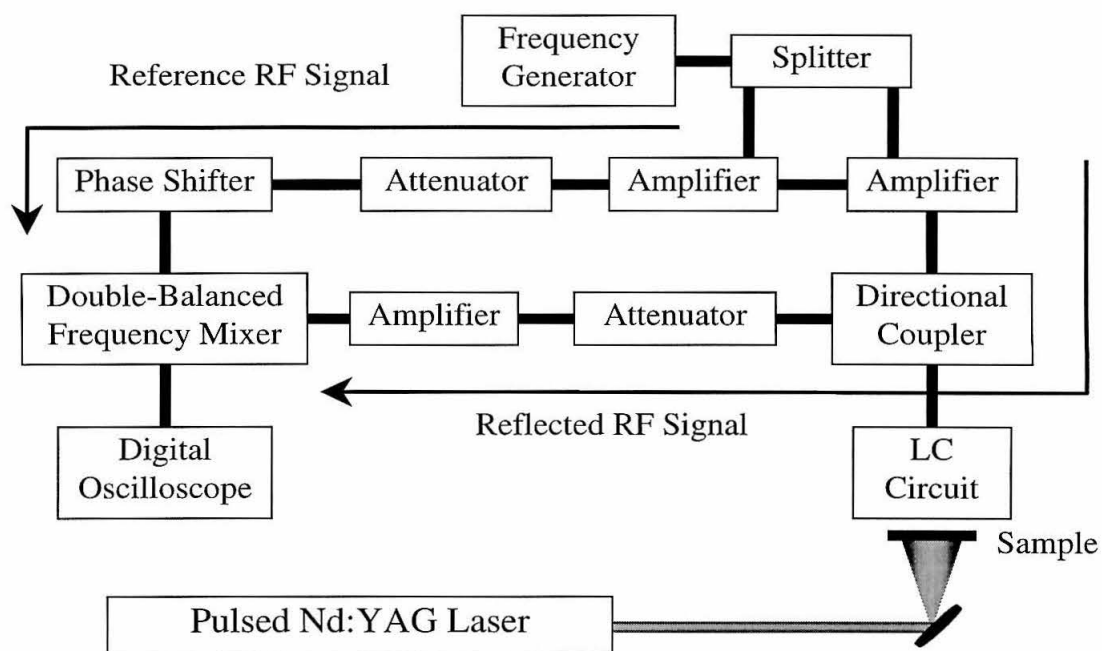


Figure 5.1: A schematic of the rf apparatus used to acquire photoconductivity decays.

The attenuator in the reference branch of the circuit was bypassed in these experiments.

III. RESULTS

A. Photoconductivity Decay Measurements of Hydrogen-Terminated Si(111) in Aqueous Acids and in Air

Figure 5.2 shows a representative rf conductivity decay signal of (111)-oriented, H-terminated Si in contact with concentrated $\text{H}_2\text{SO}_4(\text{aq})$ under low-level injection. The decays were very slow and could be fit well by a single exponential. The mean decay lifetime for samples from this wafer was $490 \pm 50 \mu\text{s}$ under low-level injection and $800 \pm 100 \mu\text{s}$ under high-level injection, which is consistent with the manufacturer's specification that the minority carrier lifetime is $> 200 \mu\text{s}$. The observed lifetime, τ , can be related to the bulk lifetime, τ_b , and surface recombination velocity, S , through the following expression:^{9,30,31}

$$S = \frac{d}{2} \left(\frac{1}{\tau} - \frac{1}{\tau_b} \right) \quad (5.1)$$

where d is the sample thickness. Assuming that the experimentally observed lifetime is dominated by surface recombination implies that $S = 19 \pm 2 \text{ cm s}^{-1}$ under low-level injection and $12 \pm 2 \text{ cm s}^{-1}$ under high-level injection. Of course, these values are an upper bound on the true surface recombination velocity because they assume that the observed lifetime is dominated only by surface recombination, with no contribution from charge-carrier recombination in the bulk of the sample.

Subsequent immersion of these samples in 48% $\text{HF}(\text{aq})$ produced somewhat shorter lifetimes of $180 \pm 60 \mu\text{s}$ under low-level injection and $460 \pm 90 \mu\text{s}$ under high-level injection. These observations are in accord with the prior observations of Yablonoitch et al. that S for H-terminated, (111)-oriented Si surfaces is a function of the acidity of the electrolyte.⁹ Re-exposure to concentrated $\text{H}_2\text{SO}_4(\text{aq})$ solutions reversed the decline in surface lifetime. Exposure of a hydrogen-terminated surface to air produced a rapid decay in the carrier lifetime, with lifetimes as short as $10 \mu\text{s}$ observed within two hours of

exposure to an atmospheric ambient (Figures 5.2). The small τ value was persistent in air, and a long lifetime could only be recovered by re-etching the Si surface and/or by re-immersion of the crystal into a highly acidic aqueous electrolyte. This behavior was observed under both low-level and high-level injection conditions.

The lifetimes measured in $\text{H}_2\text{SO}_4(\text{aq})$ are useful for setting lower bounds on the bulk lifetime in order to obtain S values for other surfaces. For many of the surfaces that will be described below, however, the measured lifetimes approach, or in some cases exceed, the values of the lifetimes obtained for the same wafer in $\text{H}_2\text{SO}_4(\text{aq})$. In these instances, it is more appropriate to use an infinite bulk lifetime for computations of S from eq 5.1. For the remainder of the discussion, the more conservative approach is typically used, and S values are reported assuming $\tau_b = \infty$. In this case, it is important to note that the reported S values represent upper limits to the true value of S . Where applicable, S values have also been computed assuming τ_b is the lifetime for the same wafer measured in $\text{H}_2\text{SO}_4(\text{aq})$; these data are presented in the tables.

B. Photoconductivity Decay Measurements of NH_4F -Etched Si(111) in CH_3OH or THF Solutions Containing Electrochemical Oxidants

Figure 5.3 displays the photoconductivity decay data observed for $\text{NH}_4\text{F}(\text{aq})$ -etched Si in contact with CH_3OH –0.05 M I_2 . The mean decay for surfaces treated in this fashion was very slow, with a lifetime of $600 \pm 300 \mu\text{s}$ (Table 5.1). Using eq 5.1, assuming an infinite bulk lifetime and $d = 195 \mu\text{m}$, an upper bound on the surface recombination velocity for this type of sample was determined to be $16 \pm 8 \text{ cm s}^{-1}$. However, when the Si sample was removed from the CH_3OH –0.05 M I_2 solution and rinsed with methanol, the lifetime observed in a $\text{N}_2(\text{g})$ ambient was significantly shorter (Figure 5.3), corresponding to $S = 810 \pm 70 \text{ cm s}^{-1}$ under high-level injection and $S = 1300 \pm 100 \text{ cm s}^{-1}$ under low-level injection (Figure 5.3, Table 5.1). The effect was completely reversible in that re-immersion of the surface into the CH_3OH –0.05 M I_2 electrolyte again

resulted in a long lifetime for the rf photoconductivity decay, and removal and rinsing again produced a short lifetime value in contact with $N_2(g)$.

Somewhat different behavior was observed for $NH_4F(aq)$ -etched Si(111) surfaces that were immersed into a $CH_3OH-0.05 M Fc^{+/0}$ electrolyte solution (Figure 5.4). The mean carrier lifetime observed in contact with this electrolyte under high-level injection conditions was $700 \pm 200 \mu s$, indicating an upper limit on the effective S value of $14 \pm 4 cm s^{-1}$ (Table 5.1). These observations are in accord with earlier measurements of the effective surface recombination velocity for silicon in contact with $CH_3OH-Me_2Fc^{+/0}$ solutions which have a Nernstian potential within 100 mV of $CH_3OH-Fc^{+/0}$.^{10,12} However, in contrast to the behavior observed for $CH_3OH-0.05 M I_2$ solutions, after rinsing with CH_3OH the value of S for this surface was only slightly higher in $N_2(g)$ than in contact with the electrolyte solution (Figure 5.4, Table 5.1). The effect observed in this solution was again completely reversible.

The reactions of (111)-oriented Si surfaces with these two electrolytes have been investigated recently using X-ray photoelectron spectroscopy and infrared spectroscopy.³² These measurements indicate that contact with $CH_3OH-0.05 M Fc^{+/0}$ primarily produces a methoxylated Si surface, as does reaction with CH_3OH-I_2 solutions.³² However, immersion of Si into CH_3OH-I_2 also leaves a low surface coverage of iodine.³² The data of Table 5.1 therefore indicate that I_2 is not needed to obtain a low effective S value for (111)-oriented Si in contact with a methanol electrolyte and in fact is deleterious to the recombination properties of such surfaces when subsequently measured in contact with a $N_2(g)$ ambient. However, the above experiments do not by themselves indicate whether formation of surface Si-alkoxide bonds is required to produce low S values in electrolyte solutions or whether some other effect dominates the observed charge-carrier recombination dynamics in contact with the liquid-phase ambients.

To address this issue, photoconductivity decay data were collected for Si surfaces

in contact with THF as the solvent. In THF–0.05 M I₂ solutions, the Si surface recombination velocity was low, $S = 40 \pm 10 \text{ cm s}^{-1}$ (Figure 5.5, Table 5.1), in qualitative accord with prior observations on this system.⁴ Similarly, the observed carrier lifetime for NH₄(aq)-etched Si samples in contact with THF–0.05 M Fc–0.005 M Fc⁺ solutions was also quite long, corresponding to S values of $50 \pm 30 \text{ cm s}^{-1}$ (Figure 5.6, Table 5.1). With this latter treatment, however, no Si-alkoxide species can be formed, nor are Si-I bonds present. Surface infrared spectroscopic measurements show nearly complete retention of the H-termination after immersion into this electrolyte.³² These results indicate that Si-alkoxide bond formation is not required to produce low effective S values in contact with these electrolyte solutions. Rinsing with solvent and contacting the sample with N₂(g) produced a high S value, and the effect was reversible in that re-immersion into THF–0.05 M Fc–0.005 M Fc⁺ or into THF–0.05 M I₂ solutions produced a long carrier decay lifetime even after observation of a short lifetime in contact with N₂(g) (Table 5.1).

Use of a redox species having a more negative redox potential, decamethylferrocene⁺⁰ (Me₁₀Fc⁺⁰), produced a significantly shorter carrier decay lifetime, and a significantly higher value of S , regardless of whether the sample had only been etched in NH₄(aq) or had been etched and then immersed into a Fc⁺–THF solution prior to contact with the THF–Me₁₀Fc⁺⁰ solution (Figure 5.6, Table 5.1). Additionally, removal of the sample from the THF–Me₁₀Fc⁺⁰ solution and immersion into the THF–Fc⁺⁰ solution restored a low effective surface recombination velocity, with $S = 40 \pm 10 \text{ cm s}^{-1}$ observed under such conditions (Table 5.1). This indicates that the electrochemical potential of the electrolyte solution is a critical factor in producing the observed surface recombination velocity values in these systems.

C. Photoconductivity Decay Measurements of Air-Oxidized Si(111) in CH₃OH or THF Solutions Containing Electrochemical Oxidants

To further elucidate the role of the electrochemical potential of the solution in determining the measured value of S , experiments were performed with oxidized surfaces to investigate systems in which no chemical reaction is feasible between the constituents of the electrolyte and the states at the Si/SiO₂ interface. Figure 5.7 shows the time-resolved rf conductivity decay dynamics of a Si sample that had been deliberately oxidized for five days in air prior to measurement of S . The S value in N₂(g) of such a sample was relatively high, as expected for an electrically-defective Si/SiO₂ interface. The XP of this interface in the Si 2p region indicated the presence of approximately 4 Å of silicon oxide on the Si surface. Despite the presence of the oxide precluding reaction of the Si surface bonds with species in the electrolyte, immersion of such a sample into CH₃OH–0.05 M I₂ or into CH₃OH–0.05 M Fc⁺ produced a long photoconductivity decay and a low effective S value. Again the effect was reversible in that removal from the solution produced a high effective S value in contact with an N₂ ambient (Table 5.2). The XP spectra of the sample after removal from the electrolyte still showed a significant amount of surface oxidation and provided no evidence for the formation of Si-alkoxide or Si-I bonds at the Si surface. Relatively high S values were then observed upon immersion of these samples into a THF–0.05 M Me₁₀Fc–0.01 M Me₁₀Fc⁺ solution, again indicating the critical role of the redox potential of the electrolyte in producing the low effective S values for Si in contact with CH₃OH–0.05 M I₂ or with CH₃OH–0.05 M Fc⁺ solutions.

D. Photoconductivity Decay Measurements of Alkylated Si(111) in Air

Figure 5.8 depicts the behavior of a methylated Si surface in air. The observed mean lifetime was $260 \pm 50 \mu\text{s}$ under low-level injection and $290 \pm 80 \mu\text{s}$ under high-level injection. Assuming τ_0 is the lifetime from the same wafer in H₂SO₄(aq), the

surface recombination velocity is computed to be 17 ± 7 and 21 ± 9 cm s^{-1} for low-level and high-level injection, respectively. As shown in Figure 5.9, these lifetimes were stable in ambient air for extended time periods, with no degradation in lifetime observed for the methylated Si surface after at least 30 days in an air ambient.

Similar experiments were performed with (111)-oriented Si surfaces that had been treated with $\text{H}_{17}\text{C}_8\text{MgBr}$ instead of with CH_3MgBr . After 168 hours of exposure to room air, an octylated Si surface exhibited lifetimes (310 ± 90 μs under low-level injection and 300 ± 100 μs under high-level injection), and hence S values, that were essentially identical to those of the methylated surfaces.

A monolayer comprised of longer alkyl chains could potentially act as an improved hydrophobic barrier towards oxidation, thereby enhancing the surface stability relative to methylated Si surfaces. However, due to methylene-methylene repulsions, alkyl chains longer than one carbon cannot be used to cover every topmost Si atom on the (111)-oriented Si surface.³³ This lack of complete reactivity might preclude passivation of the entire surface and therefore result in decreased stability after substantially longer term exposure to air.

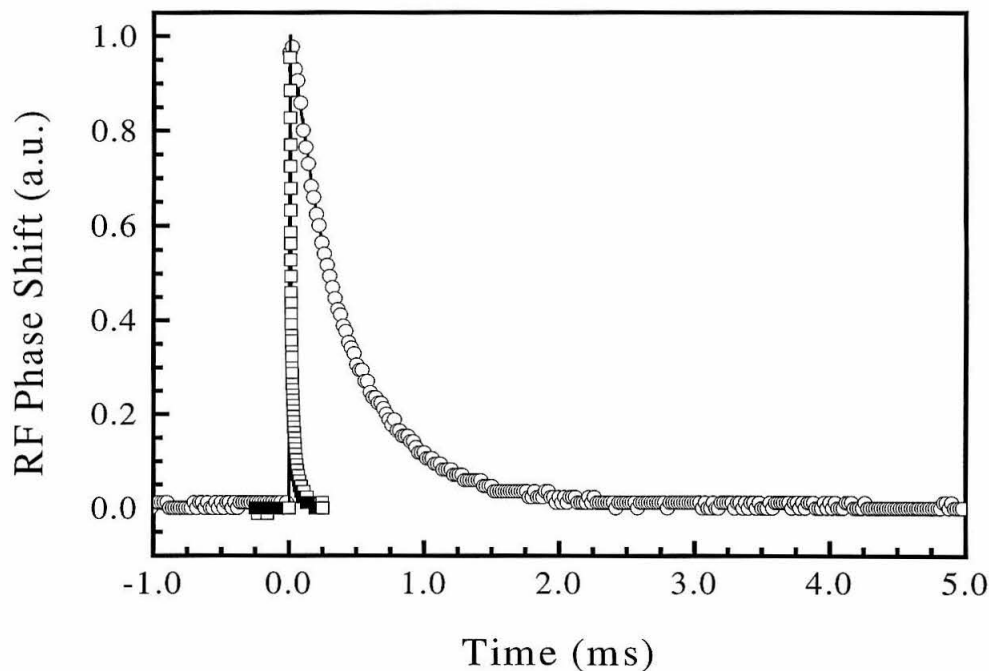


Figure 5.2: Time-resolved photoconductivity decay of hydrogen-terminated (111)-oriented n-type Si in contact with concentrated sulfuric acid (circles). Exposure of this sample to air for 30 minutes led to much more rapid conductivity decays (squares). A single-exponential fit to these decays (not shown) yielded a time constant of 434 μs for the H_2SO_4 -immersed sample and 19 μs for the air-exposed sample. Measurements were made under low-level injection conditions (1×10^{13} injected carriers cm^{-2} in a 190 μm thick sample).

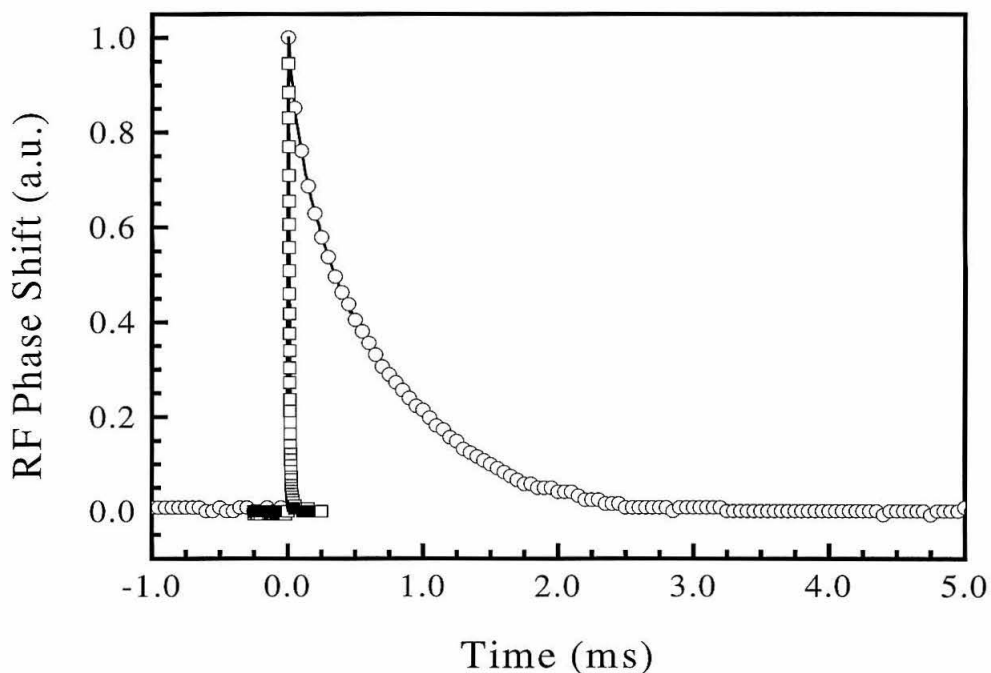


Figure 5.3: Time-resolved photoconductivity decay of NH_4F -etched (111)-oriented n-type Si in contact with CH_3OH -0.05 M I_2 (circles) and in contact with $\text{N}_2(\text{g})$ after immersion in CH_3OH - I_2 and a subsequent CH_3OH rinse (squares). A single-exponential fit to these decays (not shown) yielded a time constant of 657 μs and 10.7 μs for the CH_3OH - I_2 -immersed and the N_2 -exposed samples, respectively. Measurements were made under high-level injection conditions (5×10^{15} injected carriers cm^{-2} in a 195 μm thick sample).

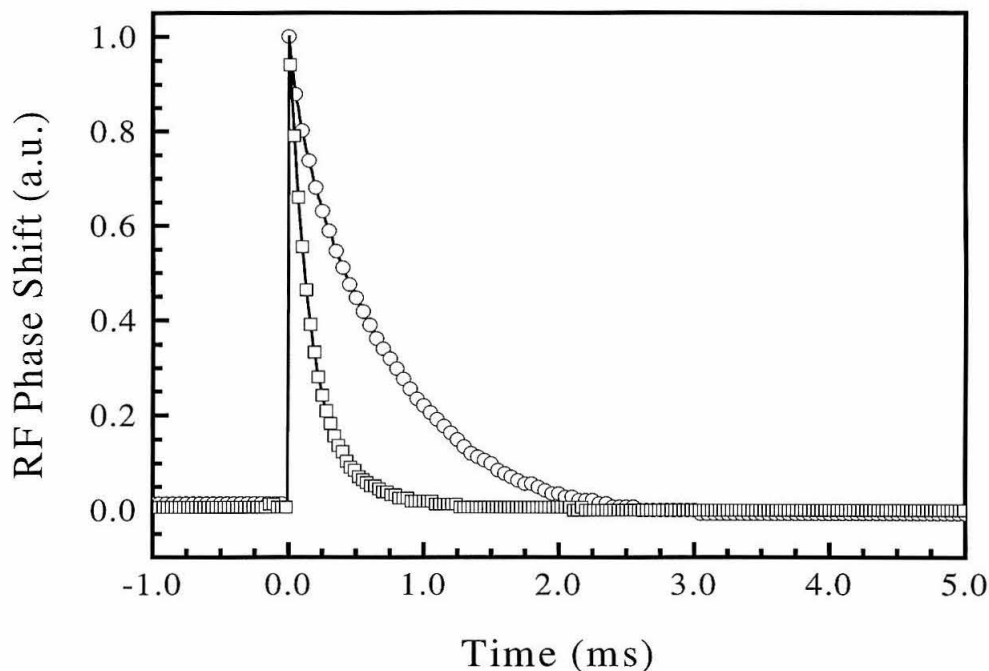


Figure 5.4: Time-resolved photoconductivity decay of NH_4F -etched (111)-oriented n-type Si in contact with CH_3OH -0.05 M $\text{Fc}^{+/0}$ (circles) and in contact with $\text{N}_2(\text{g})$ after immersion in CH_3OH -0.05 M $\text{Fc}^{+/0}$ and a subsequent CH_3OH rinse (squares). A single-exponential fit to these decays (not shown) yielded a time constant of 678 μs and 185 μs for the CH_3OH -0.05 M $\text{Fc}^{+/0}$ -immersed and the N_2 -exposed samples, respectively. Measurements were made under high-level injection conditions (5×10^{15} injected carriers cm^{-2} in a 197 μm thick sample).

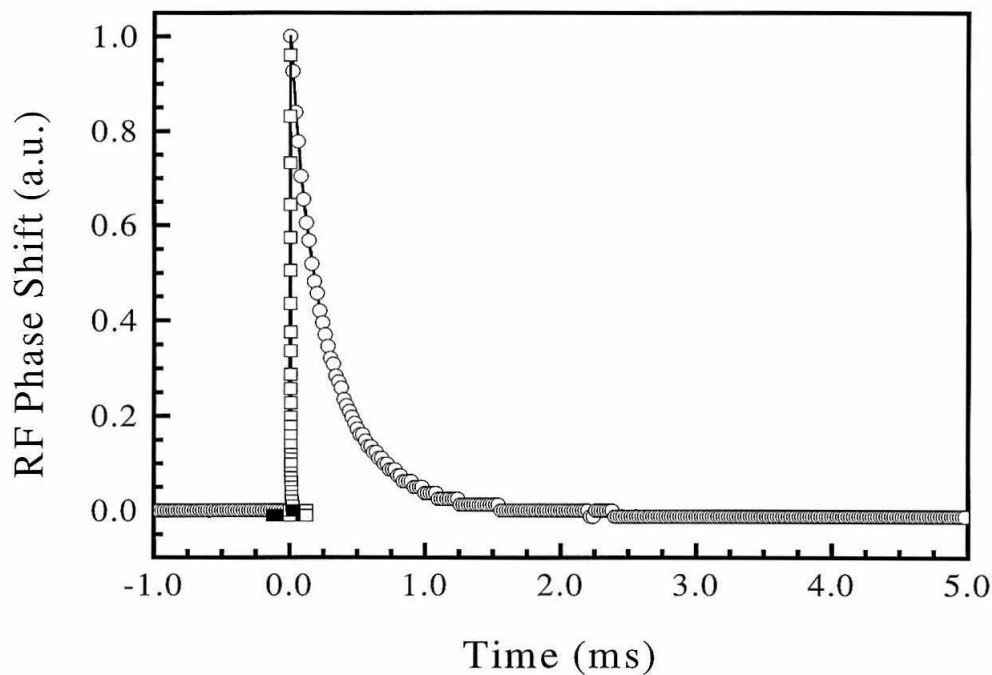


Figure 5.5: Time-resolved photoconductivity decay of NH_4F -etched (111)-oriented n-type Si in contact with $\text{THF}-0.05 \text{ M I}_2$ (circles) and in contact with $\text{N}_2(\text{g})$ after immersion in $\text{THF}-\text{I}_2$ and a subsequent THF rinse (squares). A single-exponential fit to these decays (not shown) yielded a time constant of $301 \mu\text{s}$ and $3.9 \mu\text{s}$ for the $\text{THF}-\text{I}_2$ -immersed and the N_2 -exposed samples, respectively. Measurements were made under high-level injection conditions (5×10^{15} injected carriers cm^{-2} in a $195 \mu\text{m}$ thick sample).

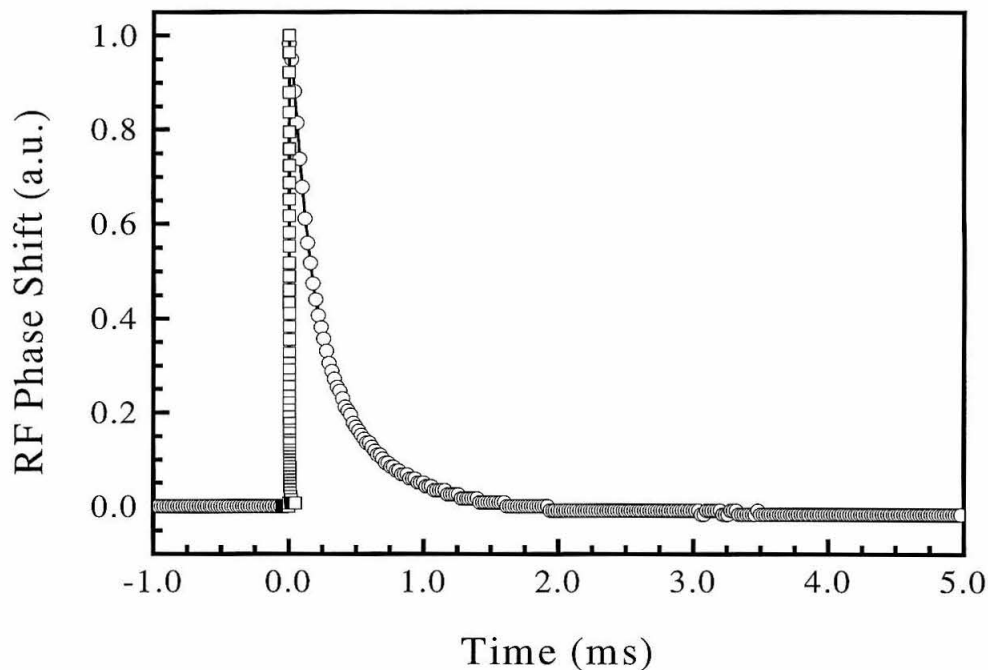


Figure 5.6: Time-resolved photoconductivity decay of NH_4F -etched (111)-oriented n-type Si in contact with THF–0.05 M Fc–0.005 M Fc^+ (circles) and in contact with THF–0.05 M Me_{10}Fc –0.01M $\text{Me}_{10}\text{Fc}^+$ (squares). A single-exponential fit to these decays (not shown) yielded a time constant of 291 μs and 3.3 μs for the THF– $\text{Fc}^{+/0}$ -immersed and the THF– $\text{Me}_{10}\text{Fc}^{+/0}$ -immersed samples, respectively. Measurements were made under high-level injection conditions (5×10^{15} injected carriers cm^{-2} in a 195 μm thick sample).

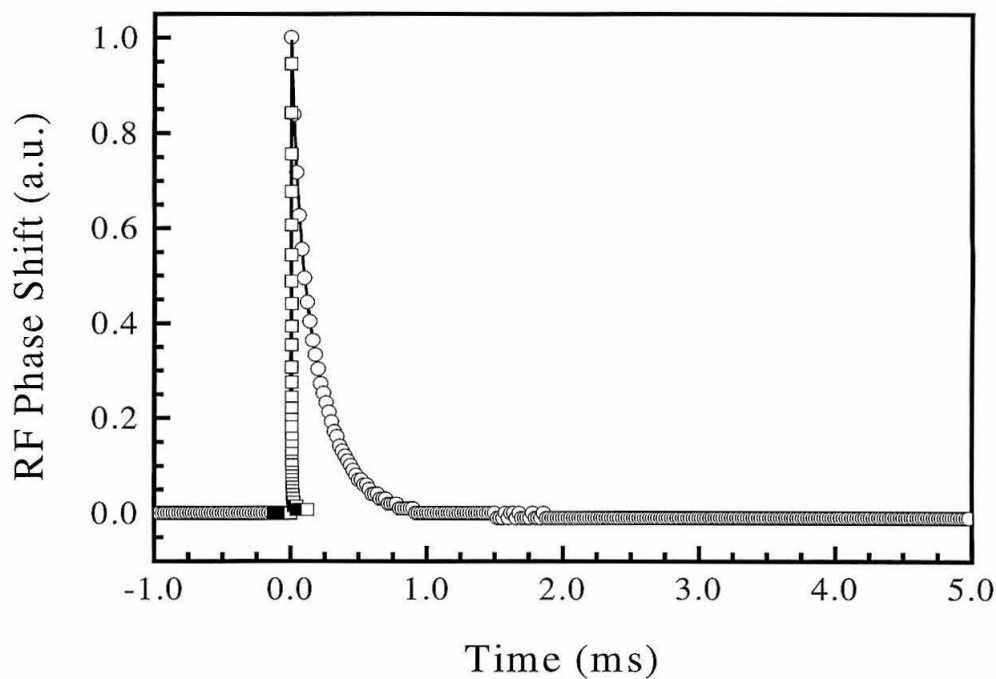


Figure 5.7: Time-resolved photoconductivity decay of air-oxidized (111)-oriented n-type Si in contact with CH_3OH -0.05 M $\text{Fc}^{+/0}$ (circles) and in contact with $\text{N}_2(\text{g})$ (squares). A single-exponential fit to these decays (not shown) yielded a time constant of 193 μs and 4.4 μs for the CH_3OH - $\text{Fc}^{+/0}$ -immersed and the $\text{N}_2(\text{g})$ -exposed samples, respectively. Measurements were made under high-level injection conditions (5×10^{15} injected carriers cm^{-2} in a 195 μm thick sample).

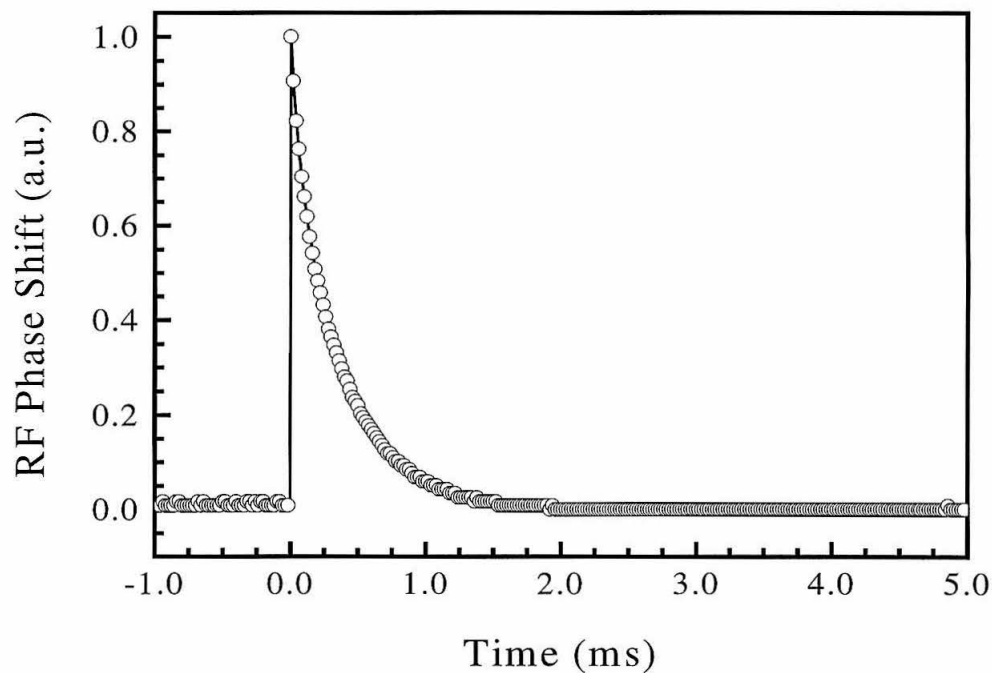


Figure 5.8: Time-resolved photoconductivity decay of methylated (111)-oriented n-Si in air under high-level injection conditions (5×10^{15} injected carriers cm^{-2} in a $190 \mu\text{m}$ thick sample) after 504 hours in an air ambient. A single-exponential fit to this decay (not shown) yielded a time constant of $342 \mu\text{s}$.

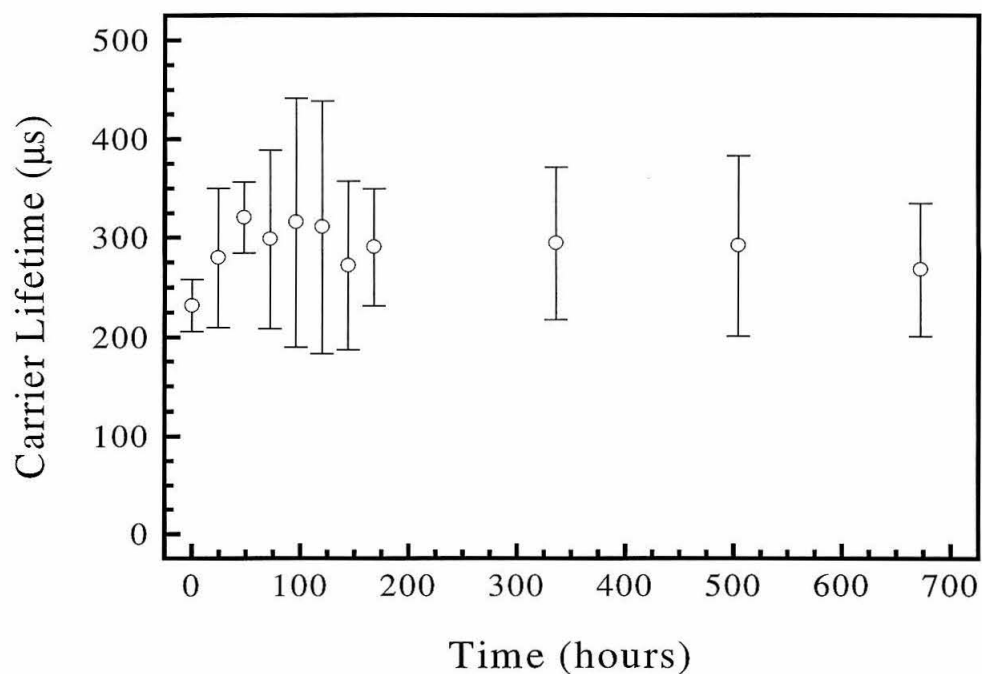


Figure 5.9: Time dependence of the mean carrier lifetimes for methylated Si in contact with air. Between measurements, the samples were stored in the dark at room temperature. All measurements were performed with a light pulse sufficient to provide high-level injection conditions. The error bars represent the standard deviations for lifetimes obtained from measurements of separate samples.

	Low Injection		High Injection	
	τ (μs)	S (cm s^{-1})	τ (μs)	S (cm s^{-1})
1) $\text{CH}_3\text{OH}-0.05 \text{ M I}_2$	520 ± 90	19 ± 3	600 ± 300	16 ± 8
2) N_2	7.8 ± 0.8	1300 ± 100	12 ± 1	810 ± 70
3) $\text{CH}_3\text{OH}-0.05 \text{ M I}_2$	500 ± 100	20 ± 4	700 ± 200	14 ± 4
1) $\text{CH}_3\text{OH}-0.05 \text{ M Fc}^0-0.05 \text{ M Fc}^+$	500 ± 100	20 ± 4	700 ± 200	14 ± 4
2) N_2	150 ± 60	70 ± 30	140 ± 40	70 ± 20
3) $\text{CH}_3\text{OH}-0.05 \text{ M Fc}^0-0.05 \text{ M Fc}^+$	470 ± 40	21 ± 2	600 ± 20	16 ± 1
4) $\text{THF}-0.05 \text{ M Me}_{10}\text{Fc}^0-0.01 \text{ M Me}_{10}\text{Fc}^+$	120 ± 20	80 ± 10	101 ± 8	98 ± 8
1) $\text{THF}-0.05 \text{ M I}_2$	280 ± 90	30 ± 10	270 ± 90	40 ± 10
2) N_2	3.7 ± 0.2	2600 ± 100	3.8 ± 0.2	2600 ± 100
3) $\text{THF}-0.05 \text{ M I}_2$	300 ± 100	30 ± 10	300 ± 100	30 ± 10
1) $\text{THF}-0.05 \text{ M Fc}^0-0.005 \text{ M Fc}^+$	280 ± 90	30 ± 10	180 ± 90	50 ± 30
2) N_2	2.7 ± 0.3	3600 ± 400	2.9 ± 0.3	3400 ± 300
3) $\text{THF}-0.05 \text{ M Fc}^0-0.005 \text{ M Fc}^+$	300 ± 100	30 ± 10	220 ± 160	40 ± 30
4) $\text{THF}-0.05 \text{ M Me}_{10}\text{Fc}^0-0.01 \text{ M Me}_{10}\text{Fc}^+$	2.6 ± 0.3	3800 ± 400	3.0 ± 0.2	3300 ± 200
1) $\text{THF}-0.05 \text{ M Me}_{10}\text{Fc}^0-0.01 \text{ M Me}_{10}\text{Fc}^+$	3.0 ± 0.7	3300 ± 800	4 ± 1	2400 ± 600
2) N_2	2.7 ± 0.3	3600 ± 400	3.4 ± 0.1	2870 ± 90
3) $\text{THF}-0.05 \text{ M Me}_{10}\text{Fc}^0-0.01 \text{ M Me}_{10}\text{Fc}^+$	2.8 ± 0.3	3500 ± 400	3.0 ± 0.4	3300 ± 400
4) $\text{THF}-0.05 \text{ M Fc}^0-0.005 \text{ M Fc}^+$	290 ± 90	30 ± 10	250 ± 60	40 ± 10

Table 5.1a: Measured lifetimes and surface recombination velocities for $\text{NH}_4\text{F}(\text{aq})$ -etched Si(111) following various surface treatments. Values for S were computed assuming an infinite bulk lifetime.

	Low Injection		High Injection	
	τ (μs)	S (cm s^{-1})	τ (μs)	S (cm s^{-1})
1) $\text{CH}_3\text{OH}-0.05 \text{ M I}_2$	520 ± 90	<i>a</i>	600 ± 300	<i>a</i>
2) N_2	7.8 ± 0.8	1200 ± 100	12 ± 1	800 ± 70
3) $\text{CH}_3\text{OH}-0.05 \text{ M I}_2$	500 ± 100	<i>a</i>	700 ± 200	<i>a</i>
1) $\text{CH}_3\text{OH}-0.05 \text{ M Fc}^0-0.05 \text{ M Fc}^+$	500 ± 100	<i>a</i>	700 ± 200	<i>a</i>
2) N_2	150 ± 60	50 ± 30	140 ± 40	60 ± 20
3) $\text{CH}_3\text{OH}-0.05 \text{ M Fc}^0-0.05 \text{ M Fc}^+$	470 ± 40	<i>a</i>	600 ± 20	<i>a</i>
4) $\text{THF}-0.05 \text{ M Me}_{10}\text{Fc}^0-0.01 \text{ M Me}_{10}\text{Fc}^+$	120 ± 20	70 ± 20	101 ± 8	87 ± 9
1) $\text{THF}-0.05 \text{ M I}_2$	280 ± 90	<i>a</i>	270 ± 90	20 ± 10
2) N_2	3.7 ± 0.2	2600 ± 100	3.8 ± 0.2	2600 ± 100
3) $\text{THF}-0.05 \text{ M I}_2$	300 ± 100	30 ± 10	300 ± 100	20 ± 10
1) $\text{THF}-0.05 \text{ M Fc}^0-0.005 \text{ M Fc}^+$	280 ± 90	<i>a</i>	180 ± 90	40 ± 30
2) N_2	2.7 ± 0.3	3600 ± 400	2.9 ± 0.3	3300 ± 300
3) $\text{THF}-0.05 \text{ M Fc}^0-0.005 \text{ M Fc}^+$	300 ± 100	<i>a</i>	220 ± 160	30 ± 30
4) $\text{THF}-0.05 \text{ M Me}_{10}\text{Fc}^0-0.01 \text{ M Me}_{10}\text{Fc}^+$	2.6 ± 0.3	3700 ± 400	3.0 ± 0.2	3200 ± 200
1) $\text{THF}-0.05 \text{ M Me}_{10}\text{Fc}^0-0.01 \text{ M Me}_{10}\text{Fc}^+$	3.0 ± 0.7	3200 ± 800	4 ± 1	2400 ± 600
2) N_2	2.7 ± 0.3	3600 ± 400	3.4 ± 0.1	2860 ± 90
3) $\text{THF}-0.05 \text{ M Me}_{10}\text{Fc}^0-0.01 \text{ M Me}_{10}\text{Fc}^+$	2.8 ± 0.3	3500 ± 400	3.0 ± 0.4	3200 ± 400
4) $\text{THF}-0.05 \text{ M Fc}^0-0.005 \text{ M Fc}^+$	290 ± 90	<i>a</i>	250 ± 60	30 ± 10

Table 5.1b: Measured lifetimes and surface recombination velocities for $\text{NH}_4\text{F}(\text{aq})$ -etched Si(111) following various surface treatments. Values for S were computed assuming lifetimes obtained for the same wafer in concentrated $\text{H}_2\text{SO}_4(\text{aq})$. Notes: ^a measured lifetime was not statistically different from the lower bound of the bulk lifetime deduced from measurements of the same wafer in concentrated $\text{H}_2\text{SO}_4(\text{aq})$.

	Low Injection		High Injection	
	τ (μs)	S (cm s^{-1})	τ (μs)	S (cm s^{-1})
1) CH_3OH –0.05 M I_2	400 ± 100	24 ± 6	500 ± 200	19 ± 8
2) N_2	16 ± 5	600 ± 200	12 ± 2	800 ± 100
3) CH_3OH –0.05 M I_2	400 ± 200	20 ± 10	500 ± 200	19 ± 8
4) THF –0.05 M $\text{Me}_{10}\text{Fc}^0$ –0.01 M $\text{Me}_{10}\text{Fc}^+$	30 ± 10	300 ± 100	23 ± 5	420 ± 90
1) CH_3OH –0.05 M Fc^0 –0.05 M Fc^+	300 ± 100	30 ± 10	300 ± 100	30 ± 10
2) N_2	7 ± 2	1400 ± 400	9 ± 2	1100 ± 200
3) CH_3OH –0.05 M Fc^0 –0.05 M Fc^+	150 ± 50	60 ± 20	220 ± 40	44 ± 8
4) THF –0.05 M $\text{Me}_{10}\text{Fc}^0$ –0.01 M $\text{Me}_{10}\text{Fc}^+$	7 ± 2	1400 ± 400	8 ± 1	1200 ± 200

Table 5.2a: Measured lifetimes and surface recombination velocities for air-oxidized Si(111) following various surface treatments. Values for S were computed assuming an infinite bulk lifetime.

	Low Injection		High Injection	
	τ (μs)	S (cm s^{-1})	τ (μs)	S (cm s^{-1})
1) CH_3OH –0.05 M I_2	400 ± 100	<i>a</i>	500 ± 200	<i>a</i>
2) N_2	16 ± 5	600 ± 200	12 ± 2	800 ± 100
3) CH_3OH –0.05 M I_2	400 ± 200	<i>a</i>	500 ± 200	<i>a</i>
4) THF –0.05 M $\text{Me}_{10}\text{Fc}^0$ –0.01 M $\text{Me}_{10}\text{Fc}^+$	30 ± 10	300 ± 100	23 ± 5	400 ± 90
1) CH_3OH –0.05 M Fc^0 –0.05 M Fc^+	300 ± 100	<i>a</i>	300 ± 100	<i>a</i>
2) N_2	7 ± 2	1400 ± 400	9 ± 2	1100 ± 200
3) CH_3OH –0.05 M Fc^0 –0.05 M Fc^+	150 ± 50	40 ± 20	220 ± 40	20 ± 10
4) THF –0.05 M $\text{Me}_{10}\text{Fc}^0$ –0.01 M $\text{Me}_{10}\text{Fc}^+$	7 ± 2	1400 ± 400	8 ± 1	1200 ± 200

Table 5.2b: Measured lifetimes and surface recombination velocities for air-oxidized Si(111) following various surface treatments. Values for S were computed assuming lifetimes obtained for the same wafer in concentrated $\text{H}_2\text{SO}_4(\text{aq})$. Notes:

^a measured lifetime was not statistically different from the lower bound of the bulk lifetime deduced from measurements of the same wafer in concentrated $\text{H}_2\text{SO}_4(\text{aq})$.

IV. DISCUSSION

The behavior of the silicon surfaces treated with solutions containing redox-active oxidants can be explained through reference to the electrochemistry of Si/liquid contacts. The electrolytes that produced low Si surface recombination velocities all had electrochemical potentials > 0 V vs. the standard calomel electrode.³⁴ In addition, in the absence of such electrolytes, higher, and variable, S values were measured, with different behavior observed, as expected, for the various chemically different Si surfaces.

This behavior can be understood in the context of the Shockley-Read-Hall treatment for surface recombination.³⁵⁻³⁷ The surface recombination rate for a surface with traps at a single energy involves the carrier-capture rate constants, $k_{n,s}$ and $k_{p,s}$, the electron and hole concentrations at the surface of the semiconductor in the dark, $n_{s,o}$ and $p_{s,o}$, respectively, and the injected electron and hole densities, Δn_s and Δp_s , respectively:

$$S = N_{t,s} \frac{k_{n,s} k_{p,s} [n_{s,o} + p_{s,o} (\Delta n_s / \Delta p_s) + \Delta n_s]}{k_{n,s} (n_{s,o} + \Delta n_s + n_{1,s}) + k_{p,s} (p_{s,o} + \Delta p_s + p_{1,s})} \quad (5.2)$$

In eq 5.2, $N_{t,s}$ is the surface trap density, and $n_{1,s}$ and $p_{1,s}$ are the electron and hole concentrations, respectively, when the Fermi level is located at the energy of the surface trap.³⁶ Redox couples that have very positive redox potentials are capable of extensive charge transfer from the Si into the electrolyte, thereby establishing an inversion layer at the surface of n-type Si.³⁸⁻⁴⁰ In this situation, even with significant values of N_t , the effective surface recombination velocity that is measured experimentally will be very low. Simulations of the surface recombination rate using an extended Shockley-Read-Hall formalism, which incorporates the effects of band bending, have in fact shown that there is a significant decrease in S with increasing positive charge at the surface of n-type Si.⁴¹ Removal of the sample from the electrolyte will generally change the surface potential in a direction that reduces the band bending, so the observed value of S should increase, and the variations in N_t can then be reflected in the measurements of S under

these conditions. This expectation is in accord with the experimental observations that the surfaces investigated in this work all exhibited higher S values in contact with $N_2(g)$ than they did in contact with the oxidizing electrolyte solutions.

Electrochemical data have located the conduction band edge of alkoxyated Si surfaces at ≈ -0.83 V vs. SCE in CH_3OH .⁴⁰ This is consistent with the observation that in air, in $N_2(g)$, or in electrolytes with moderately negative redox potentials (< 0 V vs. SCE) such as THF– $Me_{10}Fc^{+/0}$, surfaces with significant N_t values will exhibit a higher effective surface recombination velocity than they would under conditions that produced an inversion layer at the Si surface (Figure 5.10). In contrast, for electrolytes with redox potentials, $E(A/A^-)$, $> +0.2$ V vs. SCE, such as I_2 or Br_2 in CH_3OH , C_2H_5OH , or THF, or $Fc^{+/0}$ in CH_3OH or THF, the steady-state rate of surface recombination will be suppressed due to the formation of a high concentration of minority carriers at the surfaces in contact with the electrolyte solutions. The observed effect should be rapid and reversible, because only electron exchange is required to produce the electrochemically-induced change in surface carrier concentration that affects the effective S value of the interface. This expectation is also in accord with the experimental observations. In the work described herein, only etched surfaces that had been immersed in $CH_3OH-0.05$ M $Fc^{+/0}$ solutions showed low surface recombination velocities in $N_2(g)$, indicating that only these surfaces had low values of $N_{t,s}$ in contact with an ambient that did not produce an inversion layer at the Si surface.

Further evidence for charge-transfer control over the effective S value in these oxidizing electrolytes can be obtained through reference to prior electrical and electrochemical measurements on Si/liquid contacts.³⁸⁻⁴⁰ Near-surface channel conductance measurements in p^+-n-p^+ Si structures exposed to electrolytes have clearly demonstrated the formation of an inversion layer at $n-Si/CH_3OH-5.4$ mM $Me_2Fc-2.9$ mM Me_2Fc^+ contacts but not at $CH_3OH-Me_{10}Fc^{+/0}$ electrolytes.³⁸ Mott-Schottky measurements of the $n-Si/CH_3OH-Me_2Fc^{+/0}$ contact have indicated an equilibrium barrier

height of ≈ 1.03 V,^{40,42,43} which is sufficient to drive the system into carrier inversion. The surface recombination velocity of Si/CH₃OH contacts after treatment with CH₃OH–Me₂Fc⁺⁰, deduced from current density vs. potential data, is < 100 cm s⁻¹, whereas higher S values were deduced for these Si samples in contact with redox systems such as CH₃OH–Me₁₀Fc⁺⁰ that cannot produce an inversion layer at the Si surface.³⁴ Direct measurements of the surface recombination velocity of the n-Si/CH₃OH interface as a function of the electrode potential on alkoxyated Si surfaces have shown that at positive (and negative) potentials, where the surface is in inversion (accumulation), the effective surface recombination velocities are very low, whereas for surface potentials that produce moderate band-bending in the semiconductor, much higher S values are obtained.³⁴ The formation of an electrochemically-induced inversion layer has also been used to explain unexpectedly large feedback currents in scanning electrochemical microscopy experiments at Si/CH₃OH–Fc⁺⁰ and Si/CH₃OH–Me₂Fc⁺⁰ contacts.³⁹ These results are in excellent agreement with the predictions of eq 5.2 and with the experimental observations reported herein.

The lifetime measurements on alkylated silicon surfaces provide the first evidence for a chemically functionalized Si surface that has a stable, low surface recombination velocity in air. The intensity of the light pulse at high-level injection was sufficient to eliminate essentially any equilibrium potential drop that might exist in the solid. This suggests that the changes in the observed carrier recombination lifetime are primarily due to changes in surface state density and/or surface-trap carrier-capture rate constants, as opposed to changes in the electrostatic surface potential. The latter effect has been observed for native Si surfaces in contact with NH₃ and oxidizing ambients.^{44,45} Moreover, assuming a geometric cross-section for carrier capture by surface traps of 1×10^{-15} cm⁻², the observed surface recombination velocity of 2×10^1 cm s⁻¹ for methyl-terminated Si surfaces translates into only one active electrical defect for every $\approx 250,000$ surface atoms. The alkylation methodology could therefore prove useful in providing

passivation layers for Si nanoparticles, for Si surfaces in photovoltaic devices, and for other novel applications of Si surfaces in electrical device structures where low recombination velocity surfaces are beneficial.

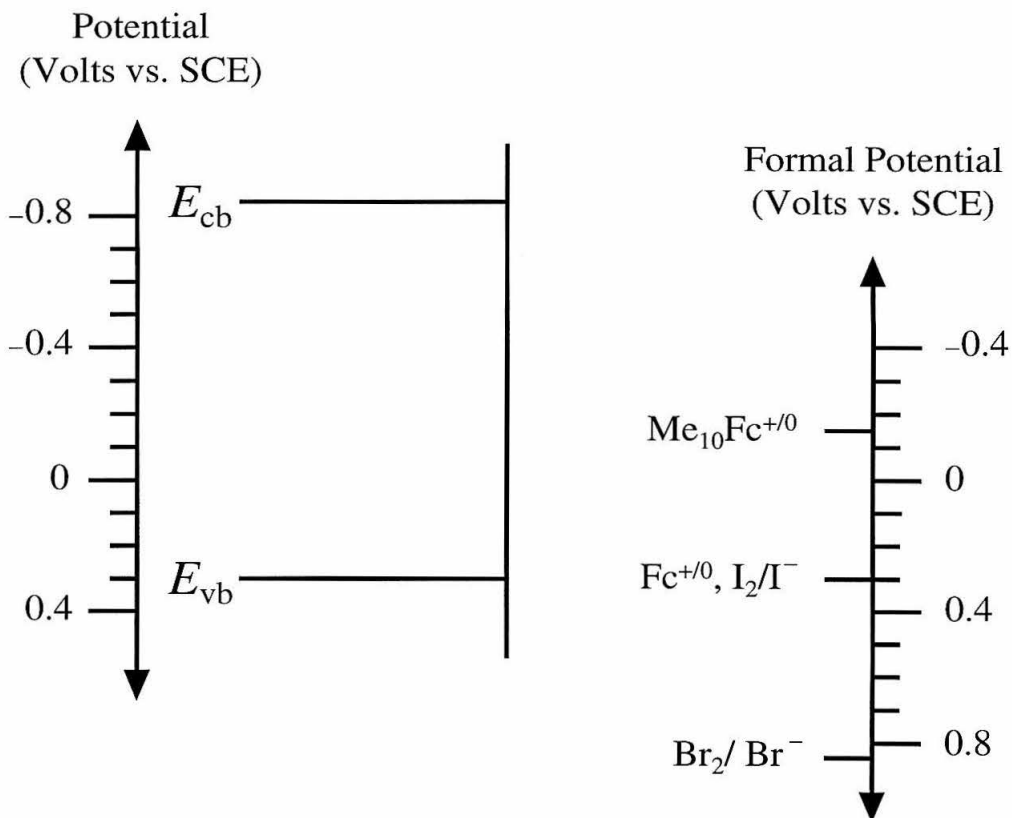


Figure 5.10: An energy diagram showing the Nernstian potentials of various redox couples relative to the potential of the bottom of the conduction band, E_{cb} , and the top of the valence band, E_{vb} , of Si. Solutions of redox couples such as $Fc^{+/0}$, I_2/I^- , and Br_2/Br^- have an electrochemical potential sufficiently positive to produce an inversion layer in Si.

V. SUMMARY

The experimentally observed charge-carrier decay dynamics for a variety of chemically treated Si surfaces can be explained in the context of the known electrochemical behavior of Si/liquid contacts. Low effective S values for Si in contact with oxidizing electrolyte solutions are observed for systems capable of undergoing interfacial charge-transfer reactions that produce an inversion layer in the Si. Except for Si surfaces exposed to CH_3OH -0.05 M $\text{Fc}^{+/0}$ solutions, these types of Si/liquid contacts are therefore potentially useful for monitoring surface contamination levels above certain trap densities in the wet etching and processing steps of Si, and for use in photoelectrochemical energy conversion systems, but do not at present appear to provide routes to the effective passivation of Si surfaces for use in applications outside of these specific media. It has been shown, however, that it is possible through molecular level control over surface chemistry, to produce Si surfaces that are highly electrically passive and which are far more stable in ambient air than H-terminated Si surfaces. The electrical properties of these alkylated surfaces in air correlate well with the improved electrochemical properties of these surfaces in contact with nonaqueous and aqueous electrolytes,^{25,26} and with the improved resistance to oxidation observed previously for such alkylated Si surfaces.^{17,18}

VI. REFERENCES

1. Sze, S. M. *The Physics of Semiconductor Devices*, 2nd ed.; Wiley: New York, 1981.
2. Fonash, S. J. *Solar Cell Device Physics*; Academic: New York, 1981.
3. Green, M. A. *Appl. Phys. Lett.* **1978**, *33*, 178.
4. Reddy, A. J.; Burr, T. A.; Chan, J. K.; Norga, G. J.; Michel, J.; Kimerling, L. C. *Mat. Sci. Forum* **1997**, *258-263*, 1719.
5. Reddy, A. J.; Chan, J. V.; Burr, T. A.; Mo, R.; Wade, C. P.; Chidsey, C. E. D.; Michel, J.; Kimerling, L. C. *Physica B* **1999**, *273-274*, 468.
6. Lewis, N. S.; Rosenbluth, M. L. *Theory of Semiconductor Materials. In Photocatalysis: Fundamentals and Applications*; Serpone, N., Pelizzetti, E., Eds.; John Wiley & Sons: New York, 1989.
7. Yablonovitch, E.; Gmitter, T. J. *Sol. St. Electron.* **1992**, *35*, 261.
8. Eades, W. D.; Swanson, R. M. *J. Appl. Phys.* **1985**, *58*, 4267.
9. Yablonovitch, E.; Allara, D. L.; Chang, C. C.; Gmitter, T.; Bright, T. B. *Phys. Rev. Lett.* **1986**, *57*, 249.
10. Forbes, M. D. E.; Lewis, N. S. *J. Am. Chem. Soc.* **1990**, *112*, 3682.
11. Tan, M. X.; Kenyon, C. N.; Lewis, N. S. *J. Phys. Chem.* **1994**, *98*, 4959.
12. Tan, M. X.; Kenyon, C. N.; Krüger, O.; Lewis, N. S. *J. Phys. Chem. B* **1997**, *101*, 2830.
13. Stephens, A. W.; Green, M. A. *Sol. Energ. Mat. Sol. Cells* **1997**, *45*, 255.
14. Stephens, A. W.; Green, M. A. *J. Appl. Phys.* **1996**, *80*, 3897.
15. M'saad, H.; Michel, J.; Lappe, J. J.; Kimerling, L. C. *J. Elect. Mat.* **1994**, *23*, 487.
16. Horányi, T. S.; Pavelka, T.; Tüttö, P. *Appl. Surf. Sci.* **1993**, *63*, 306.
17. Bansal, A.; Li, X.; Lauermann, I.; Lewis, N. S.; Yi, S. I.; Weinberg, W. H. *J. Am. Chem. Soc.* **1996**, *118*, 7225.
18. Linford, M. R.; Fenter, P.; Eisenerger, P. M.; Chidsey, C. E. D. *J. Am. Chem. Soc.* **1995**, *117*, 3145.
19. Linford, M. R.; Chidsey, C. E. D. *J. Am. Chem. Soc.* **1993**, *115*, 12631.
20. Teplyakov, A. V.; Kong, M. J.; Bent, S. F. *J. Am. Chem. Soc.* **1997**, *119*, 11100.

21. de Villeneuve, C. H.; Pinson, J.; Bernard, M. C.; Allongue, P. *J. Phys. Chem. B* **1997**, *101*, 2415.
22. Buriak, J. M.; Allen, M. J. *J. Am. Chem. Soc.* **1998**, *120*, 1339.
23. Buriak, J. M.; Stewart, M. P.; Geders, T. W.; Allen, M. J.; Choi, H. C.; Smith, J.; Raftery, D.; Canham, L. T. *J. Am. Chem. Soc.* **1999**, *121*, 11491.
24. Gurtner, C.; Wun, A. W.; Sailor, M. J. *Angew. Chem. Int. Edit.* **1999**, *38*, 1966.
25. Bansal, A.; Lewis, N. S. *J. Phys. Chem. B* **1998**, *102*, 4058.
26. Bansal, A.; Lewis, N. S. *J. Phys. Chem. B* **1998**, *102*, 1067.
27. Hendrickson, D. H.; Sohn, Y. S.; Gray, H. B. *Inorg. Chem.* **1971**, *10*, 1559.
28. Pomykal, K. E.; Fajardo, A. M.; Lewis, N. S. *J. Phys. Chem.* **1995**, *99*, 8302.
29. Tufts, B. J.; Kumar, A.; Bansal, A.; Lewis, N. S. *J. Phys. Chem.* **1992**, *96*, 4581.
30. Yablonovitch, E.; Swanson, R. M.; Eades, W. D.; Weinberger, B. R. *Appl. Phys. Lett.* **1986**, *48*, 245.
31. Kunst, M.; Sanders, A. *Semicond. Sci. Tech.* **1992**, *7*, 51.
32. Haber, J. A.; Vaid, T. P.; Michalak, D.; Lewis, N. S. *J. Phys. Chem. B* **2000**, in press.
33. Fidélis, A.; Ozanam, F.; Chazalviel, J. N. *Surf. Sci.* **2000**, *444*, L7.
34. Rosenbluth, M. L.; Lewis, N. S. *J. Am. Chem. Soc.* **1986**, *108*, 4689.
35. Shockley, W.; Read, W. T. *Phys. Rev.* **1952**, *87*, 835.
36. Schroder, D. K. *Semiconductor Material and Device Characterization*; John Wiley & Sons: New York, 1990.
37. Hall, R. N. *Phys. Rev.* **1952**, *87*, 387.
38. Laibinis, P. E.; Stanton, C. E.; Lewis, N. S. *J. Phys. Chem.* **1994**, *98*, 8765.
39. Shreve, G. A.; Karp, C. D.; Pomykal, K. E.; Lewis, N. S. *J. Phys. Chem.* **1995**, *99*, 5575.
40. Pomykal, K. E.; Fajardo, A. M.; Lewis, N. S. *J. Phys. Chem.* **1996**, *100*, 3652.
41. Aberle, A. G.; Glunz, S.; Warta, W. *J. Appl. Phys.* **1992**, *9*, 4422.
42. Kobayashi, H.; Takeda, N.; Sugahara, H.; Tsubomura, H. *J. Phys. Chem.* **1991**, *95*, 813.
43. Tomkiewicz, M. *Electrochim. Acta* **1990**, *35*, 1631.

44. Buck, T. M.; McKim, F. S. *J. Electrochem. Soc.* **1963**, *343*, 709.
45. Many, A.; Goldstein, Y.; Grover, N. B. *Semiconductor Surfaces*; North-Holland: New York, 1965.

Chapter 6

Electrochemical Measurements of Interfacial Electron Transfer at Chemically Modified Silicon Electrodes

I. INTRODUCTION

Electron-transfer reactions play a significant role in numerous chemical and biological processes. In systems such as redox proteins¹⁻⁴ and photosynthetic reaction centers,⁵⁻⁷ electron transfer can occur over remarkably long distances via molecular bridges that link electron donors and electron acceptors. For many years, considerable efforts have been made to elucidate the influence of the chemical and electronic properties of molecular linkers on long-range electron-transfer rates. While the kinetics of such reactions have been studied extensively in homogeneous solutions,^{8,9} there are relatively few reports concerning long-range electron transfer at solid electrodes.

To date, most studies of long-range electron-transfer kinetics in heterogeneous systems have employed metal electrodes with attached alkyl monolayers.¹⁰⁻¹⁵ Chidsey reported the first such measurements using Au electrodes modified with ferrocene-terminated alkanethiols.¹⁰ By varying the alkane chain lengths in these systems, Chidsey and co-workers showed that the attenuation of electronic coupling, β , with increases in the charge-transfer distance was similar to that observed for alkane-based linkers in homogeneous liquid systems (i.e., with $\beta \approx 1 \text{ \AA}^{-1}$).¹¹ Similar observations have also been reported for alkanethiol-modified Au electrodes having either pendant pentaamine(pyridine)-ruthenium¹² or ferrocenecarboxamide¹³ functionality and for alkanthiol-modified Au and Hg electrodes in contact with solutions containing freely diffusing redox species.^{14,15}

Due primarily to the relative difficulty in preparing well characterized, stable monolayers on semiconductor surfaces, there have been only a few studies of long-range electron transfer at semiconductor electrodes. Recently, Waldeck and co-workers measured interfacial electron-transfer rates at alkanethiol-terminated n-InP and alkylsiloxane-terminated n-Si/SiO₂ electrodes in contact with solutions containing Fe(CN)₆^{4-/3-}.¹⁶⁻¹⁸ In these systems, the attenuation of electron-transfer rates with alkyl chain length was found to be significantly smaller than that observed for other

heterogeneous and homogeneous systems (i.e., with $\beta < 0.5 \text{ \AA}^{-1}$). Moreover, studies of solid-state n-Si-SiO₂-alkane-Al device structures have suggested that the tunneling current in these devices is completely independent of alkyl chain length.^{19,20} These observations stand in stark contrast to the behavior reported for long-range electron transfer reactions in homogeneous systems.

In this chapter, electrochemical measurements of alkyl-terminated Si surfaces have been performed to provide further insight into the distance-dependence of electron transfer rates at semiconducting electrodes. Various surface orientations and surface modification procedures were evaluated prior to the work described herein, and in only one instance was electron transfer found to be rate-limiting: (100)-oriented Si derivatized by a two-step, wet chemical alkylation procedure. The results are consistent with the solid-state measurements described above which indicate that there is no appreciable dependence of the current on alkyl chain length. However, the possibility that the observed behavior results from pinhole defects in the monolayer structure cannot be excluded.

II. EXPERIMENTAL

A. Electrodes and Solutions

Single-crystal, n-type, (100)-oriented Si wafers (P-doped) were obtained from Silicon Sense Inc. Four-point probe measurements were used to determine the resistivities of each Si wafer ($0 - 10 \Omega \text{ cm}$), and the wafers were then cut into rectangular electrodes having dimensions of $20 \times 12 \text{ mm}$.

Prior to chemical modification, Si electrodes were etched twice for 1 minute in 48% HF(aq) (Mallinckrodt, Inc.). After each etch, the electrodes were rinsed with distilled H_2O ($18 \text{ M}\Omega \text{ cm}$) and dried under a stream of $\text{N}_2(\text{g})$. The samples were then alkylated using a two-step chlorination-alkylation procedure that has been described previously for (111)-oriented Si surfaces.²¹ All chlorination reagents, organomagnesium reagents, and anhydrous solvents were obtained from Aldrich and used without further purification. X-ray photoelectron spectroscopy was used to characterize the modified surfaces as detailed in a previous report.²¹ Following alkylation reactions, the samples were stored for less than 24 hours under ultrahigh vacuum before being transferred into an inert atmosphere for electrochemical analysis. During the transfer, the electrodes were exposed briefly to an air ambient during which time Ga:In eutectic was applied to the unpolished backsides of the electrodes to form ohmic contacts.

Methyl viologen dichloride (MV^{2+}) was obtained from Aldrich and dried for 12 hours under vacuum at $60 \text{ }^\circ\text{C}$. Ferrocenium (Fc^+) was obtained from Aldrich and recrystallized from a mixture of THF and acetonitrile. Methanol was purchased from EM Science and distilled over Mg turnings prior to use. Lithium chloride (EM Science) was dried under vacuum for 24 hours at $250 \text{ }^\circ\text{C}$. The reduced form of methyl viologen (MV^+) was prepared in situ by electrolyzing MV^{2+} in a $\text{LiCl-CH}_3\text{OH}$ solution with a Pt foil working electrode, a $\text{CH}_3\text{OH-LiCl}$ saturated calomel reference electrode (-0.55 V vs. SCE), and a Pt gauze counter electrode isolated from the solution by a Vycor frit. All reagents were stored in a $\text{N}_2(\text{g})$ -purged drybox containing less than $10 \text{ ppm O}_2(\text{g})$ as

determined by the absence of visible fumes from diethylzinc.

B. Electrochemical Cells and Instrumentation

Electrochemical measurements were performed in a $N_2(g)$ -purged drybox using a Delrin cell in a three-electrode configuration. The working Si electrode was sealed against an open wall of the cell using a viton o-ring, yielding an exposed electrode area of 2.12 cm^2 . Electrical contact to the Ga:In eutectic was made by pressing a strip of Cu foil against the back of the Si electrode. Pt gauze was used for the counter electrode, and a Pt wire was used to reference the working electrode to the redox-active solution. The mass-transport limit, the concentration overpotential, and the solution resistance were determined by replacing the Si working electrode with a Pt foil working electrode and performing current-potential measurements using the same instrument parameters as those used for the modified Si electrodes.²²

Current density-potential (J - E) measurements were performed using a Solartron Model 1287 potentiostat or an EG&G PAR Model 173 potentiostat equipped with an EG&G PAR Model 175 universal programmer. Measurements were taken at a slow scan rate (10 mV s^{-1}) to avoid mass-transport limitations. Capacitance-voltage data were obtained using a Solartron Model 1260 impedance analyzer interfaced with a Solartron Model 1287 potentiostat. Impedance spectra were recorded for reverse DC biases ranging from 0 mV to 800 mV, in 50 mV increments, at frequencies between 100 kHz and 100 Hz. Evaluation of diode quality factors and barrier heights were made as described in previous studies.²²⁻²⁴

III. RESULTS

Figure 6.1 shows representative $\ln(J)$ - E curves for a $C_{12}H_{25}$ -terminated Si(100) electrode in contact with CH_3OH -1.0 M LiCl-10 mM MV^{2+} -10 mM MV^+ and in contact with CH_3OH -1 M LiCl-100 mM MV^{2+} -10 mM MV^+ . Both curves have been corrected for resistance losses and concentration overpotential as described previously.²² The measured diode quality factor was 1.27 for the CH_3OH -1 M LiCl-10 mM MV^{2+} -10 mM- MV^+ -immersed sample and 1.22 for the CH_3OH -1 M LiCl-100 mM MV^{2+} -10 mM MV^+ -immersed sample, indicating a near first-order dependence of the measured current on the surface electron concentration.²²⁻²⁴ In addition, the mean separation between the curves displayed in Figure 6.1, averaged over the entire current range, is 48 ± 15 mV, suggesting a first-order dependence of the current on the redox-acceptor concentration.²²⁻²⁴

Table 6.1 lists average values of the diode quality factors and mean $\ln(J)$ - E curve separations for Si(100) surfaces terminated with various chain length alkyl groups. With the exception of C_4H_9 -terminated surfaces, all derivatized surfaces exhibited diode quality factors and current-voltage curve separations indicating a first-order dependence of the measured current on the concentrations of both surface electrons and redox acceptors. Current-potential curves for surfaces terminated with C_4H_9 alkyl chains exhibited diode quality factors near 2.0 and showed no significant dependence on redox acceptor concentration, suggesting a different rate-limiting transport process in this system.

A typical Mott-Schottky plot for a $C_{12}H_{25}$ -terminated sample in contact with CH_3OH -1 M LiCl-10 mM MV^{2+} -10 mM MV^+ is shown in Figure 6.2. The dopant density determined from the capacitance-voltage (C^{-2} - E) data ($2.1 \times 10^{15} \text{ cm}^{-3}$) is in good agreement with the dopant density measured for the same wafer using a four-point probe apparatus ($1.8 \times 10^{15} \text{ cm}^{-3}$). Although a slight frequency dependence was observed in the C^{-2} - E data, extrapolation of the data to infinite capacitance yielded values for the built-in

voltage with minimal frequency dispersion (approximately 20 – 30 mV). For the system shown in Figure 6.2, the average barrier height was determined to be 0.73 ± 0.02 volts. The barrier heights for other systems examined in this work are listed in Table 6.1. In all cases, the barrier heights were significantly larger than that measured for HF-etched, $\text{CH}_3\text{OH-Fc}^+$ -treated Si(100).

Figure 6.3 shows current-voltage curves for Si(100) surfaces terminated with various chain length alkyl groups. The current observed for each surface at a given potential is nearly identical despite XPS data (not shown) which indicates that there is a monotonic increase of carbon coverage with increasing alkyl chain length.

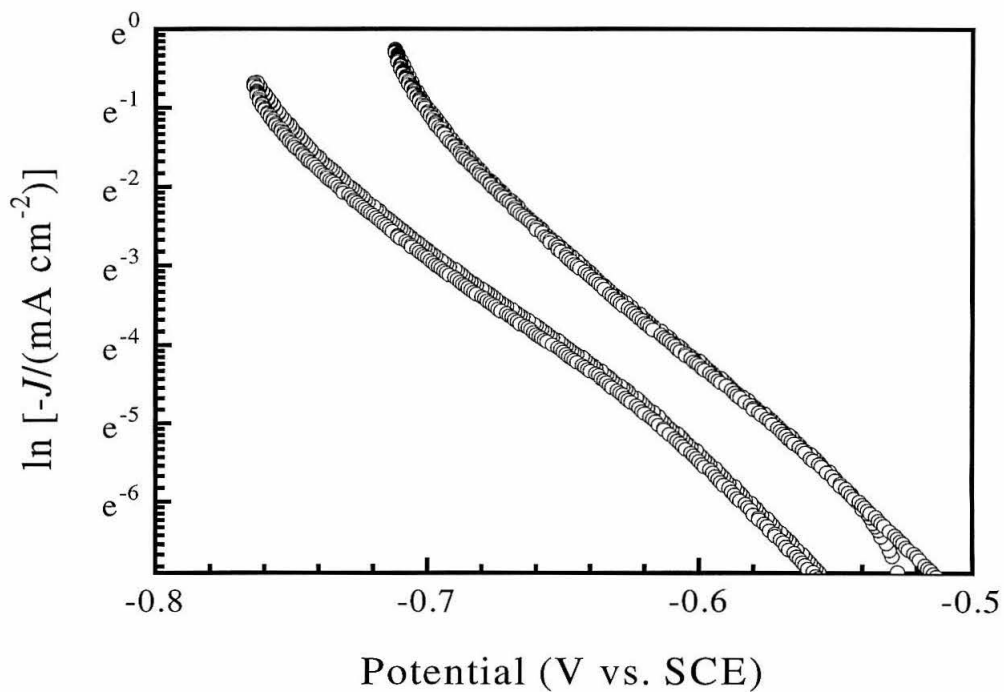


Figure 6.1: A plot of $\ln(J)$ vs. E for a $C_{12}H_{25}$ -terminated Si(100) surface in contact with $CH_3OH-1\text{ M LiCl}-10\text{ mM }MV^{2+}-10\text{ mM }MV^+$ (left data set) and in contact with $CH_3OH-1\text{ M LiCl}-100\text{ mM }MV^{2+}-10\text{ mM }MV^+$ (right data set). The diode quality factors determined from the slopes of these curves were 1.27 (left) and 1.22 (right), and the mean separation between the curves was $48 \pm 15\text{ mV}$.

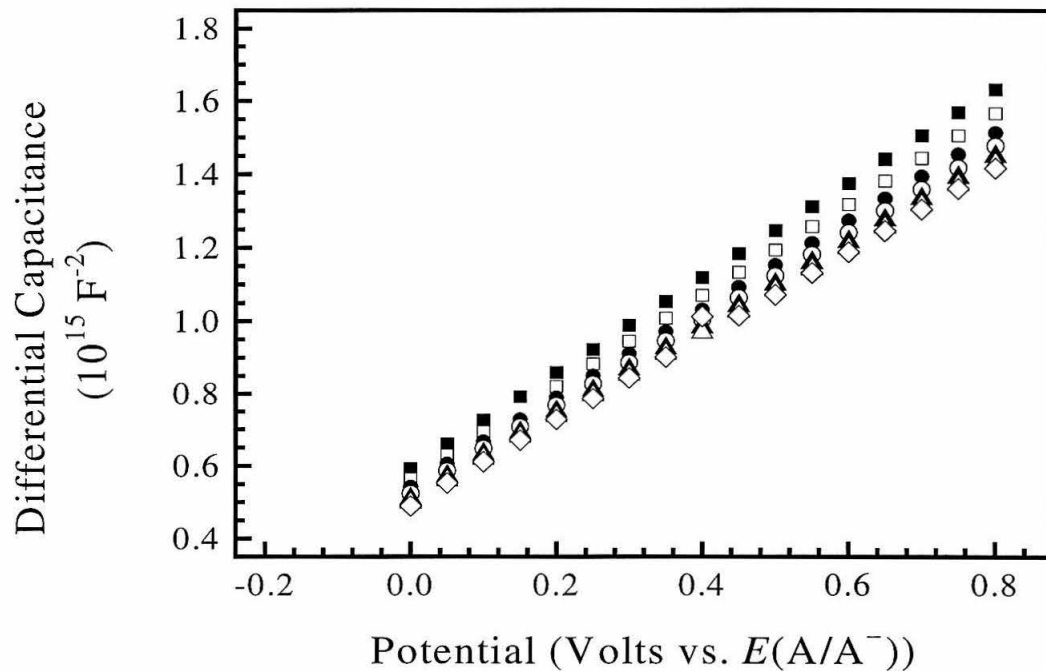


Figure 6.2: A Mott-Schottky plot for a C₁₂H₂₅-terminated Si(100) surface in contact with CH₃OH–1 M LiCl–10 mM MV²⁺–10 mM MV⁺. The data shown were taken at frequencies of 25.1 kHz (filled squares), 15.8 kHz (unfilled squares), 10.0 kHz (filled circles), 6.31 kHz (unfilled circles), 3.98 (filled triangles), 2.51 (unfilled triangles), and 1.58 kHz (unfilled diamonds). Linear extrapolation of these curves yielded a built-in voltage of 0.483 ± 0.015 volts.

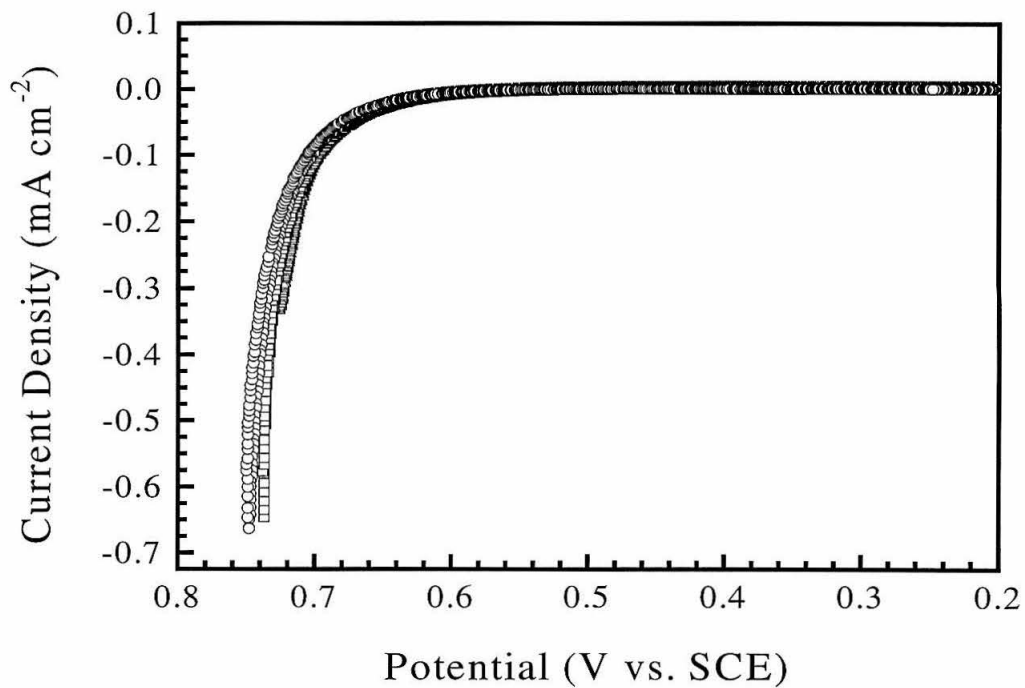


Figure 6.3: A plot of current density vs. potential for Si(100) surfaces terminated with 3 different-length alkyl chains, including C₁₂H₂₅ (circles), C₁₄H₂₉ (squares), and C₁₈H₃₇ (triangles). All curves have been corrected for resistance losses and concentration overpotentials.

	Diode quality factor ^a	<i>E</i> shift with [A] (mV)	Barrier height ^a (V)
HF-Etched Si(100)	1.05 ± 0.08	56 ± 7	0.515 ± 0.008
C ₄ H ₉ -Si(100)	1.80 ± 0.19	7 ± 8	0.75 ± 0.03
C ₁₂ H ₂₅ -Si(100)	1.27 ± 0.11	51 ± 13	0.73 ± 0.02
C ₁₄ H ₂₉ -Si(100)	1.38 ± 0.11	70 ± 12	0.75 ± 0.02
C ₁₈ H ₃₇ -Si(100)	1.39 ± 0.09	48 ± 19	0.78 ± 0.03

Table 6.1: Measured kinetic parameters for chemically modified and unmodified Si(100) surfaces in CH₃OH–MV^{2+/+} solutions. ^a Determined for surfaces in contact with CH₃OH–1 M LiCl–10 mM MV²⁺–10 mM MV⁺.

IV. DISCUSSION

The first-order dependence on both surface electron concentration and redox acceptor concentration observed for most of the chemically modified Si(100) electrodes examined in this work indicates that interfacial electron transfer dominates the current-voltage properties for these semiconductor/liquid contacts.^{22–26} Such behavior is consistent with earlier electrochemical measurements of NH_4F -etched, $\text{CH}_3\text{OH}-\text{Fc}^+$ -treated Si(100) electrodes in contact with $\text{CH}_3\text{OH}-\text{MV}^{2+/+}$, which have also been shown to be kinetically limited by interfacial electron transfer.^{22,27} The similarities between the modified and unmodified surfaces are not unexpected since recent surface recombination velocity measurements have shown that alkylated Si surfaces, like $\text{CH}_3\text{OH}-\text{Fc}^+$ -treated surfaces, have relatively few electrical defects that could contribute to other charge-transport processes.²⁸ While the dominant kinetic mechanism is similar for both chemically modified and unmodified electrodes, the energetics of these surfaces appear to be quite different, with the flat-band potential of the chemically-modified surface shifted over -200 mV relative to the unmodified surface. Such differences have not previously been observed between chemically modified and unmodified Si(111) electrodes in contact with other redox systems.²⁹

The most striking feature of the data described above is that there is no dependence of the interfacial electron-transfer current on the length of the alkyl chain in the surface overlayer. Although this behavior is consistent with previous measurements of current-voltage behavior in solid-state n-Si-SiO₂-alkane-Al device structures, which show no dependence of tunneling current on alkyl chain length,^{19,20} the results contradict experimental measurements of interfacial electron transfer in other heterogeneous systems as well as theoretical predictions for such processes. One possible explanation for the lack of chain-length dependence that cannot be excluded based on the results of this work is that the current is dominated by electron transfer through pinhole defects in the blocking layer. This possibility warrants further investigation.

V. SUMMARY

To date, experimental studies of long-range electron transfer at semiconductor interfaces have indicated a shallower dependence of electron-transfer rate with distance than that expected from theory. Although the results presented in this chapter are in agreement with previous experimental measurements, the data do not preclude the possibility that overlayer defects contribute to anomalously large currents in all of the semiconductor/liquid systems examined.

VI. REFERENCES

1. Gray, H. B.; Winkler, J. R. *Annu. Rev. Biochem.* **1996**, *65*, 537.
2. Moser, C. C.; Page, C. C.; Farid, R.; Dutton, P. L. *J. Bioenerg. Biomembr.* **1995**, *27*, 263.
3. Palmer, G. *Long-Range Electron Transfer in Biology*; Springer-Verlag: Berlin, 1991; Vol. 75.
4. McLendon, G. *Acc. Chem. Res.* **1988**, *21*, 160.
5. Deisenhofer, J.; Michel, H. *Angew. Chem. Int. Ed. Engl.* **1989**, *28*, 829.
6. Feger, G.; Allen, J. P.; Okamura, M. Y.; Rees, D. C. *Nature* **1989**, *339*, 111.
7. Franzen, S.; Goldstein, R. F.; Boxer, S. G. *J. Phys. Chem.* **1993**, *97*, 3040.
8. Marcus, R. A.; Sutin, N. *Biochim. Biophys. Acta.* **1985**, *811*, 265.
9. Barbara, P. F.; Meyer, T. J.; Ratner, M. A. *J. Phys. Chem.* **1996**, *100*, 13148.
10. Chidsey, C. E. D. *Science* **1991**, *251*, 919.
11. Smalley, J. F.; Feldberg, S. W.; Chidsey, C. E. D.; Linford, M. R.; Newton, M. D.; Liu, Y. P. *J. Phys. Chem.* **1995**, *99*, 13141.
12. Finklea, H. O.; Liu, L.; Ravenscroft, S.; Punturi, S. *J. Phys. Chem.* **1996**, *100*, 18852.
13. Weber, K.; Hockett, L.; Creager, S. *J. Phys. Chem. B* **1997**, *101*, 8286.
14. Terrettaz, S.; Becka, A. M.; Traub, M. J.; Fettingner, J. C.; Miller, C. J. *J. Phys. Chem.* **1995**, 11216.
15. Slowinski, K.; Chamberlain, R. V.; Miller, C. J.; Majda, M. *J. Am. Chem. Soc.* **1997**, *119*, 11910.
16. Gu, Y.; Waldeck, D. H. *J. Phys. Chem.* **1996**, *100*, 9573.
17. Gu, Y.; Waldeck, D. H. *J. Phys. Chem. B* **1998**, *102*, 9015.
18. Gu, Y.; Akhremitchev, B.; Walker, G. C.; Waldeck, D. H. *J. Phys. Chem. B* **1999**, *103*, 5220.
19. Boulas, C.; Davidovits, J. V.; Rondelez, F.; Vuillaume, D. *Phys. Rev. Lett.* **1996**, *76*, 4797.
20. Vuillaume, D.; Boulas, C.; Collet, J.; Davidovits, J. V.; Rondelez, F. *Appl. Phys. Lett.* **1996**, *69*, 1646.

21. Bansal, A.; Li, X.; Lauermann, I.; Lewis, N. S.; Yi, S. I.; Weinberg, W. H. *J. Am. Chem. Soc.* **1996**, *118*, 7225.
22. Fajardo, A. M.; Lewis, N. S. *J. Phys. Chem.* **1997**, *101*, 11136.
23. Pomykal, K. E.; Fajardo, A. M.; Lewis, N. S. *J. Phys. Chem.* **1996**, *100*, 3652.
24. Pomykal, K. E.; Lewis, N. S. *J. Phys. Chem. B* **1997**, *101*, 2476.
25. Lewis, N. S. *J. Phys. Chem. B* **1998**, *102*, 4843.
26. Lewis, N. S. *Annu. Rev. Phys. Chem.* **1991**, *42*, 543.
27. Fajardo, A. M.; Lewis, N. S. *Science* **1996**, *274*, 969.
28. Royea, W. J.; Juang, A.; Lewis, N. S. *Appl. Phys. Lett.* **2000**, in press.
29. Bansal, A.; Lewis, N. S. *J. Phys. Chem. B* **1998**, *102*, 1067.